CH_3 Radical Generation in Microplasmas for Up-Conversion of Methane

Mackenzie Meyer[1], Sanjana Kerketta[1], Ryan Hartman[2], and Mark J. Kushner[1,*]

[1] University of Michigan, Electrical Engineering and Computer Science Department, 1301 Beal Ave., Ann Arbor, MI 48109-2122 USA maemeyer@umich.edu, sanjanakerketta@gmail.com, mjkush@umich.edu

[2] New York University, Department of Chemical and Biomolecular Engineering, New York, NY, 11201 USA ryan.hartman@nyu.edu

[*] Author to whom correspondence should be addressed.

Abstract

The conversion of methane, CH_4, into higher value chemicals using low temperature plasmas is challenged by both improving efficiency and selectivity. One path towards selectivity is capturing plasma produced methyl radicals, CH_3, in a solvent for aqueous processing. Due to the rapid reactions of methyl radicals in the gas phase, the transport distance from production of the CH_3 to its solvation should be short, which then motivates the use of microplasmas. The generation of CH_3 in $Ar/CH_4/H_2O$ plasmas produced in nanosecond pulsed dielectric barrier discharge microplasmas is discussed using results from a computational investigation. The microplasma is sustained in the channel of a microfluidic chip in which the solvent flows along one wall or in droplets. CH_3 is primarily produced by electron-impact of and dissociative excitation transfer to CH_4, as well as CH_2 reacting with CH_4. CH_3 is rapidly consumed to form C_2H_6 which, in spite of being subject to these same dissociative processes, accumulates over time, as do other stable products including C_3H_8 and CH_3OH. The gas mixture and electrical properties were varied to assess their effects on CH_3 production. CH_3 production is largest with 5% CH_4 in the $Ar/CH_4/H_2O$ mixture due to an optimal balance of electron-impact dissociation, which increases with CH_4 percentage, and dissociative excitation transfer and CH_2 reacting with CH_4, which decrease with CH_4 percentage. Design parameters of the microchannels were also investigated. Increasing the permittivity of the dielectrics in contact with the plasma increased the ionization wave intensity which increased CH_3 production. Increased energy deposition per pulse generally increased CH_3 production as does lengthening pulse length up to a certain point. The arrangement of the solvent flow in the microchannel can also affect the CH_3 density and fluence to the solvent. The fluence of CH_3 to the liquid solvent is increased if the liquid is immersed in the plasma as a droplet or is a layer on the wall where the ionization wave terminates. The solvation dynamics of CH_3 with varying numbers of droplets was also examined. The maximum density of solvated methyl radicals CH_{3aq} occurs with a large number of droplets in the plasma. However, the solvated CH_{3aq} density can rapidly decrease due to desolvation, emphasizing the need to quickly react the solvated species in the solvent.

I. Introduction

In spite of its abundance, methane (CH_4) serves a minor role as a feedstock material in the chemical industry [1]. The use of CH_4 as a chemical feedstock is limited by the difficulty in activating the C-H bond and poor selectivity in product formation as many of the intermediate species are more reactive than CH_4. Plasma-assisted catalysis of CH_4 for its up-conversion to higher value C_xH_y and oxygenated species is a rapidly evolving area of research due to the ability of plasma to activate the C-H bond at lower temperatures with potentially higher selectivity compared to purely thermal driven processes [2–4]. Cleaving the strong C-H bond in CH_4 using plasmas can be accomplished in either an oxidative manner in the presence of CO_2 or O_2 [5–7] or relying on non-oxidative processes [8–10]. Conversion of CH_4 in mixtures with noble gases, including He and Ar, have been investigated as a means to improve efficiency [11,12]. For example, Rahmani and Nikravech showed that the conversion of CH_4 and CO_2 improved when the plasma was diluted with Ar because both the electron density and mean electron energy increased [13].

The identity and concentration of products formed by plasma-assisted catalysis of CH_4 depends on several parameters such as temperature, pressure, manner of energy deposition, and intrinsic chemical reactivities of species. Dielectric barrier discharges (DBDs) have often been employed for plasma-assisted conversion of methane using AC power (sinusoidal waveforms) or nanosecond pulsed discharges (ns-DBDs) [8,9]. Miura et al. investigated the consequences of different voltage waveforms in a CH_4 DBD and found that ns pulses increased the energy efficiency of H_2 production [14]. Changing the power source from AC to ns-DBDs alters product formation pathways. ns-DBDs typically offer better performance in terms of lower energy cost and less heating with more energy coupling into electronically excited states of CH_4 [15,16].

Several studies have focused on CH_4 conversion in DBDs. Zhang et al. reported CH_4 conversion of up to 9.6% in a pure CH_4 microsecond-pulsed DBD [9]. Products of the CH_4 conversion included H_2 and C_2H_6. Chen et al. observed up to 31.9% CH_4 conversion in a pure CH_4 ns-DBD, with C_2H_6 being the dominant hydrocarbon product [10]. Results of a global plasma chemistry model matched the experimental results and showed that CH_3 was the dominant radical produced before combining to form C_2H_6. Oxidative environments, particularly with admixtures of CO_2 in CH_4, have also been investigated. Bai et al. modeled a CH_4/CO_2 ns-DBD using a 1-dimensional fluid model and showed that CH_3 production was maximum at 70% CO_2 [17]. Mei

et al. investigated CH_4 and CO_2 conversion in a ns-DBD and found that while the conversion increased with applied voltage and length of the cylindrical DBD, energy efficiency decreased [18]. Montesano et al. showed that by shortening the pulse repetition frequency, the conversion of CH_4 increased by 50% and the conversion of CO_2 doubled [19]. Wang et al. modeled the conversion of CH_4 and CO_2 in a DBD in the presence of several additives, including O_2, H_2O, H_2, and N_2 [20]. They found that adding N_2 increased the CH_4 and CO_2 conversion, attributing this increase to reactions of CH_4 and CO_2 with metastable N_2 species. Zhang et al. investigated CH_4 and CO_2 conversion in a DBD by chemical kinetics modeling [21]. Electron-impact dissociation of CH_4 and CO_2 was the most important loss mechanism for those species.

Inexpensive and easily accessible starting materials have received attention in recent years for the discovery of more sustainable synthetic methodologies. Methylation, or the addition of a methyl group (CH_3) to an organic compound, is relevant in pharmaceutical and materials applications [22,23]. Transition-metal complexes can also be used to capture CH_3 [24–26] for the preparation of catalysts from abundant compounds. A variety of homogeneous, catalytic or stoichiometric, methylations can occur under mild conditions, including C-H activation, C-H oxidation, and chain reactions, among the most common [27–33]. These transformations, however, typically require reaction times of up to 24 hours, or orders of magnitude greater than the direct addition by plasmas. Conventional syntheses of activated transition-metal complexes themselves are generally prepared by multiple reaction steps and intermediary workups, generating large amounts of toxic chemicals and solvent waste. Energy intensive separations, e.g., distillation, are necessary to recycle the solvent and chemical waste. Other workups common in organic synthesis, such as filtration, condensation, and reprecipitation are also solvent/energy intensive. Direct methylations by plasmas could circumvent laborious, time consuming, and energy intensive procedures that generate significant chemical waste.

One of the challenges in selective plasma conversion of methane is that the most abundantly generated radical, CH_3, is highly reactive. In conversion schemes which rely on surface processes, such as catalysis or solvation into a processing fluid, capturing the CH_3 is transport limited. That is, the challenge is to have the CH_3 transport to the surface before reacting in the gas phase. To reduce the transport time, the volume of the plasma producing the radicals should be physically small or the plasma should be produced in the immediate vicinity of the surface. In this way, the radicals have greater likelihood of reaching the surface before reacting in

the gas phase. Both goals are at least partially met by microplasma configurations. One of the goals of chemical conversion is to process large quantities of feedstock, which might appear to be inconsistent with plasma conversion using microplasmas. That said, microplasmas can be constructed in large arrays powered in parallel by single power supplies in a manner that will process large volumes of gas.

Microfluidics was primarily introduced to incorporate microreactor technology for process intensification in flow chemistry [34,35]. Microfluidic devices capitalize on flow channels, a few hundred microns to 0.1 mm wide, that are smaller than the scale length of typical boundary layers and turbulence, which results in highly laminar flow that can be guided by channels fabricated in substrates [36]. These well-defined flow patterns enable finer degree of control of mass and heat transfer between reactants contained in adjacent flow streams. Microreactor technology offers new routes for chemical synthesis with the added advantage of miniaturization of analytical devices. The integration of plasmas with microfluidics, microplasmas, enables added benefit of electron-impact dissociation of feedstocks to aid in chemical conversion [37–42]. With microplasma reactors typically operating at atmospheric pressure, the reduction in dimensions of the reactor shifts the Paschen curve to the left on the pd (pressure × dimension) scale, enabling breakdown to be achieved, and self-sustaining plasmas to occur, at lower voltages [41]. As with conventional microplasma reactors, plasma-enhanced microfluidics (PEM) can sustain high power densities at lower gas temperatures due to the regulation of temperature by the small thermal diffusion length. PEM also enables more rapid transport of plasma-generated species to liquids within the channel, thereby also enabling beneficial plasma-liquid interactions.

In this paper, we discuss results from a computational investigation of the plasma chemistry resulting from ns-DBDs sustained microfluidic channels. The gas mixture is $Ar/CH_4/H_2O$ with the goal of producing CH_3 radicals that will solvate into liquids bounding the channels. The intent of the solvated CH_3 is to react with organic radical acceptors or transition-metal complexes leading to up-conversion of CH_3 as an alternative to conventional synthetic methodologies [27–33]. The model geometry is a square microchannel, hundreds of microns wide, with a liquid flowing along one wall or a liquid in the form of injected droplets. The intended gas mixture is Ar/CH_4, with the addition of small amounts of H_2O acknowledging evaporation from the water-based solutions in the channel. These investigations were performed with *GlobalKin* (a 0-dimensional global plasma chemistry model) and *nonPDPSIM* (a 2-dimensional plasma hydrodynamics model). The role of

nonPDPSIM is to resolve the spatial dynamics of the plasma, while *GlobalKin* enables modeling of multiple pulses and detailed chemistry. The final goal of this work is to assess the ability of plasma-produced CH_3 to solvate into a liquid solvent, to catalyze the formation of products relevant for the pharmaceutical industry including higher degree alkanes, substituted arenes, and amine derivatives. To this end, the solvent here is simply water, which is included in the simulation to estimate the rates of solvation of CH_3 into the bounding liquids and to include solvent-relevant electric properties.

The two models used in this work are described in Section II. The reactor geometry and conditions are discussed in Section III. The plasma chemistry of the base case ($Ar/CH_4/H_2O$ = 89.9/10/0.1) is discussed in Section IV. Parametric studies addressing the consequences of gas composition, microchannel materials (and permittivity in particular), and pulse power waveform on CH_3 generation are discussed in Sections V and VI. The configuration of the solvent flow and suggestions to improve CH_3 solvation into the liquid are discussed in Section VII. Concluding remarks are presented in Section VIII.

II. Description of Models

Two plasma models, *GlobalKin* and *nonPDPSIM*, were used in this investigation of CH_3 generation in PEM devices. *GlobalKin* and *nonPDPSIM* are described in detail in Refs. [43] and [44], respectively, and are only briefly discussed here.

GlobalKin is a 0-dimensional (0D) global plasma chemistry model that assumes, to first order, plasma generation inside a well-stirred reactor [43]. The model consists of a set of rate equations whose integration produces the density and temperature of species in the plasma as a function of time. The rate equations include sources or losses of species due to electron-impact and heavy particle reactions, flow (either volume averaged or plug flow), and diffusion to the walls of the reactor, specified by a diffusion length. The average electron energy or temperature is calculated using the electron energy conservation equation. Electron energy distributions for use in computing electron transport and electron-impact rate coefficients are obtained from solutions of the stationary Boltzmann equation. In this work, the power deposition is specified as a function of time. *GlobalKin* also has the ability to model plasma-liquid interactions. The liquid is treated as a separate, well-mixed volume with a specified area in contact with the plasma. Henry's law equilibrium is used to limit the rate of solvation and desolvation of neutral species into and out of

the liquid.

nonPDPSIM is a 2-dimensional (2D) plasma hydrodynamics model that simultaneously integrates Poisson's equation for the electric potential and continuity equations for charged species densities and surface charge on an unstructured numerical mesh [44]. These equations are implicitly solved using Newton-Raphson iteration techniques. The electron temperature is then updated using the electron energy conservation equation using a fully implicit method of successive over-relaxation. Radiation transport and photoionization are included using a Green's function approach. In this study, the typical time steps during the plasma period are dynamically chosen and were on the order of 10^{-13} to 10^{-11} s. *nonPDPSIM* employs time-slicing algorithms to resolve discharge dynamics occurring over μm spatial scales with time steps of a few ps to calculate species evolution over time scales of up to few microseconds. Following the discharge pulse, the neutral plasma option, one of the time-slicing options, was used [45]. In this option, Poisson's equation is not solved, while enforcing charge neutrality. The time steps in the neutral period were dynamically chosen, with typical values varying from 1 ns to 50 ns.

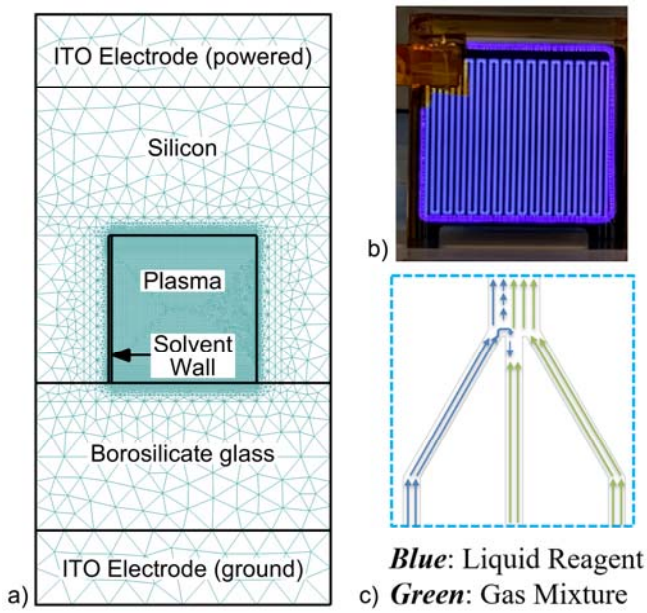

Figure 1. Geometry of the PEM investigated. a) Microchannel geometry with numerical mesh used in *nonPDPSIM*, b) plasma generation inside the microchannel sustained in a mixture of Ar/CH_4, and c) solvent flow arrangement inside the microchannel.

III. Reactor Geometry and Conditions

The cross-section of the microreactor that was modeled in *nonPDPSIM* with the numerical mesh is shown in Fig. 1a. The device that motivates this study is the microfluidic device shown in Fig. 1b whose channel length is 1 m long. The microfluidic device has a channel of 500 μm × 500 μm etched into a silicon wafer using reactive ion etching techniques. A 500 μm thick Borosilicate glass (BG) slide was secured to the Si wafer using anodic bonding. The BG layer and Si had relative permittivities of ε_r = 4.6 and 11.68, respectively. 300 nm thick indium tin oxide

(ITO) layers deposited on the top and bottom of the device function as electrodes. The thickness of the ITO layers was increased in *nonPDPSIM* relative to the experimental device; however, the difference does not affect the results of the model. The ITO layers were represented as metals in the model which are treated as equipotential surfaces. As a result, the mesh resolution inside the electrodes has low refinement. The mesh refinement was increased to a spatial resolution of about 5 μm inside the microchannel to capture the plasma dynamics and gas phase plasma chemistry. The numerical mesh contains 7811 nodes with 5489 nodes in the plasma region. The effective capacitance of this geometry was 6.8×10^{-2} pF/cm^2, meaning the capacitor charged at short time scales (within ns). Gas flow is perpendicular to the channel cross section shown in Fig. 1c. Liquid flows downstream of the junction along the left side of the channel having a thickness of 10 μm.

In experiments, to be reported on elsewhere, the plasma in the microchannel (Fig. 1b) was sustained in a mixture of Ar/CH_4 = 90/10 using high voltage pulses of 4 kV – 20 kV at 1-10 kHz repetition rates and pulse widths of 30 ns. The system was operated at room temperature and atmospheric pressure. The direction of the applied electric field was perpendicular to the direction of fluid flow along the microchannel. Gas and liquid were injected into the microchannel using separate inlets using an arrangement with differential flow velocities to establish a stable gas-liquid interface as shown in Fig. 1c.

The conditions modeled in *nonPDPSIM* and *GlobalKin* closely replicated those of the experiments. The plasma was sustained in $Ar/CH_4/H_2O$ = 89.9/10/0.1 at atmospheric pressure in the base case. H_2O was included in the simulation to represent water vapor in the gas phase from evaporation of the solvent flowing along the sidewall. The species included in the model are listed in Table 1. The model includes 105 species and 2270 reactions in *GlobalKin*. To increase computational speed, the reaction mechanism was reduced to 91 species and 1751 reactions in *nonPDPSIM*. The reaction mechanism for Ar/H_2O was based on Van Gaens et al. [46]. The reactions involving CH_4 and other hydrocarbon species are listed in the supporting information, and a summary of important reactions is given in Table 2. The mechanism includes vibrational states of CH_4, CH_3, CH_2, and C_2H_6. The vibrational modes of a particular species are lumped into a single representative vibrational state in the reaction mechanism. All reactions with CH_4, CH_3, CH_2, or C_2H_6 as a reactant are duplicated for $CH_4(v)$, $CH_3(v)$, $CH_2(v)$, and $C_2H_6(v)$ with the activation energy decreased by the respective vibrational state energy. V-T (vibrational-translational) relaxation is included for 2 classes of species – atomic and molecular. In

nonPDPSIM, secondary electron emission is included for all positive ions with a yield of 0.25. Photoionization of H_2O and CH_4 from Ar(4P) → Ar is included with cross-sections of 2.3×10^{-17} cm^2 and 10^{-17} cm^2, respectively.

In *GlobalKin*, the energy delivered to the plasma in 1 discharge pulse was 10 mJ cm^{-3} (peak power of 42.74 W or 228 kW cm^{-3}). The power ramped up over 15 ns, stayed constant for 30 ns, and fell over 15 ns (pulse width of 60 ns). The pulse repetition rate was 10 kHz (100 μs period), and 20 pulses were modeled. The diffusion length was 112.5 μm based on the 500 μm plasma channel.

In *nonPDPSIM*, the voltage pulse was 6 kV. The voltage ramped up over 5 ns, stayed constant for 15 ns, and fell for 10 ns (pulse width of 30 ns). The voltage pulse width was decreased in *nonPDPSIM* relative to *GlobalKin* for computational efficiency. The neutral plasma option was turned on at 40 ns, or 10 ns after the voltage had decreased to zero. The simulation ended at 100 μs, capturing the dynamics of one pulse. The electron density was initially uniform within the channel at 10^{12} cm^{-3}. A 10 μm thick dielectric layer was modeled on one side wall of the reactor geometry in Fig. 1a to represent the liquid reagent present in the experiments. Liquid phase chemistry was not tracked inside the solvent, but fluxes of CH_3 to the solvent were recorded. The relative permittivity of the dielectric solvent layer was 80, that of water. The conductivity of the dielectrics, including the solvent, was 5×10^{-6} S/cm. The energy deposited in one pulse in *nonPDPSIM* was 2.3 mJ/cm^3.

Liquid water droplets were included in *GlobalKin* to assess the ability of capturing CH_3 radicals in these distributed solvents. The gas phase chemistry was unchanged with CH_3 solvating with a Henry's law constant of 3.47×10^{-2}, estimated to be the same as CH_4 as data for CH_3 is not available [47]. A Henry's law constant below 1 indicates that the CH_3 density will be larger in the gas phase than the liquid phase. Electrons solvated upon encountering the droplet. No reactions occurred in the liquid; only solvation and desolvation of electrons and CH_3 were considered for the purpose of assessing strategies for capturing CH_3 in the liquid. Different numbers of droplets were examined while keeping the total liquid volume constant. Therefore, the radius of the droplet(s) and surface area in contact with the plasma were changed. The diffusion length was based on the average distance between the droplets $(NV)^{-1/3}$, where N is the number of droplets and V is the reactor volume. These properties are listed in Table 3 for the different numbers of droplets examined.

IV. CH_3 Production

The rates of the dominant reactions involving CH_3 are shown in Fig. 2. The major pathways for CH_3 production, shown in Fig. 2a, are

$$e + CH_4 \rightarrow CH_3 + H + e, \quad (1)$$

$$Ar^* + CH_4 \rightarrow CH_3 + H + Ar, \quad (2)$$

$$CH_2 + CH_4 \rightarrow CH_3 + CH_3. \quad (3)$$

Breaking a single C-H bond in CH_4 requires 435 kJ/mol (4.5 eV) [48]. However, electron-impact dissociative excitation has a threshold energy of 10 eV which is readily accessible by electrons during the discharge pulse. In the *GlobalKin* simulations of 20 pulses, electron-impact dissociation of CH_4 is the largest contributor to CH_3 production, accounting for 43% of the CH_3 generated over the last pulse. The maximum rate of electron-impact dissociation is 4.2×10^{22} cm^{-3} s^{-1} at 15 ns into the last pulse, as shown in Fig. 2a. The rate decreases after 15 ns due to the decrease in the electron temperature, discussed further in Section IV.B. As the power ramps down, electron-impact dissociation of CH_4 rapidly decreases. Electron-impact excitation to Ar(1s$_1$), Ar(1s$_2$), Ar(1s$_3$), and Ar(1s$_4$) requires energies above 11.5 eV. These excited states are collectively represented as Ar^* in reaction 2 and can break C-H bonds in CH_4 through dissociative excitation transfer (DET), contributing 9% of the CH_3 production over the last pulse. This reaction rate peaks at 9.9×10^{21} cm^{-3} s^{-1} at 16 ns into the last pulse. The Ar^* density decreases after 16 ns due to quenching of Ar^*. DET from Ar_2^* is not included, as the energy of Ar_2^* is 10.9 eV and the dissociation threshold of CH_4 is 10 eV.

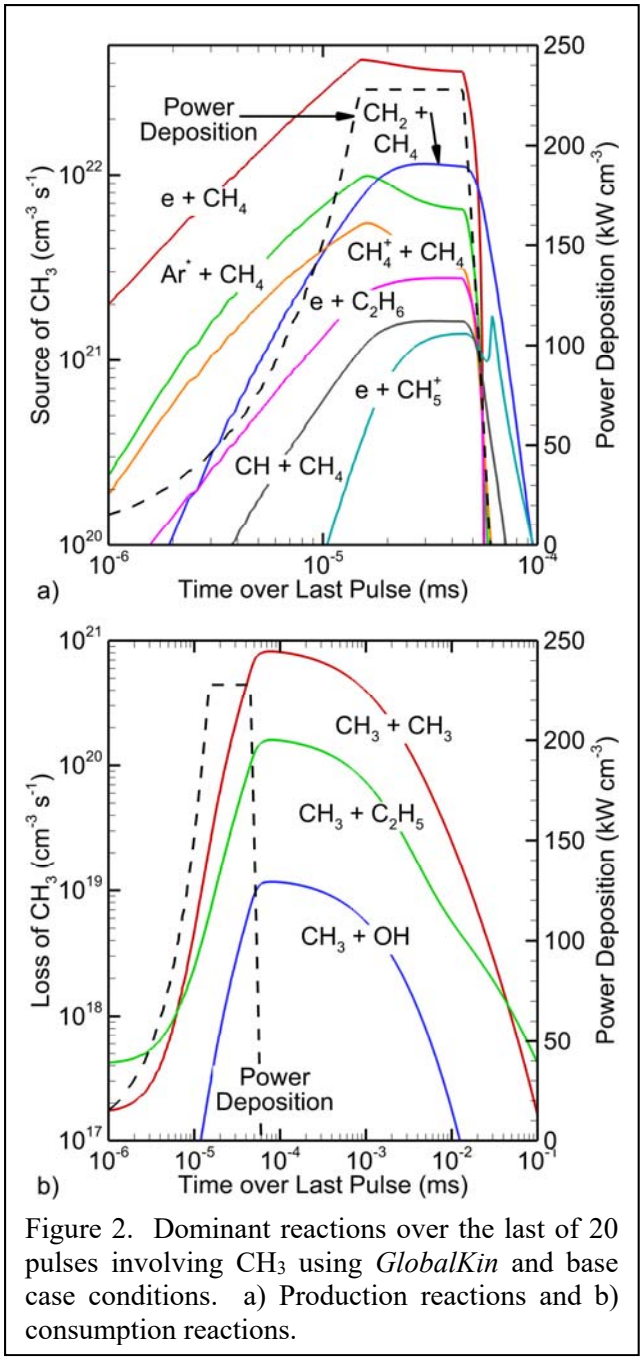

Figure 2. Dominant reactions over the last of 20 pulses involving CH_3 using *GlobalKin* and base case conditions. a) Production reactions and b) consumption reactions.

CH_2 reacting with CH_4 (reaction 3) generates 28% of the CH_3 produced over the last pulse. The reaction rate peaks at 1.1×10^{22} cm^{-3} s^{-1} at 30 ns into the last pulse, later than the previous two reactions. CH_2 first must be produced during the pulse by DET and electron-impact dissociation of CH_4. Other important pathways for the formation of CH_3 radicals, also shown in Fig. 2a, include

$$e + C_2H_6 \rightarrow CH_3 + CH_3 + e, \quad (4)$$

$$CH_4^+ + CH_4 \rightarrow CH_5^+ + CH_3, \quad (5)$$

$$CH + CH_4 \rightarrow CH_2 + CH_3, \quad (6)$$

$$e + CH_5^+ \rightarrow CH_3 + H + H. \quad (7)$$

The maximum rates of these reactions are below 5.5×10^{21} cm^{-3} s^{-1} over the last pulse, implying they play a smaller role in forming CH_3 relative to reactions 1-3. Electron-impact dissociation of ethane (reaction 4) contributes 6% of CH_3 generation, associative charge-exchange (reaction 5) contributes 5%, hydrogen abstraction by CH (reaction 6) contributes 2%, and dissociative recombination of CH_5^+ (reaction 7) contributes 2%.

CH_3 is a reactive species. As shown in Fig. 2b, CH_3 rapidly reacts to form higher order hydrocarbons and oxygenated species by

$$CH_3/CH_3(v) + CH_3 \rightarrow C_2H_6, \quad (8)$$

$$CH_3 + C_2H_5 \rightarrow C_3H_8. \quad (9)$$

$$CH_3 + OH \rightarrow CH_3OH. \quad (10)$$

The most common product was ethane (C_2H_6), with a maximum rate of formation of 8.2×10^{20} cm^{-3} s^{-1} over the last pulse. C_2H_6 formation contributes 88% of the CH_3 consumption over the last pulse. Formation of propane (C_3H_8) when CH_3 radicals react with C_2H_5 (reaction 9) was also a significant source of loss of CH_3 radicals, contributing 10%. The rate of formation of C_3H_8 was much lower than C_2H_6 with a maximum at 1.6×10^{20} cm^{-3} s^{-1} over the last pulse. Finally, methanol (CH_3OH) is formed with a maximum rate of 1.2×10^{19} cm^{-3} s^{-1} over the last pulse, contributing 0.5% of CH_3 consumption. The rate of CH_3OH formation was limited by the amount of OH formed in the plasma. The rates of formation of C_2H_6, C_3H_8, and CH_3OH peak shortly after the pulse and decrease into the afterglow as the densities of radicals (CH_3, C_2H_5, and OH) decrease.

The consumption of CH_3 to make C_2H_6 is the major loss channel. This reaction, in principle a 3-body process, has a high pressure limit for the 2-body equivalent rate coefficient of $6.0 \times 10^{-}$

^{11} cm^3 s^{-1} [49]. The high pressure limit occurs at 10 Torr [50]. As a result, operation at atmospheric pressure is well into the saturated regime.

A. Ionization Wave Propagation

The evolution of the electron-impact ionization source, electron density, and CH_3 density as modeled in *nonPDPSIM* during a single pulse is shown in Fig. 3 at different times during the pulse. At 5 ns, the voltage has risen from 0 kV to 6 kV. An ionization wave propagating from the Si to the BG forms, as shown by the source of electrons due to electron-impact reactions S_e having a maximum value of 2.8×10^{23} cm^{-3} s^{-1} in the head of the ionization wave. The E/N (electric field/gas density) in the head of the ionization wave (IW) is 440 Td (1 Td = 10^{-17} V-cm^2) and electron density of 1.1×10^{13} cm^{-3}. Combined with charging of the lower dielectric surface which removes voltage from the gap, the conductive column reduces the E/N in the plasma column to 36 Td at 5 ns, which essentially extinguishes the ionization source. While the source of electrons due to electron-impact ionization has decreased, the electron density persists in a gas mixture which is at best weakly attaching. Electrons are lost dominantly by diffusion and dissociative recombination. Electrons are also produced by Penning ionization and photoionization after the ionization wave passes.

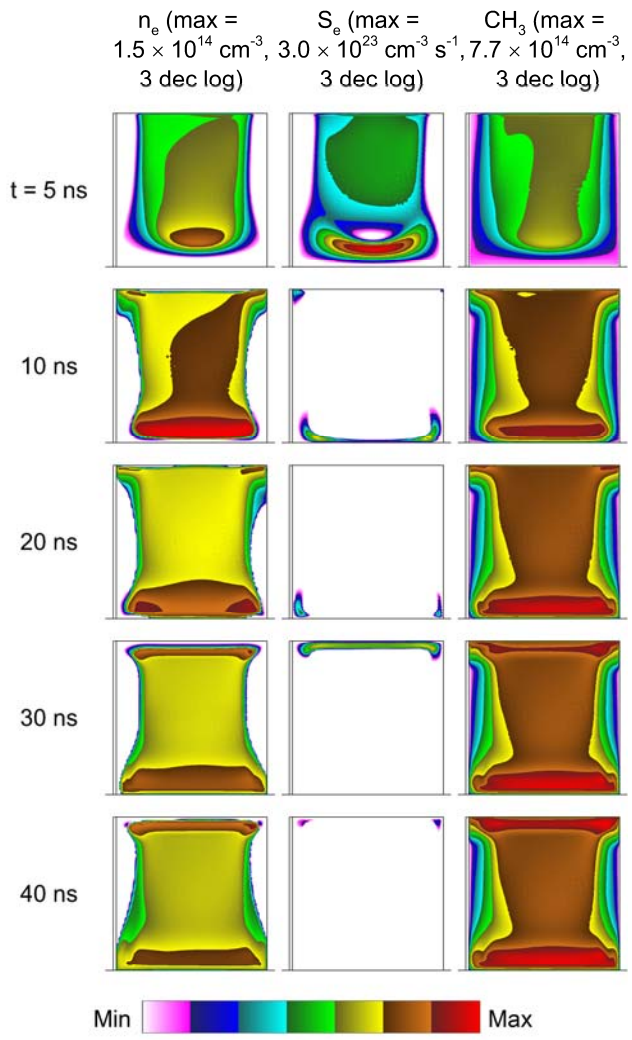

Figure 3. Spatial distribution of the electron density, source of electrons due to electron-impact collisions, and CH_3 radicals over the pulse in *nonPDPSIM*.

Rev. 1-2

The CH_3 density largely follows the path of electrons with a peak value at 7.7×10^{14} cm^{-3} at 40 ns adjacent to the dielectrics where E/N is largest. The formation of CH_3 due to reaction 1 by electron-impact dissociation of CH_4 directly follows the ionization rate, and has largely ceased

by the end of the discharge pulse due to charging of the dielectrics. There is longer term production of CH_3 due to DET from excited states (reaction 2) and radicals (reaction 3) that persist beyond the transit of the ionization wave. Since the Ar/CH_4 plasma does not result in a large density of negative ions, positive molecular ions dominantly undergo dissociative recombination with electrons as opposed to ion-ion neutralization. Dissociative recombination of Ar_2^+ produces Ar^*, which can continue to producing CH_3 through DET to CH_4, while dissociative recombination of CH_4^+ and CH_5^+ have branching to CH_3. Although CH_3 production after passage of the ionization wave does diminish, these secondary processes continue to produce CH_3 into the afterglow.

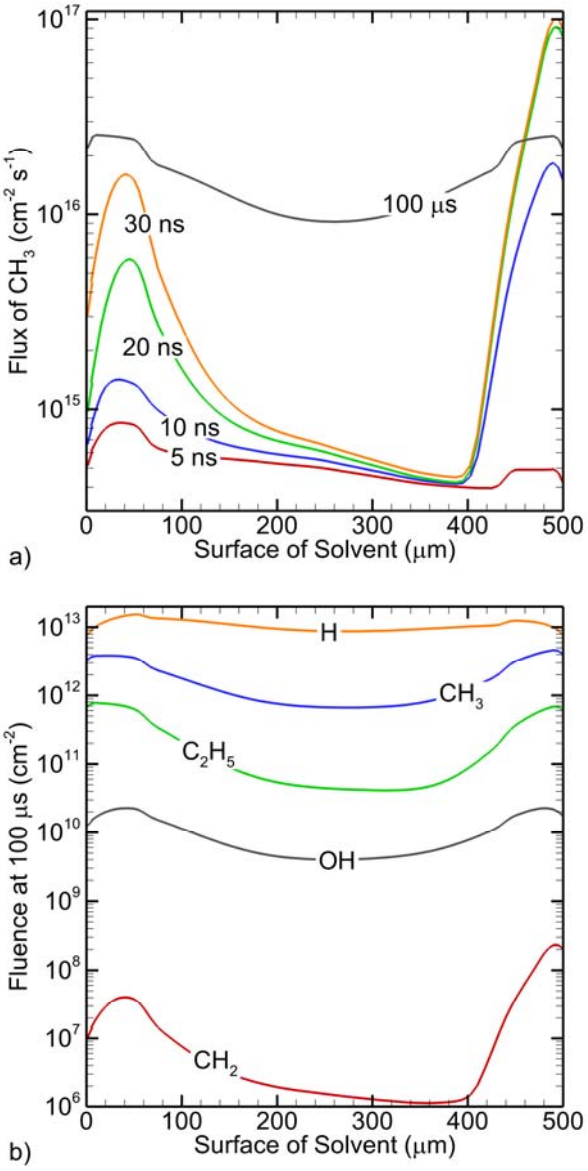

Figure 4. Delivery of radicals to the solvent layer over the pulse using *nonPDPSIM*. a) Flux of CH_3 and b) fluence of CH_3 and other radicals. 0 µm corresponds to the bottom of the solvent layer, and 500 µm corresponds to the top of the solvent layer.

The flux of CH_3 radicals to the solvent layer on the left side of the channel is shown in Fig. 4a at different times during the pulse. The location 0 µm corresponds to the bottom of the solvent layer, and 500 µm corresponds to the top of the solvent layer. As with ionization, electric field enhancement in the corners of the channel produce higher rates of CH_3 production, in addition to the larger rates of production in the head of the IW which stalls at the bottom surface. At 5 ns, the flux of CH_3 to the solvent is low but relatively uniform, which reflects the uniform passage of the IW in the near vicinity of the solvent layer. At 10 ns, a maximum in the flux occurs near the top of the solvent layer where charging of the top surface produces local electric field enhancement and propagation of a SIW near the solvent. While the

CH_3 density in the microchannel is maximum near the bottom of the solvent layer at this time, this CH_3 has not diffused to the edge of the reactor. The maximum in CH_3 flux at the top of the solvent layer persists at 20 ns and 30 ns while the CH_3 flux near the bottom of the solvent layer at 20 ns progressively increases, as CH_3 produced at the bottom surface diffuses to the solvent layer. At 100 μs, the density of CH_3 in the reactor is decreasing, with a maximum of 6.5×10^{13} cm^{-3}, and the density is becoming more homogenous due to diffusion of CH_3 throughout the reactor. The end result is a larger and more uniform flux of CH_3 to the solvent layer.

The fluences of CH_3 and other radicals (CH_2, C_2H_5, H, and OH) to the solvent layer at 100 μs are shown in Fig. 4b. (Fluence is time integral of flux.) CH_3 has a fluence of 6.6×10^{11} cm^{-2} to 4.6×10^{12} cm^{-2}, varying by a factor of 7. For all of the radicals, local maximum fluences occur near the top and bottom of the solvent layer where electric enhancement occurs and ionization waves propagate over the adjacent dielectric surfaces. Overall, H has the largest fluence to the solvent layer (maximum of 1.5×10^{13} cm^{-2}) and CH_2 has the lowest fluence (maximum of 2.3×10^{8} cm^{-2}).

B. Hydrocarbon Chemistry Over Multiple Pulses

The densities of short-lived plasma produced radicals predicted using *GlobalKin* are shown in Fig. 5a over the last of 20 pulses. In general, the densities of these short-lived species increase during the pulse and decrease shortly after the power decreases. CH_3 radicals are generated within a few nanoseconds of the pulse due to the hot electrons, Ar^*, and CH_2 (reactions 1-3), with the CH_3 density increasing for the duration of the pulse as the production outweighs the consumption. CH_3 has a peak density of 3.7×10^{15} cm^{-3}. When the power terminates, CH_3 radicals are quickly consumed in recombination reactions to form higher order hydrocarbons and oxygenates, primarily C_2H_6, C_3H_8, and CH_3OH (reactions 8 - 10). The lifetime of CH_3 radicals is short (< 1 ms).

Other radicals formed in the plasma include CH_2, which has a peak density of 1.9×10^{14} cm^{-3} at 31 ns, a factor of 20 lower than the peak density of CH_3. The dominant production mechanism of CH_2 is DET by

$$Ar^* + CH_4 \rightarrow CH_2 + H + H + Ar, \qquad (11)$$

where Ar^* represents the sum of all electronically excited states [$Ar(1s_1)$, $Ar(1s_2)$, $Ar(1s_3)$, and $Ar(1s_4)$, Ar(4p), Ar(4d)]. Reaction 11 contributes 52% of CH_2 formation over the last pulse.

Other important mechanisms of CH_2 production are electron-impact dissociation of CH_4 and C_2H_4 by

$$e + CH_4 \rightarrow CH_2 + H_2 + e, \qquad (12)$$

$$e + C_2H_4 \rightarrow CH_2 + CH_2 + e. \qquad (13)$$

Reactions 12 and 13 represent 23% and 13%, respectively, of CH_2 formation over the last pulse. CH_2 is primarily consumed by reaction 3, forming CH_3, and

$$CH_2 + CH_4 \rightarrow C_2H_5 + H, \qquad (14)$$

forming C_2H_5. These reactions begin consuming CH_2 during the pulse, creating a maximum in the density of CH_2 at 31 ns into the last pulse, and continue into the afterglow. Together, reactions 3 and 14 consume 89% of the CH_2 formed.

C_2H_5 is dominantly produced by

$$C_2H_4 + H \rightarrow C_2H_5. \qquad (15)$$

Reaction 15 represents 75% of C_2H_5 formation over the last pulse. C_2H_5 is also generated by CH_2 and CH_4 (reaction 14), contributing 21% of C_2H_5 formation over the last pulse. As C_2H_5 is not a saturated hydrocarbon, C_2H_5 is rapidly consumed in the afterglow by hydrogen abstraction,

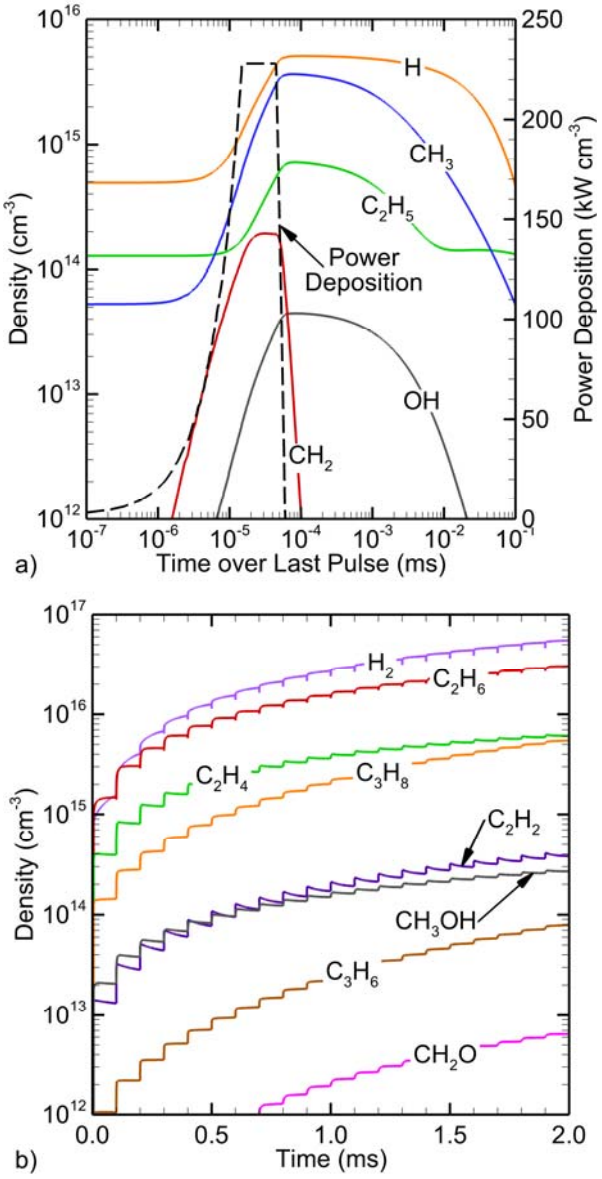

Figure 5. Densities of a) short-lived species over the last pulse and b) species that accumulate over 20 pulses using *GlobalKin*.

$$C_2H_5 + H \rightarrow C_2H_4 + H_2, \qquad (16)$$

contributing 83% of the C_2H_5 depletion over the last pulse. Formation of C_3H_8 (reaction 9) also contributes to C_2H_5 consumption (16% over the last pulse). Although C_2H_5 is produced and consumed with each pulse, the production is marginally larger than consumption, resulting in a pulse-to-pulse increase in C_2H_5 and a density of 1.3×10^{14} cm^{-3} after 20 pulses.

H is produced during the pulse primarily by electron-impact dissociation of CH_4 (reaction 1), contributing 35% of the H generated over the last pulse. Other important production mechanisms of H include DET to CH_4 to form CH_2 (reaction 11, 27% over the last pulse) or to form CH_3 (reaction 2, 7% contribution over the last pulse), and formation of C_2H_5 (reaction 14, 11% contribution over the last pulse). H is consumed in many reactions, both during and after the pulse. The dominant consumption mechanisms of H following the pulse include formation of C_2H_5 (reaction 15, 41% over the last pulse) and formation of C_2H_4 (reaction 16, 46% over the last pulse). H is also consumed by recombination to produce H_2 (10% over the last pulse),

$$H + H + M \rightarrow H_2 + M, \quad M = Ar, CH_4. \tag{17}$$

As Ar and CH_4 are not modulated over the pulse, the dependence of this reaction on time relative to the pulse relies only on H concentration.

The oxygen content in the plasma comes from H_2O, and, in particular, the reactive oxygen species OH. OH is produced during the pulse by

$$e + H_2O \rightarrow OH + H + e, \tag{18}$$

$$e + H_2O \rightarrow OH + H^-, \tag{19}$$

$$Ar^* + H_2O \rightarrow OH + H + Ar. \tag{20}$$

Reaction 18 produces 38% of the OH over the last pulse, reaction 19 produces 22%, and reaction 20 produces 21%. In this system, OH is primarily consumed by CH_3OH formation (reaction 10, 41% over the last pulse). Other important consumption mechanisms include

$$H + OH + M \rightarrow H_2O + M, \quad M = Ar, CH_4, \tag{21}$$

$$CH_4/CH_4(v) + OH \rightarrow H_2O + CH_3. \tag{22}$$

Reactions 21 and 22 each contribute 25% of OH consumption over the last pulse.

The densities of species that accumulate in the plasma over multiple pulses are shown in Fig. 5b. H_2 accumulation produces a density of 5.5×10^{16} cm^{-3} at the end of 20 pulses. H_2 is formed during the pulse by electron-impact dissociation of CH_4, both through reaction 12 (9% over the last pulse) and

$$e + CH_4 \rightarrow CH + H_2 + H + e, \tag{23}$$

contributing 5% of H_2 production over the last pulse. As ground state H_2 accumulates with successive pulses, its density briefly decreases due to electron-impact rotational and vibrational excitation during the pulse. However, this small depletion is compensated for by production during the afterglow between pulses. With accumulation of C_2H_5, the main production mechanism of H_2 during the afterglow is C_2H_4 formation (reaction 16, 72% over the last pulse), which represents circular H-atom chemistry. H recombination (reaction 17, 8% over the last pulse) plays a minor role in regenerating H_2.

C_2H_x species are produced in abundance. C_2H_6, ethane, is the most abundant hydrocarbon product reaching a density of 3.0×10^{16} cm^{-3} after 20 pulses. C_2H_6 is formed primarily by recombination of CH_3 (reaction 8, 99.6% over the last pulse). Following the pulse, C_2H_4 is created from H reacting with C_2H_5 (reaction 16, 93% over the last pulse). C_2H_2 (acetylene) reaches a density of 3.8×10^{14} cm^{-3} after 20 pulses. C_2H_2 is formed immediately following the pulse by dissociative electron-ion recombination

$$e + C_2H_5^+ \rightarrow C_2H_2 + H_2 + H, \quad (24)$$

$$e + C_2H_5^+ \rightarrow C_2H_2 + H + H + H, \quad (25)$$

whose rate coefficient, proportional to the inverse of the electron temperature, increases in the early afterglow. $C_2H_5^+$ is formed from charge-exchange and association reactions involving CH_5^+ and CH_3^+. Reaction 24 produces 34% of the C_2H_2 formed over the last pulse, and reaction 25 produces 19% over the last pulse. Another important formation mechanism of C_2H_2 that occurs during the afterglow is

$$C_2H_3 + H \rightarrow C_2H_2 + H_2. \quad (26)$$

Reaction 26 produces 28% of the C_2H_2 over the last pulse. C_2H_3 is formed from dissociative recombination of $C_2H_5^+$ and

$$C_2H_2 + H \rightarrow C_2H_3, \quad (27)$$

which also consumes C_2H_2 in the afterglow.

C_3H_x species are also formed. C_3H_8 (propane) is produced in abundance, reaching a density of 5.5×10^{15} cm^{-3} after 20 pulses, formed by reactions between CH_3 and C_2H_5 (reaction 9, 98% over the last pulse). C_3H_6 (propene), with a density of 7.9×10^{13} cm^{-3} after 20 pulses, is produced following the pulse by

$$CH_3 + C_2H_3 \rightarrow C_3H_6, \quad (28)$$

$$C_3H_7 + CH_3 \rightarrow CH_4 + C_3H_6, \quad (29)$$

$$C_3H_5 + H \rightarrow C_3H_6. \quad (30)$$

Reaction 28 produces 50% of the C_3H_6 over the last pulse, while reaction 29 produces 22% and reaction 30 produces 17%.

Due to the production of OH from water vapor, oxygenated compounds accumulate in t he plasma, dominantly CH_3OH (methanol) with a density of 2.7×10^{14} cm^{-3} after 20 pulses, and CH_2O (formaldehyde), 6.5×10^{12} cm^{-3} after 20 pulses. CH_3OH is primarily formed by CH_3 combining with OH (reaction 10, 98% over the last pulse). CH_2O is produced primarily from

$$CH_3O + H \rightarrow CH_2O + H_2, \quad (31)$$

producing 74% of the CH_2O formed over the last pulse. CH_3O is produced from electron-impact dissociation of CH_3OH. Little formaldehyde is produced due to this 2-step process.

V. Gas Composition

The gas mixture of the plasma can greatly affect the products formed and the pathways of formation. For example, as CH_4 mole fraction in the Ar/CH_4 mixture decreases, DET by Ar^* plays a larger role in CH_3 production as more power is channeled into the Ar. However, as CH_4 mole fraction increases, electron-impact dissociation of CH_4 can become the dominant pathway for CH_3 formation. In this section, the consequences of CH_4 and H_2O mole fractions in $Ar/CH_4/H_2O$ on CH_3 and other hydrocarbon production are discussed.

A. CH_4 Mole Fraction

The mole fraction of CH_4 in Ar plays an important role in optimizing the production of CH_3 radicals. The consequences of CH_4 mole fraction on IW properties as determined by *nonPDPSIM* are shown in Fig. 6 at 5 ns (after the rise of the pulse). With 0.1% CH_4, the electron density has a peak value of 1.8×10^{13} cm^{-3} occurring near the BG, lowest of the mole fractions investigated. The E/N in the center of the channel is 118 Td. This larger value of E/N leads to a higher electron temperature as needed to excite or ionize Ar with higher threshold energies than electron-impact processes for CH_4. The microchannel operates as a DBD, which terminates the electron avalanche process when the capacitance of the series dielectric surfaces are charged to a significant fraction of the applied voltage. That said, with a positive applied voltage, the bottom

dielectric and its underlying electrode appear cathode-like, thereby forming a cathode-fall like sheath at the surface of the bottom electrode. The E/N in the sheath exceeds 520 Td. As CH_4 content increases above 0.1%, E/N in the center of the channel decreases to below 100 Td, producing lower electron temperatures and lower rates of electron-impact processes. This is, in part, due to the larger plasma density at higher CH_4 fractions, which supports a lower electric field and more rapid charging of the dielectric surfaces, which reduces the voltage across the bulk.

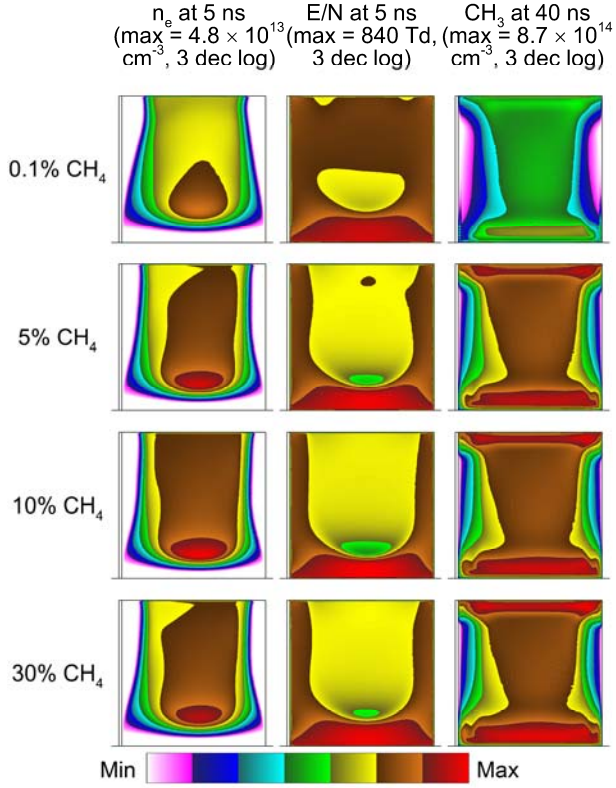

Figure 6. Electron density and E/N at 5 ns and CH_3 at 40 ns using *nonPDPSIM* for different CH_4 fractions.

The CH_3 density is maximum adjacent to the top and bottom surfaces due to the cathode-like sheath formation on the primary and reverse ionization waves. The maximum volume averaged density of CH_3 (inventory divided by volume) occurs from about 4 μs (0.1% CH_4) to 0.8 μs (30% CH_4). The maximum density increases from 6.6×10^{14} cm^{-3} for 0.1% CH_4 to 1.8×10^{15} cm^{-3} for 5% CH_4. and 2.0×10^{15} cm^{-3} for 30% CH_4. This significantly less than linear scaling of CH_3 density with CH_4 mole fraction results, in part, from the finite energy deposition during the pulse which sets the upper limit on CH_3 production. The poor scaling is also, in part, due to the non-uniform energy deposition which is concentrated near the upper and lower surfaces. This local energy deposition produces locally large densities of CH_3 which are then more susceptible to depletion by ethane formation.

The results of *nonPDPSIM* evaluate the consequences of CH_4 content on the plasma properties over one pulse. The consequences of CH_4 mole fraction of 0.1% to 30% over 20 pulses was examined with *GlobalKin*. The water content was held constant at 0.1% with the balance being Ar. The differing production of CH_3, C_2H_x, and CH_3OH with CH_4 mole fraction is shown in Fig. 7. The CH_3 density over the last pulse is shown in Fig. 7a, while the maximum densities

over the last pulse for C_xH_y and CH_3OH are shown in Fig. 7b. The yield of stable products is shown in Figure 7c. The peak CH_3 density was highest at 4.1×10^{15} cm^{-3} with 5% CH_4 in the $Ar/CH_4/H_2O$ mixture.

The dominant reactions producing and consuming CH_3 change as CH_4 content changes. At low CH_4 contents (0.1% and 0.5%), none of the dominant production mechanisms of CH_3 identified at 10% are important. At 0.1% CH_4, this difference in mechanism is partly due to the depletion of CH_4 by over an order of magnitude from its initial density. With the majority of C-compounds being those other than methane, the dominant production mechanisms for CH_3 at 0.1% CH_4 during the last pulse include

$$CH_2 + H_2 \rightarrow CH_3 + H, \quad (32)$$

$$CH + H_2 \rightarrow CH_3, \quad (33)$$

$$e + CH_3OH \rightarrow CH_3 + OH + e, \quad (34)$$

and electron-impact dissociation of C_2H_6 (reaction 4, 15% of CH_3 over the last pulse). Reaction 32 provides 21% of the production of CH_3 over the last pulse, reaction 33 provides 13%, and reaction 34 provides 9%. DET of CH_4 contributes only 3% of the CH_3 formed. The increased importance of CH_3OH to CH_3 production at 0.1% CH_4 is due to the relative concentrations of CH_4 and H_2O. At 0.1% CH_4, the initial mole fractions of CH_4 and H_2O are equal. CH_3 is consumed in C_2H_6 formation (reaction 8, 55% over the last pulse) and CH_3OH formation (reaction 10, 32% over the last pulse). As the CH_4 mole fraction increases to 0.5%, CH_4 after 20 pulses is less depleted, decreasing in density by a factor of 3 over the 20 pulses. The dominant production mechanism for CH_3 is CH_2 reacting with H_2 (reaction 32, 19% over the last pulse). Electron-impact dissociation of C_2H_6 and DET of CH_4 (reaction 2) also play a role in CH_3 formation, contributing 13% each over the last pulse. CH_2 reacting with CH_4 (reaction 3) contributes 12%, and

$$CH_2 + C_2H_6 \rightarrow CH_3 + C_2H_5, \quad (35)$$

contributes 12%. At 0.5% CH_4, C_2H_6 formation (reaction 8, 70%) is the dominant consumption mechanism of CH_3.

As the CH_4 fraction increases to 1%, CH_2 reacting with CH_4 (reaction 2) becomes the dominant production mechanism for CH_3 over the last pulse (21%), while the importance of CH_2 reacting with H_2 decreases (14%). DET of CH_4 also increases in importance (18%). C_2H_6 production (reaction 8) remains the dominant consumption mechanism of CH_3 (76%). At 5% CH_4,

the reactions producing CH_3 are similar to those for 10% CH_4. CH_2 reacting with CH_4 (reaction 3) is the dominant generation mechanism of CH_3, accounting for 31% of total production over the last pulse. Electron-impact dissociation of CH_4 contributes 29%, while DET (reaction 2) contributes 14% over the last pulse. A mole fraction of 5% CH_4 produces the largest density CH_3. The rates of DET (reaction 2) and CH_2 reacting with CH_4 (reaction 3) decrease from 5% CH_4 to 10% CH_4, outweighing the increase in the rate of electron-impact dissociation (reaction 1). At 20% and 30% CH_4, the role of electron-impact dissociation on CH_3 production is similar to that at 10% CH_4, but the roles of DET of CH_4 and CH_2 reacting with CH_4 are greatly reduced, leading to a decrease in CH_3 density. With larger mole fractions of CH_4, electron temperature decreases and production of Ar* also decreases.

As the CH_4 mole fraction increases, the time at which the maximum CH_3 density occurs shortens, shifting closer to the end of the discharge pulse as shown in Fig. 7a. At 0.1% CH_4, the maximum occurs at 1.4 μs, indicating that the production mechanisms of CH_3 after the pulse (that is, other than electron-impact dissociation) are important. As the CH_4 mole fraction increases, the maximum in density shifts closer to the end of the pulse, occurring at 72 ns at 20% and 30%. This shift in the maximum CH_3 density from the afterglow towards the end of the discharge pulse where the electron density is large occurs as electron-impact

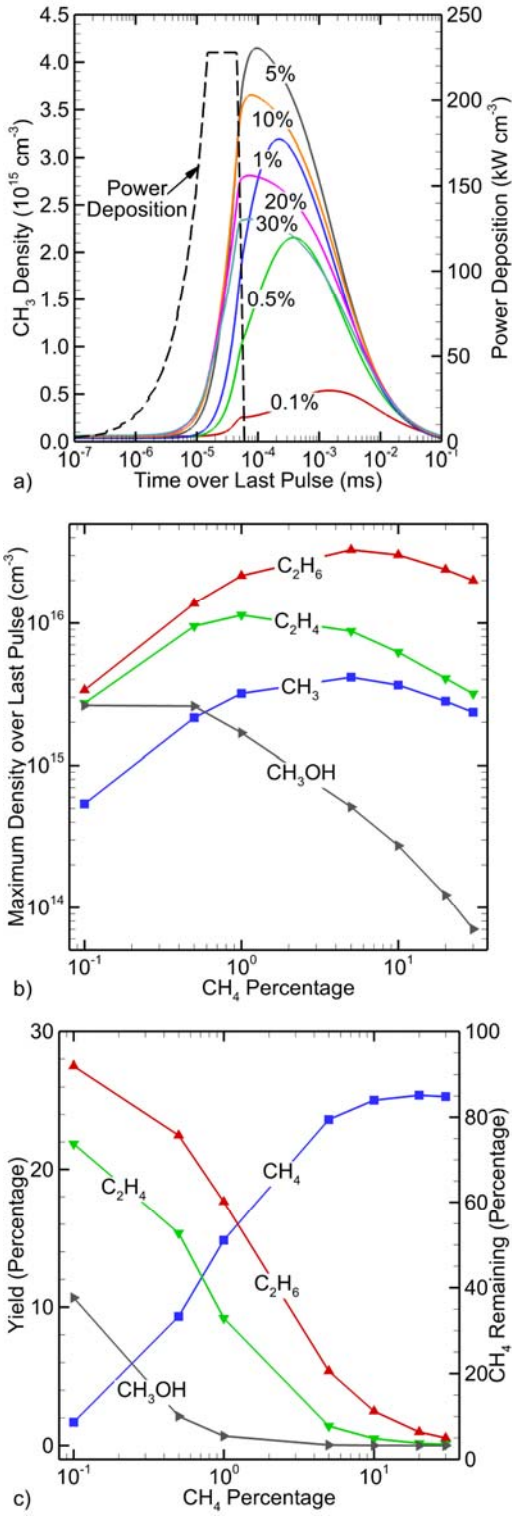

Figure 7. Effect of CH_4 percentage on a) CH_3 density over the last pulse, b) maximum densities over the last pulse, and c) yields and CH_4 conversion at the end of the simulation using *GlobalKin*.

dissociation becomes the dominant mechanism of CH_3 production.

The maximum densities of other hydrocarbon and oxygenated hydrocarbon species are also shown in Fig. 7b. Regardless of the mole fraction of CH_4, C_2H_6 is produced by CH_3 recombination (reaction 8). Therefore, the density of C_2H_6 follows the same trends as CH_3, reaching a maximum density of 3.3×10^{16} cm^{-3} at 5% CH_4. While C_2H_6 is the dominant hydrocarbon product at all CH_4 mole fractions, at low CH_4 mole fractions, C_2H_4 is an important product with a density of 2.7×10^{15} cm^{-3} compared to a density of 3.4×10^{15} cm^{-3} for C_2H_6 at 0.1% CH_4. The relative abundance of C_2H_4 is explained by the rates of formation of C_2H_4 compared to C_2H_6. C_2H_4 is produced from C_2H_5 reacting with H (reaction 15), limited primarily by the C_2H_5 concentration as H is abundant at all CH_4 mole fractions. However, the rate of C_2H_6 formation depends on the square of the CH_3 density and is therefore more limited at low CH_4 percentages when the density of CH_3 is low. The densities of oxygenated hydrocarbons generally decrease as CH_4 content increases. As CH_4 content increases relative to H_2O, radicals increasingly form other hydrocarbon species such as C_2H_6 due to the lack of availability of OH radicals.

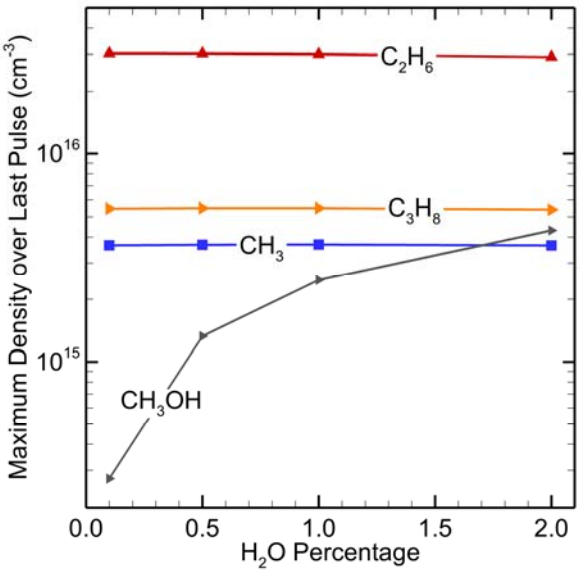

Figure 8. Maximum organic species densities over the last pulse using *GlobalKin* for different H_2O percentages.

The yields of C_2H_6, C_2H_4, and CH_3OH are shown in Fig. 7c. The yields Y are based on carbon accounting and are calculated using the densities at the end of twenty pulses,

$$Y_{C_xH_y} = \frac{x \cdot n_{C_xH_y}}{n_{iCH_4}} \tag{36}$$

where n_{iCH_4} is the initial density of CH_4. The yield for CH_4 is simply the ratio of the final to initial CH_4 density and is related to the CH_4 conversion. Only long-lived species are considered, as the short-lived species have negligible density at the end of the last afterglow. At 0.1% CH_4, the yield of CH_4 is 8.7%, indicating that the majority of CH_4 has been depleted and converted into other compounds. The carbon is converted dominantly into C_2H_6 and C_2H_4, with yields of 27.5% and

21.8%, respectively. CH_3OH is also relatively abundant with a yield of 10.7%. As initial CH_4 mole fraction increases to 0.5%, the yields of C_2H_6, C_2H_4, and CH_3OH all decrease as less CH_4 is converted (33.3% initial CH_4 remains). As CH_4 percentage increases above 0.5%, CH_4 yield increases (indicating less conversion), rising to 84.9% at 30% CH_4. Therefore, the yields of C_2H_6, C_2H_4, and CH_3OH decrease, as less CH_4 is converted to other compounds.

B. H_2O Content

The consequences of increasing H_2O mole fraction are discussed in this section using results from *GlobalKin*. The maximum H_2O percentage considered is 2%, representing saturated vapor pressure of the gas.

The maximum densities of hydrocarbon species over the last pulse are shown in Fig. 8 as a function of H_2O percentage. The densities of the pure hydrocarbon species (CH_3, C_2H_6, and C_3H_8) change by < 4% as H_2O percentage increases. The production mechanisms of CH_3 remain largely unchanged as H_2O percentage increases. This is surprising, as the electron density decreases from 1.1×10^{14} cm^{-3} at 0.1% H_2O to 5.8×10^{13} cm^{-3} at 2% H_2O, due in part to an increase in the density of negative ions as H_2O content increases. This decrease in electron density is outweighed by an increase in the steady-state T_e as H_2O percentage increases. At the time the power begins to decrease, T_e increases from 3.03 eV at 0.1% H_2O to 3.16 eV at 2% H_2O. This increase in T_e, albeit small, leads to larger electron-impact rate coefficients for dissociative processes over the pulse, as well as increased rates of production of Ar^* as the power begins to decrease (45 ns). Since the rate coefficient for electron-impact processes increases while the electron density decreases, the overall rate remains nearly constant.

Since the CH_3 density remains relatively constant with increasing H_2O fraction, C_2H_6 and C_3H_8 also remain relatively constant. As H_2O content increases, the OH density linearly increases as OH is primarily produced by electron-impact dissociation and DET of H_2O (reactions 18-20). As CH_3OH is formed by OH reacting with CH_3 (reaction 10), and the reaction is limited by the availability of OH, the density of CH_3OH increases as the density of OH increases.

VI. Electrical Properties

Electrical properties of the reactor change the electron density and temperature, as well as the reduced electric field E/N. As the CH_3 radical density is related to electron-impact reactions,

whether directly or indirectly through CH_2 or DET with Ar^*, the CH_3 radical density is also affected by the reactor electrical properties. In this section, the consequences of these electrical properties are discussed. In Section VI.A., the permittivity of the dielectric BG is changed, and the results are analyzed using *nonPDPSIM*. In Section VI.B., the effect of energy deposition per pulse is examined using *GlobalKin*. In Section VI.C., the pulse length is varied in *nonPDPSIM*.

A. Dielectric Permittivity

The choice of material for a DBD reactor is typically based on the material's dielectric constant and chemical and thermal stability. Borosilicate glass (BG) is a widely used dielectric material for microreactors owing to its ease of fabrication at small scales and its low reactivity towards plasma-produced species. However, increasing the permittivity of the materials for the reactor can increase the energy deposition by increasing the RC (resistance × capacitance) time constant for charging the dielectric (which is typically in series with the applied voltage). The consequences of permittivity of the dielectric on discharge properties during a single pulse was investigated using *nonPDPSIM*.

The consequences of the relative permittivity of the dielectric on the propagation of the IW are shown in Fig. 9. IWs are shown for relative permittivities of 4.6 (corresponding to BG), 10 (alumina), and 100. The IW begins at 4 ns. For $\varepsilon_r = 4.6$, the IW is weak with a maximum value of 8.0×10^{21} cm^{-3} s^{-1}. These differences in initial propagation of the IW are largely explained by the polarization of the bounding dielectrics which expel electric potential out of high permittivity materials into the lower permittivity of the gas gap. This produces an initially larger E/N in the gap for the higher permittivity material. For

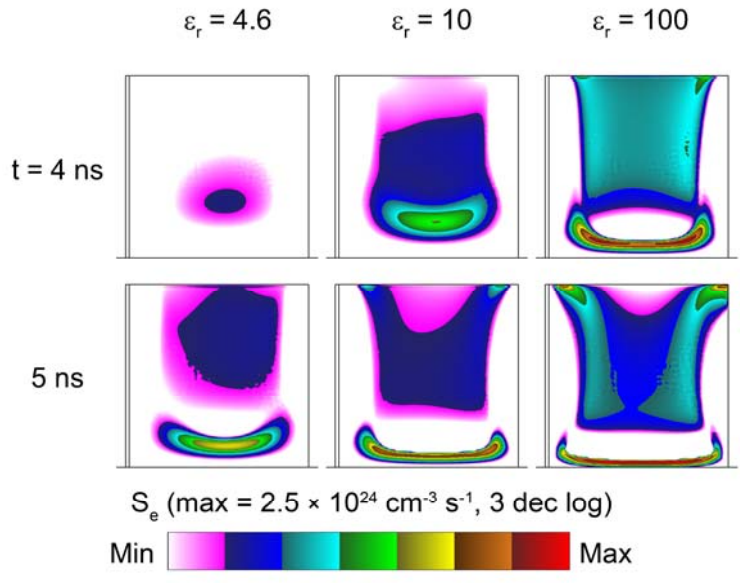

Figure 9. Effect of dielectric permittivity on IW propagation across the gap using *nonPDPSIM*.

ε_r = 100, the IW propagates across the gap in 4-5 ns with a maximum ionization rate of 1.5-2.5 × 10^{24} cm^{-3} s^{-1}. For ε_r = 4.6, the IW requires nearly 10 ns to fully cross the gap, with a maximum ionization rate of 2.8 × 10^{23} cm^{-3} s^{-1}. The shape of the IWs is also sensitive to the permittivity. At the low value of permittivity, the IW propagates as conventional bulk IW whereas at the higher permittivity, electric field enhancement in corners influence propagation.

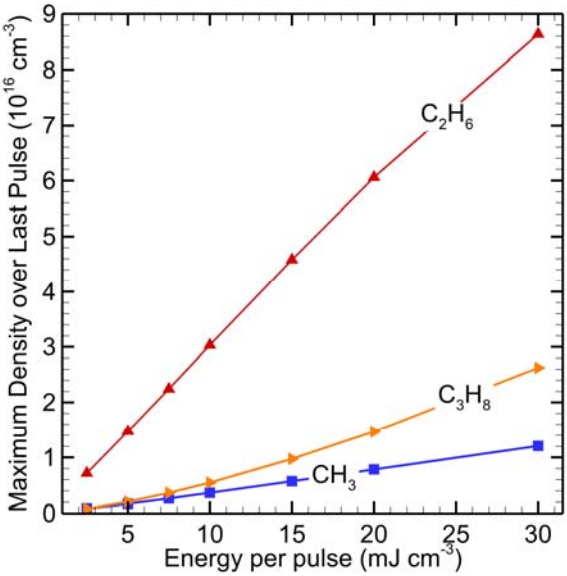

Figure 10. Maximum hydrocarbon densities over the last pulse using *GlobalKin* for different energy depositions per pulse.

With the bottom dielectric serving in the role of a cathode, a sheath is produced with a large E/N above its surface, resulting in local production of CH_3. The maximum CH_3 density after the IW has crossed the gap at 40 ns increases from 7.7 × 10^{14} cm^{-3} at ε_r = 4.6 to 2.8 × 10^{15} cm^{-3} at ε_r = 10 and 8.4 × 10^{15} cm^{-3} at ε_r = 100.

B. Energy per Pulse

The energy per pulse was varied using *GlobalKin* by changing the peak power while holding the pulse length and rise and fall times constant. In *GlobalKin*, the E/N applied across the plasma is not specified. A power profile as a function of time is specified, which is then included the electron energy equation. The electron temperature and density are then computed that will deliver the specified power. The power integrated over time then gives energy per pulse. The consequences of energy deposition per pulse on the maximum hydrocarbon densities over the last pulse are shown in Fig. 10. The gas mixture was $Ar/CH_4/H_2O$ = 89.9/10/0.1, as for the base case. As the energy per pulse increases, the maximum electron density over the last pulse linearly increases from 3.2 × 10^{13} cm^{-3} for 2.5 mJ cm^{-3} to 2.5 × 10^{14} cm^{-3} for 30 mJ cm^{-3}. The peak electron temperature also nominally increases from 4.9 eV to 5.3 eV as the energy per pulse increases from 2.5 mJ cm^{-3} to 30 mJ cm^{-3}. The nominally linear increase in electron density with energy deposition indicates that multistep processes, such as ionization of excited states, are not the dominant sources of ionization.

The CH_3 density also increases nearly linearly with energy deposition, from 8.5×10^{14} cm^{-3} for 2.5 mJ cm^{-3} to 1.2×10^{16} cm^{-3} for 30 mJ cm^{-3}. This linear increase follows the linear increase in the electron density. The rates of formation of CH_3 either directly depend on the electron density through electron-impact dissociation of CH_4 (or, at high powers, C_2H_6) or indirectly through DET of CH_4 by Ar^* or CH_2 reacting with CH_4. Since the density of CH_3 increases linearly with energy per pulse, the densities of C_2H_6 and C_3H_8 also increase linearly. These linearities also result from CH_4 not being significantly depleted (< 40% depleted).

C. Pulse Length

The length of the voltage pulse primarily affects the propagation of the IW, which in turn determines the electron and radical densities. To examine these relationships, the voltage pulse length was varied in *nonPDPSIM*. A constant 5 ns rise time and 10 ns fall time was maintained for each pulse length while varying the constant voltage portion of the pulse. The neutral plasma option described in Section II begins 10 ns after the voltage reaches zero.

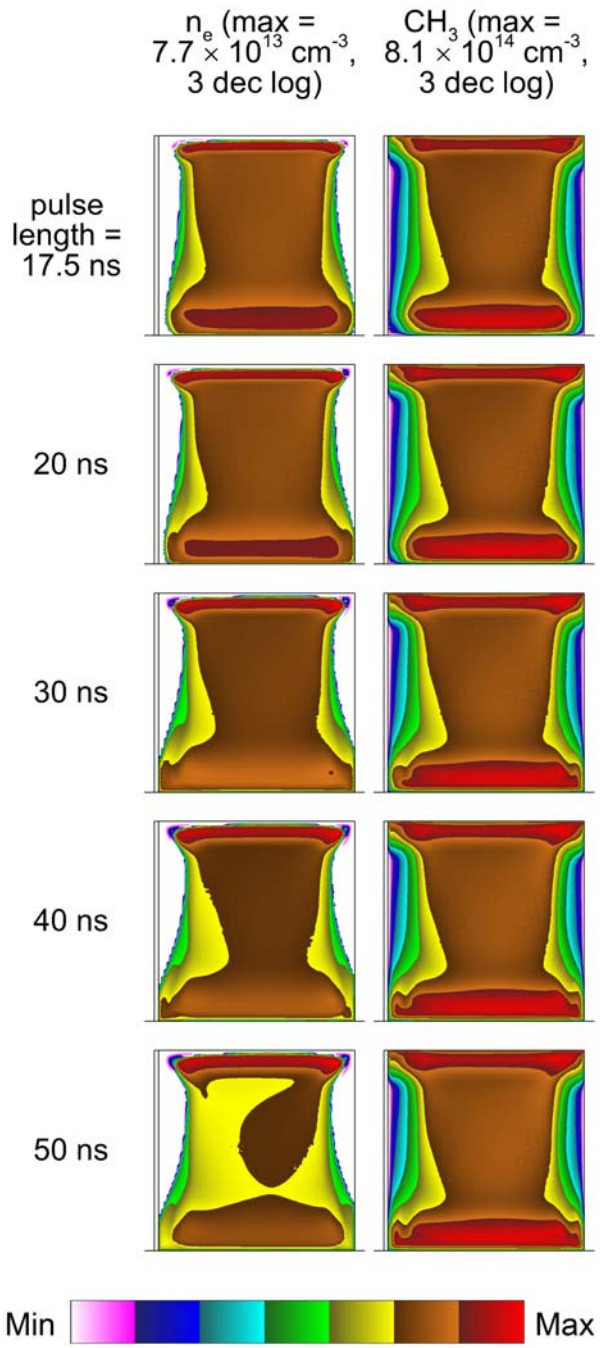

Figure 11. Electron and CH_3 densities 10 ns after the pulse ends using *nonPDPSIM* for different pulse lengths.

The electron density and CH_3 density at 10 ns after the pulse ends are shown for different pulse lengths in Fig. 11. Since the rise time is constant for all pulse lengths, the IW propagation on the rise of the pulse is nearly unchanged. As the pulse lengthens, the electron density near the

BG (bottom) 10 ns after the pulse ends decreases, despite having the same density for all pulse lengths at earlier times. This decrease is due primarily to recombination of electrons and ions after the IW passes. As the constant voltage portion of the pulse was lengthened, fewer electrons survive to the fall of the voltage pulse. The traversal of the IW across the gap in large part charges the capacitance of the BG which results in a reduction of current flow and a lowering of the electric field in the bulk plasma – similar to the operation of a DBD. With ionization by electron-impact processes terminated at approximately the same time for all voltage pulse lengths, the longer afterglow period of the longer pulse length produces a larger reduction in plasma density. The power deposition over the pulse also changes as the pulse length changes. At 17.5 ns, 1.8 mJ cm^{-3} is deposited in the plasma, compared to 2.3 mJ cm^{-3} at 30 ns. After 30 ns, the power deposition increases less rapidly with increasing pulse length, only reaching 2.4 mJ cm^{-3} at 50 ns.

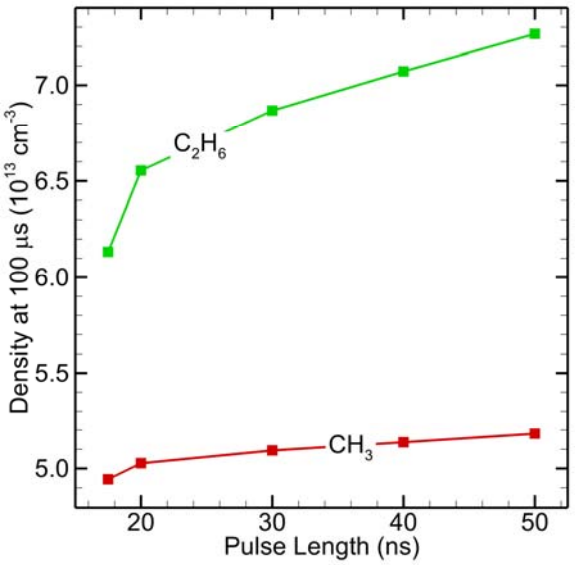

Figure 12. Volume-averaged densities of CH_3 and C_2H_6 at 100 µs for different pulse lengths using *nonPDPSIM*.

The reverse IW that occurs during the fall of the voltage pulse does somewhat depend on the pulse length. The electron and CH_3 densities at the top of the reactor are generally lower for shorter pulses. The intensity of the reverse ionization wave depends, in part, on the plasma channel having a finite resistivity. A highly conductive channel is unable to support the large electric fields that produce ionization and excitation in the head of an IW. With shorter pulses, there has been insufficient time to allow for recombination and attachment in the plasma channel formed by the forward IW to increase its resistivity and so support a strong reverse IW.

The volume-averaged densities of CH_3 and C_2H_6 at 100 µs are shown in Fig. 12 for different pulse lengths, a time that is long compared to the pulse lengths. On these time scales, the discharge pulses appear to provide initial conditions for evolution during the afterglow. Densities of both CH_3 and C_2H_6 have only moderate increases when increasing pulse length from 17.5 ns to 50 ns – 5% for CH_3 and 18% for C_2H_6. Production of CH_3 by electron-impact dissociation is

slowed during the pulse after the IW passes. The production of CH_3 by DET (reaction 2) and CH_2 reacting with CH_4 (reaction 3) are not directly dependent upon the IW, though production of Ar^* and CH_2 does depend on the IW. This is also reflected by the slowing increase of power deposition over the pulse beyond a pulse length of 30 ns. Therefore, the growth rate of CH_3 slows as the pulse length increases. Extrapolating to longer pulses, the CH_3 produced would likely reach a constant value. The more rapid increase in C_2H_6 is a result of the spatial distribution of the CH_3 produced during the pulse. For longer pulse lengths, a larger fraction of the CH_3 is produced in high density regions near the upper and lower surfaces. Since the formation of C_2H_6 depends on the square of the CH_3 density, more rapid formation of C_2H_6 occurs due to the concentration of CH_3 near the boundaries.

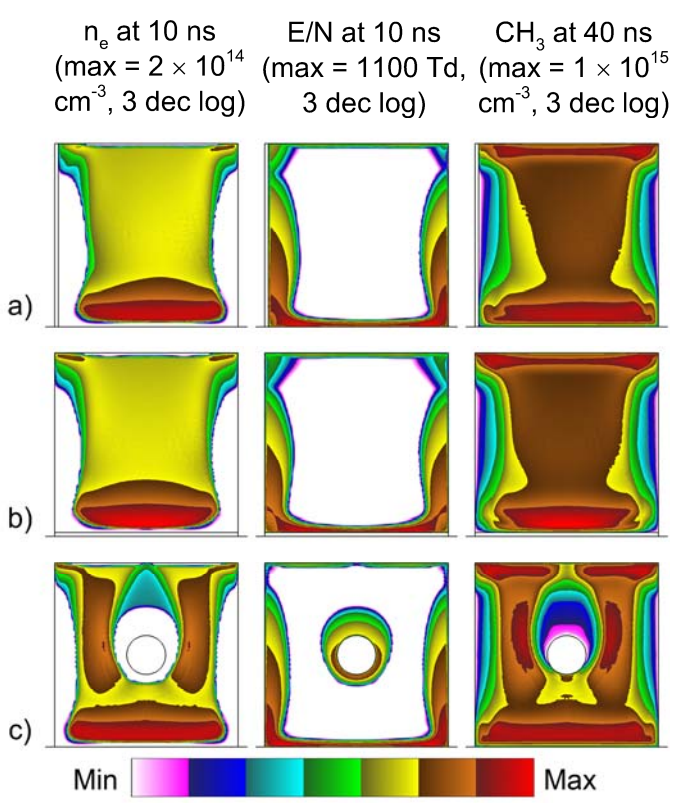

Figure 13. Electron density at 10 ns, E/N at 10 ns, and CH_3 density at 40 ns for different flow arrangements using *nonPDPSIM*. a) solvent along left wall, b) solvent along bottom wall and c) solvent as a droplet.

VII. Solvent Flow Arrangement

To trap the CH_3 radicals generated in the gas phase into an organic acceptor in the liquid, the original motivation for this work, the radicals should be generated in close proximity of the solvent to avoid loss of CH_3 to, for example, formation of C_2H_6. Different geometrical configurations of liquid flow into the microchannel were investigated using *nonPDPSIM*. to optimize the fluence of radicals reaching the solvent. In the first case, the liquid solvent was flowed along the left wall, with the liquid flow rate adjusted to establish a stable gas-liquid interface shown in Fig. 1c. In the second arrangement, the solvent was flowed along the bottom wall. In the third arrangement, the liquid was flowed in the form of droplets in the center of the

microchannel. The relative permittivity of the solvent in all cases was kept at 80, mirroring that of water. The solvent layer along the wall was 10 μm thick in both cases, and the droplet was 106 μm in diameter.

The electron density and reduced electric field E/N at 10 ns, and CH_3 density in the microchannel at 40 ns are shown in Fig. 13 for solvent flowing along the left wall (Fig. 13a), bottom wall (Fig. 13b), and as a droplet (Fig. 13c). There are small differences in these quantities between the solvent flowing along the left wall and along the bottom wall. The electron density is enhanced above the bottom solvent layer more than above the bottom BG dielectric, with a maximum of 2.0×10^{14} cm^{-3} compared to 1.5×10^{14} cm^{-3}, leading to an enhancement of the CH_3 density. This is due to the larger capacitance in the direction of current flow with the solvent layer on the bottom of the channel.

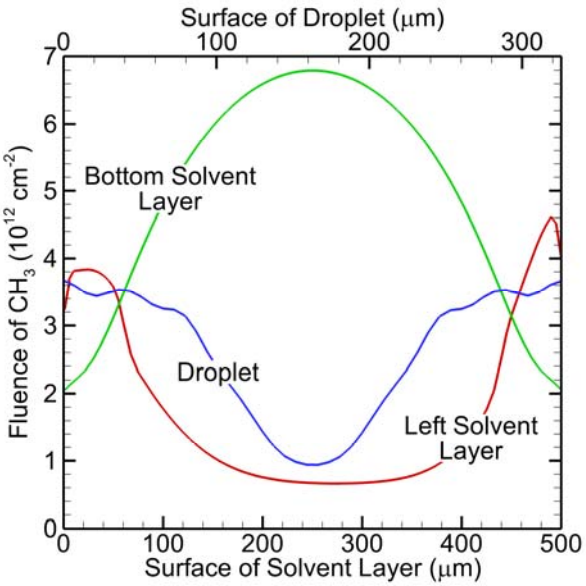

Figure 14. Fluence of CH_3 to the solvent at 100 μs using *nonPDPSIM*.

With the applied electric field largely axial, the droplet in the center of the microchannel polarizes, producing electric field enhancement at the poles (parallel to the applied electric field) and a decrease in electric field at the equator. At the same time, the droplet charges, producing a sheath around the droplet. Due to this polarization and formation of a sheath around the droplet, the electron density decreases substantially in the vicinity of the droplet. There is some shadowing of droplet by the IW that decreases CH_3 formation in its wake.

The fluences (integrated fluxes) of CH_3 radicals reaching the solvent are shown in Fig/ 14 after 100 μs for these three configurations of solvent. The solvent layer on the bottom has a higher fluence than the solvent layer on the left in the center of the solvent layer. This increase in CH_3 fluence occurs as the solvent is positioned near the maximum CH_3 density where the IW terminates on the bottom surface. The fluence to the solvent on the side wall is maximum at either end, adjacent to the local maxima in the density of CH_3 density where the forward and reverse IWs terminate. The fluence of CH_3 to the droplet is generally larger than the left solvent layer. With

the droplet immersed in the plasma, the distance CH_3 radicals must travel before encountering the solvent is shorter, thereby reducing transit time and reducing the likelihood that CH_3 will be consumed by other processes. In spite of the initial density of CH_3 being smaller around the droplet, transport dominates, producing larger fluences. However, the CH_3 fluence to the droplet is lower than to the bottom solvent layer, as the IW produces the largest CH_3 density adjacent to the bottom solvent layer.

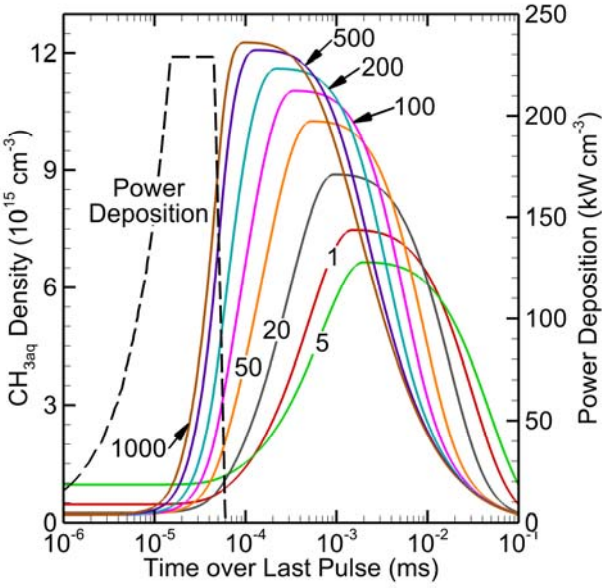

Figure 15. Effect of number of droplets on CH_{3aq} density in droplets for different numbers of droplets for constant droplet volume. These results were produced using *GlobalKin.*

Integrating the fluences of CH_3 to the solvent over the surface area of the solvent provides a measure of the total inventory of CH_3 molecules encountering the solvent. The fluences are expressed as per-cm of depth perpendicular to the plane displayed in Fig. 13. The solvent on the bottom receives 2.5×10^{15}/cm CH_3 molecules following a single discharge pulse, while the solvent on the left side receives 8.7×10^{14}/cm CH_3 molecules. The droplet, represented as a cylindrical rod in the 2D simulation, receives 8.5×10^{14}/cm CH_3 molecules. The differences between the number of CH_3 molecules encountering the solvent layers (top or side) is driven by the difference in fluence since their areas are the same. However, while the droplet has a larger fluence of CH_3 than the left solvent layer, the droplet encounters smallest inventory of CH_3 molecules because the surface area of the single droplet is low compared to the solvent layers.

While flowing the solvent as a droplet can increase the fluence of CH_3, there are practical drawbacks to this method. Experimentally, the droplet could stick to the inside the walls due to charge accumulation which would result in disruption of desired flow pattern inside the microchannel. Other solvent properties such as hydrophobicity, vapor pressure, polar vs non-polar solvent can affect CH_3 uptake by the solvent. Examples of solvents that can be employed for radical trapping include polar solvents like diethyl azodicarboxylate (DEAD) and acrylic acid or non-polar solvents such as heptane, toluene, and xylene [41,42]. Noteworthy is that droplet-based microfluidics are readily modeled in non-plasma systems. A number of studies have shown

enhanced mass transport at liquid-liquid or gas-liquid interfaces that could facilitate refreshing rates of the CH_3 at polar solvent interfaces on times scales of micro-to-milliseconds [51–54]. Optimization of the multiphase microfluidic and plasma physics is expected to influence the overall selectivity in CH_4 reactions.

The density of CH_{3aq} produced in droplets was investigated for different numbers of droplets and radii using *GlobalKin* as described in Section III. (The aq subscript means an aqueous species.) The total liquid volume was held constant, and the number of droplets and their radii were varied as shown in Table 3. Reactions in the liquid were neglected. The resulting CH_{3aq} densities over the last pulse are shown in Fig. 15 for 1 to 1000 droplets. At the beginning of the last pulse, CH_{3aq} is similar regardless of the droplet number.

In the 1 – 10 μs after the pulse, the CH_{3aq} density does depend on the number of droplets. The peak density of CH_{3aq} increases as the number of droplets increases beyond 5. With 1000 droplets having a radius of 5 μm, the concentration of CH_{3aq} increases over 600 times compared to the beginning of the pulse, reaching a maximum at 1.2×10^{16} cm^{-3}. This increase in CH_{3aq} is due to the decrease in diffusion length for CH_3 to reach any given droplet, enabling more CH_3 to diffuse to the liquid and solvate, and the larger surface-to-volume ratio of that droplet. While the CH_{3aq} density largely increases as droplet number increases, the CH_{3aq} density decreases from a single droplet to 5 droplets. This decrease is due to the differing diffusion lengths. For a single droplet, the diffusion length is based on the distance from the droplet to the walls of the reactor; however, for 5 droplets, the diffusion length is based on the distance between the droplets, larger than the diffusion length to the wall. In reality, there would be diffusion to both the droplets and to the walls of the reactor.

As CH_3 is depleted in the gas phase by gas phase reactions, such as conversion to C_2H_6, , the droplets become super-saturated, resulting in desolvation of CH_{3aq} to maintain Henry's law equilibrium. The rate of desolvation is larger for smaller droplets due to the larger surface-to-volume ratio.

Due to the small liquid volume (0.2% of the total), CH_3 in the gas phase at any given time is largely unaffected by the solvation of CH_3. The density of CH_3 in the gas phase changes by at most 3% by storing methyl radicals as CH_{3aq}. That said, in the absence of reactions in the droplet, the uptake of CH_3 is limited by Henry's law equilibrium of CH_3. Reactions in the liquid that consume CH_{3aq} would enable continued solvation and uptake of CH_3. The timescale of these

reactions would need to be shorter than the desolvation time of CH_{3aq}.

VIII. Concluding Remarks

ns-DBD in microfluidic devices is a rapidly evolving field with potential benefits in the field of plasma catalysis and development of novel pathways for production of chemicals. The generation of CH_3 radicals in a microfluidic ns-DBD has been computationally investigated using a global plasma chemistry model and a 2D plasma hydrodynamics model.

A plasma was initially generated in $Ar/CH_4/H_2O$ = 89.9/10.0/0.1 at 1 atm. In this mixture, CH_3 is formed primarily from electron-impact dissociation of CH_4, dissociative excitation transfer (DET) to CH_4 from Ar^*, and CH_2 reacting with CH_4 (reactions 1-3). IWs traverse the microfluidic channel during the rise (forward IW) and fall (reverse IW) of the voltage pulse, and the CH_3 density profile followed that of the electrons with local maxima near the top Si surface and bottom BG surface. While only electron-impact dissociation of CH_4 directly relates the electron density to the CH_3 density, DET and CH_2 reacting with CH_4 are indirectly related to the electron density. DET relies on electron-impact excitation of Ar to Ar^*, while the CH_2 concentration relies on electron-impact and DET of CH_4.

The dominant radicals formed in the plasma are CH_3, CH_2, C_2H_5, H, and OH. Following the pulse, these radicals formed higher-order hydrocarbons such as C_2H_6, C_2H_4, C_2H_2, C_3H_8, and C_3H_6, as well as oxygenated species including CH_3OH and CH_2O. CH_3 was primarily consumed forming C_2H_6. CH_3 was also consumed through formation of C_3H_8 and CH_3OH, though these processes occurred at a lower rates than formation of C_2H_6.

The production of CH_3 radicals varies with gas composition. While the source of CH_3 due to electron-impact reactions of CH_4 largely increased as CH_4 content increased, the source due to DET of CH_4 by Ar^* and CH_2 reacting with CH_4 decreased. The optimum mixture for producing large densities of CH_3 was found to be 5% CH_4. Separately, the effect of H_2O content in the gas mixture was investigated. CH_3 concentration was constant up to 2% H_2O. From 0.1% H_2O to 2% H_2O, the increase in T_e outweighed the decrease in the electron density, keeping the production of CH_3 nearly constant.

The consequences of electrical properties of the materials used to construct the microfluidic device were also investigated. Increase in permittivity of the dielectric material from 4.6 (Borosilicate glass) to 100 resulted in an increase in the ionization wave intensity and led to a

resulting increase of over an order of magnitude in the maximum CH_3 density. Increasing the energy deposited into the plasma over one pulse linearly increased the CH_3 density. An increase in the pulse length increased CH_3 density up to pulse lengths of 30 ns, with saturating increases from 30 ns to 50 ns.

Finally, the advantages and disadvantages of flowing solvent as a droplet versus flowing the solvent along one of the walls (left or bottom) were discussed. The flux of CH_3 to the layer on the bottom was increased compared to the layer along the left wall and droplet; however, the flux may be dependent upon solvent properties like polarity. The variation in the density of CH_{3aq} with differing numbers of droplets was discussed. This discussion was in the context of solvation dynamics and neglected reactions in the liquid. CH_{3aq} reached the highest values inside the droplet as the number of droplets increased, but also desolvated more rapidly. If the timescale of CH_{3aq} reacting in the droplet is short relative to the desolvation time, there is an advantage to using larger numbers of smaller droplets to capture CH_3 prior to reactions in the gas depleting its density.

Supporting Information

Reactions included in *GlobalKin* involving CH_4 and other hydrocarbon species.

Acknowledgements

This work was supported by the National Science Foundation under Award No. ECO-CBET-2032604 and CBET-2032664. This work was also supported by the Department of Energy Office of Fusion Energy Sciences (DE-SC0020232), and the Army Research Office MURI program (W911NF-20-1-0105).

Conflict of Interest

The authors have no conflicts of interest to disclose.

Data Availability

The data that support the findings of this study are contained in the paper and available from the corresponding author upon reasonable request.

References

[1] R. Franz, E. A. Uslamin and E. A. Pidko, "Challenges for the utilization of methane as a chemical feedstock", Mendeleev Commun. **31,** 584 (2021).

[2] L. Bromberg, D. R. Cohn, A. Rabinovich and N. Alexeev, "Plasma catalytic reforming of methane", Int. J. Hydrogen Energy **24,** 1131 (1999).

[3] T. Nozaki and K. Okazaki, "Non-thermal plasma catalysis of methane: Principles, energy efficiency, and applications", Catal. Today **211,** 29 (2013).

[4] A. Bogaerts, X. Tu, J. C. Whitehead, G. Centi, L. Lefferts, O. Guaitella, F. Azzolina-jury, H. Kim, A. B. Murphy, W. F. Schneider, et al., "The 2020 plasma catalysis roadmap", J. Phys. D. Appl. Phys. **53,** 443001 (2020).

[5] X. Tu and J. C. Whitehead, "Plasma dry reforming of methane in an atmospheric pressure AC gliding arc discharge: Co-generation of syngas and carbon nanomaterials", Int. J. Hydrogen Energy **39,** 9658 (2014).

[6] C. De Bie, J. van Dijk and A. Bogaerts, "The Dominant Pathways for the Conversion of Methane into Oxygenates and Syngas in an Atmospheric Pressure Dielectric Barrier Discharge", J. Phys. Chem. C **119,** 22331 (2015).

[7] B. Wanten, S. Maerivoet, C. Vantomme, J. Slaets, G. Trenchev and A. Bogaerts, "Dry reforming of methane in an atmospheric pressure glow discharge: Confining the plasma to expand the performance", J. CO2 Util. **56,** 101869 (2022).

[8] M. Scapinello, E. Delikonstantis and G. D. Stefanidis, "A study on the reaction mechanism of non-oxidative methane coupling in a nanosecond pulsed discharge reactor using isotope analysis", Chem. Eng. J. **360,** 64 (2019).

[9] S. Zhang, Y. Gao, H. Sun, H. Bai, R. Wang and T. Shao, "Time-resolved characteristics and chemical kinetics of non-oxidative methane conversion in repetitively pulsed dielectric barrier discharge plasmas", J. Phys. D. Appl. Phys. **51,** 274005 (2018).

[10] X. Chen, S. Zhang, S. Li, C. Zhang, J. Pan, A. B. Murphy and T. Shao, "Temperature-independent, nonoxidative methane conversion in nanosecond repetitively pulsed DBD plasma", Sustain. Energy Fuels **5,** 787 (2021).

[11] N. R. Pinhão, A. Janeco and J. B. Branco, "Influence of Helium on the Conversion of Methane and Carbon dioxide in a Dielectric Barrier Discharge", Plasma Chem. Plasma Process. **31,** 427 (2011).

[12] S. Jo, D. Hoon Lee and Y.-H. Song, "Product analysis of methane activation using noble gases in a non-thermal plasma", Chem. Eng. Sci. **130,** 101 (2015).

[13] A. Rahmani and M. Nikravech, "Impact of Argon in Reforming of (CH4 + CO2) in Surface Dielectric Barrier Discharge Reactor to Produce Syngas and Liquid Fuels", Plasma Chem. Plasma Process. **38,** 517 (2018).

[14] T. Miura, K. Takahashi, K. Takaki and Y. Nishida, "Influence of Waveform of Applied Voltage on H2 Production From Methane Reforming Using Dielectric Barrier Discharge", IEEE Trans. Plasma Sci. **49,** 147 (2021).

[15] M. Scapinello, E. Delikonstantis and G. D. Stefanidis, "Direct methane-to-ethylene conversion in a nanosecond pulsed discharge", Fuel **222,** 705 (2018).

[16] N. Pourali, M. M. Sarafraz, V. Hessel and E. V. Rebrov, "Simulation study of a pulsed DBD with an electrode containing charge injector parts", Phys. Plasmas **28,** 013502 (2021).

[17] C. Bai, L. Wang, L. Li, X. Dong, Q. Xiao, Z. Liu, J. Sun and J. Pan, "Numerical investigation on the CH4/CO2 nanosecond pulsed dielectric barrier discharge plasma at atmospheric pressure", AIP Adv. **9,** 035023 (2019).

[18] D. Mei, P. Zhang, G. Duan, S. Liu, Y. Zhou, Z. Fang and X. Tu, "CH4 reforming with CO2 using a nanosecond pulsed dielectric barrier discharge plasma", J. CO2 Util. **62,** 102073 (2022).

[19] C. Montesano, M. Faedda, L. M. Martini, G. Dilecce and P. Tosi, "CH4 reforming with CO2 in a nanosecond pulsed discharge. The importance of the pulse sequence", J. CO2 Util. **49,** 101556 (2021).

[20] W. Wang, R. Snoeckx, X. Zhang, M. S. Cha and A. Bogaerts, "Modeling Plasma-based CO2 and CH4 Conversion in Mixtures with N2, O2 , and H2O: The Bigger Plasma Chemistry Picture", J. Phys. Chem. C **122,** 8704 (2018).

[21] L. Zhang, S. Heijkers, W. Wang, L. M. Martini, P. Tosi, D. Yang, Z. Fang and A. Bogaerts, "Dry reforming of methane in a nanosecond repetitively pulsed discharge: chemical kinetics modeling", Plasma Sources Sci. Technol. **31,** 055014 (2022).

[22] J. Huang, Z. Chen and J. Wu, "Recent Progress in Methyl-Radical-Mediated Methylation or Demethylation Reactions", ACS Catal. **11,** 10713 (2021).

[23] G. Yan, A. J. Borah, L. Wang and M. Yang, "Recent Advances in Transition Metal-

Catalyzed Methylation Reactions", Adv. Synth. Catal. **357,** 1333 (2015).

[24] D. G. Kelley, A. Marchaj, A. Bakac and J. H. Espenson, "Formation and Homolysis of Organonickel(III) Complexes", J. Am. Chem. Soc. **113,** 7583 (1991).

[25] J. Campos, J. López-Serrano, R. Peloso and E. Carmona, "Methyl Complexes of the Transition Metals", Chem. - A Eur. J. **22,** 6432 (2016).

[26] S. K. Kariofillis, B. J. Shields, M. A. Tekle-Smith, M. J. Zacuto and A. G. Doyle, "Nickel/Photoredox-Catalyzed Methylation of (Hetero)aryl Chlorides Using Trimethyl Orthoformate as a Methyl Radical Source", J. Am. Chem. Soc. **142,** 7683 (2020).

[27] N. J. Gunsalus, A. Koppaka, S. H. Park, S. M. Bischof, B. G. Hashiguchi and R. A. Periana, "Homogeneous Functionalization of Methane", Chem. Rev. **117,** 8521 (2017).

[28] X. Guo, G. Fang, G. Li, H. Ma, H. Fan, L. Yu, C. Ma, X. Wu, D. Deng, M. Wei, et al., "Direct, Nonoxidative Conversion of Methane to Ethylene, Aromatics, and Hydrogen", Science **344,** 616 (2014).

[29] R. A. Periana, D. J. Taube, S. Gamble, H. Taube, T. Satoh and H. Fujii, "Platinum Catalysts for the High-Yield Oxidation of Methane to a Methanol Derivative", Science **280,** 560 (1998).

[30] A. Hu, J.-J. Guo, H. Pan and Z. Zuo, "Selective functionalization of methane, ethane, and higher alkanes by cerium photocatalysis", Science **361,** 668 (2018).

[31] K. T. Smith, S. Berritt, M. González-Moreiras, S. Ahn, M. R. Smith, M.-H. Baik and D. J. Mindiola, "Catalytic borylation of methane", Science **351,** 1424 (2016).

[32] A. K. Cook, S. D. Schimler, A. J. Matzger and M. S. Sanford, "Catalyst-controlled selectivity in the C–H borylation of methane and ethane", Science **351,** 1421 (2016).

[33] C. Díaz-Urrutia and T. Ott, "Activation of methane: A selective industrial route to methanesulfonic acid", Science **363,** 1326 (2019).

[34] B. Gutmann, D. Cantillo and C. O. Kappe, "Continuous-Flow Technology-A Tool for the Safe Manufacturing of Active Pharmaceutical Ingredients", Angew. Chemie Int. Ed. **54,** 6688 (2015).

[35] L. N. Protasova, M. Bulut, D. Ormerod, A. Buekenhoudt, J. Berton and C. V. Stevens, "Latest Highlights in Liquid-Phase Reactions for Organic Synthesis in Microreactors", Org. Process Res. Dev. **17,** 760 (2013).

[36] G. M. Whitesides, "The origins and the future of microfluidics", Nature **442,** 368 (2006).

[37] O. T. Olabanji and J. W. Bradley, "The development and analysis of plasma microfluidic devices", Surf. Coatings Technol. **205,** S516 (2011).

[38] L. Patinglag, D. Sawtell, A. Iles, L. M. Melling and K. J. Shaw, "A Microfluidic Atmospheric-Pressure Plasma Reactor for Water Treatment", Plasma Chem. Plasma Process. **39,** 561 (2019).

[39] C. Ishii, S. Stauss, K. Kuribara, K. Urabe, T. Sasaki and K. Terashima, "Atmospheric pressure synthesis of diamondoids by plasmas generated inside a microfluidic reactor", Diam. Relat. Mater. **59,** 40 (2015).

[40] N. Pourali, V. Hessel and E. V. Rebrov, "The Effects of Pulse Shape on the Selectivity and Production Rate in Non-oxidative Coupling of Methane by a Micro-DBD Reactor", Plasma Chem. Plasma Process. **42,** 619 (2022).

[41] L. Lin, H. Quoc Pho, L. Zong, S. Li, N. Pourali, E. Rebrov, N. Nghiep Tran, K. (Ken) Ostrikov and V. Hessel, "Microfluidic plasmas: Novel technique for chemistry and chemical engineering", Chem. Eng. J. **417,** 129355 (2021).

[42] Y. Liu, J. C. Sabio and R. L. Hartman, "A counter-current flow micro-packed-bed DBD plasmatron for the synthesis of a methylated cobaloxime", J. Phys. D. Appl. Phys. **54,** 194003 (2021).

[43] A. M. Lietz and M. J. Kushner, "Air plasma treatment of liquid covered tissue: Long timescale chemistry", J. Phys. D. Appl. Phys. **49,** 425204 (2016).

[44] S. A. Norberg, E. Johnsen and M. J. Kushner, "Formation of reactive oxygen and nitrogen species by repetitive negatively pulsed helium atmospheric pressure plasma jets propagating into humid air", Plasma Sources Sci. Technol. **24,** 035026 (2015).

[45] J. Kruszelnicki, A. M. Lietz and M. J. Kushner, "Atmospheric pressure plasma activation of water droplets", J. Phys. D. Appl. Phys. **52,** 355207 (2019).

[46] W. Van Gaens and A. Bogaerts, "Kinetic modelling for an atmospheric pressure argon plasma jet in humid air", J. Phys. D. Appl. Phys. **46,** 275201 (2013).

[47] R. Sander, "Compilation of Henry's law constants (version 4.0) for water as solvent", Atmos. Chem. Phys. **15,** 4399 (2015).

[48] R. Lü and J. Lin, "A interpretation of stepwise bond dissociation energies of CH4", Comput. Theor. Chem. **1037,** 10 (2014).

[49] D. L. Baulch, C. T. Bowman, C. J. Cobos, R. A. Cox, T. Just, J. A. Kerr, M. J. Pilling, D.

Stocker, J. Troe, W. Tsang, et al., "Evaluated Kinetic Data for Combustion Modeling. Supplement II", J. Phys. Chem. Ref. Data **34,** 757 (2005).

[50] W. Tsang and R. F. Hampson, "Chemical Kinetic Data Base for Combusion Chemistry. Part I. Methane and Related Compounds", J. Phys. Chem. Ref. Data **15,** 1087 (1986).

[51] A. Günther and K. F. Jensen, "Multiphase microfluidics: from flow characteristics to chemical and materials synthesis", Lab Chip **6,** 1487 (2006).

[52] J. G. Kralj, H. R. Sahoo and K. F. Jensen, "Integrated continuous microfluidic liquid–liquid extraction", Lab Chip **7,** 256 (2007).

[53] M. T. Kreutzer, F. Kapteijn, J. A. Moulijn and J. J. Heiszwolf, "Multiphase monolith reactors: Chemical reaction engineering of segmented flow in microchannels", Chem. Eng. Sci. **60,** 5895 (2005).

[54] H. Song, D. L. Chen and R. F. Ismagilov, "Reactions in Droplets in Microfluidic Channels", Angew. Chemie Int. Ed. **45,** 7336 (2006).

[55] H. Chatham, D. Hils, R. Robertson and A. Gallagher, "Total and partial electron collisional ionization cross sections for CH4, C2H6, SiH4, and Si2H6", J. Chem. Phys. **81,** 1770 (1984).

[56] H. F. Winters, "Dissociation of methane by electron impact", J. Chem. Phys. **63,** 3462 (1975).

[57] P. Tosi, D. Bassi, B. Brunetti and F. Vecchiocattivi, "Molecular processes in CH4-H2 plasmas diluted with rare gases: reactions of X* atoms and X+ ions (X = Ne and Ar) with methane molecules", Int. J. Mass Spectrom. Ion Process. **149–150,** 345 (1995).

[58] M. Hayashi, "Electron Collision Cross-Sections for Molecules Determined from Beam and Swarm Data", Swarm Studies and Inelastic Electron-Molecule Collisions, 167–187 (1987).

[59] A. I. Florescu-Mitchell and J. B. A. Mitchell, "Dissociative recombination", Phys. Rep. **430,** 277 (2006).

[60] Y. Itikawa and N. Mason, "Cross Sections for Electron Collisions with Water Molecules", J. Phys. Chem. Ref. Data **34,** 1 (2005).

[61] A. C. Gentile, "Kinetic Processes and Plasma Remediation of Toxic Gases", "Kinetic Processes and Plasma Remediation of Toxic Gases," Ph.D. Thesis (University of Illinois at Urbana-Champaign, 1995).

[62] X. Xu, "Dynamics of High- and Low-Pressure Plasma Remediation", "Dynamics of High- and Low-Pressure Plasma Remediation," Ph.D. Thesis (University of Illinois at Urbana-Champaign, 2000).

[63] R. K. Janev and D. Reiter, "Collision processes of C2,3Hy and C 2,3Hy+ hydrocarbons with electrons and protons", Phys. Plasmas **11,** 780 (2004).

[64] S. I. Stoliarov, V. D. Knyazev and I. R. Slagle, "Experimental study of the reaction between vinyl and methyl radicals in the gas phase. Temperature and pressure dependence of overall rate constants and product yields", J. Phys. Chem. A **104,** 9687 (2000).

[65] W. Tsang, "Chemical Kinetic Data Base for Combustion Chemistry. Part 3: Propane", J. Phys. Chem. Ref. Data **17,** 887 (1988).

[66] M. Lucas, Y. Liu, R. Bryant, J. Minor and J. Zhang, "Vacuum ultraviolet photodissociation dynamics of methanol at 121.6 nm", Chem. Phys. Lett. **619,** 18 (2015).

[67] S. Satyapal, J. Park, R. Bersohn and B. Katz, "Dissociation of methanol and ethanol activated by a chemical reaction or by light", J. Chem. Phys. **91,** 6873 (1989).

[68] C. C. Marston, K. Weide, R. Schinke and H. U. Suter, "Product selectivity of vibrationally mediated photofragmentation of methanol", J. Chem. Phys. **98,** 4718 (1993).

[69] S.-H. Lee, H.-I. Lee and Y. T. Lee, "Distributions of angular anisotropy and kinetic energy of products from the photodissociation of methanol at 157 nm", J. Chem. Phys. **121,** 11053 (2004).

[70] A. A. Konnov, "Implementation of the NCN pathway of prompt-NO formation in the detailed reaction mechanism", Combust. Flame **156,** 2093 (2009).

Table 1. Species included in the reaction mechanism.

e, Ar, Ar($1s_1$), Ar($1s_2$), Ar($1s_3$), Ar($1s_4$), Ar(4P), Ar(4D), Ar^+, Ar_2^*, Ar_2^+, ArH^+
H, H^*, H^+, H^-, H_2, H_2(r), H_2(v), H_2^*, H_2^+, H_3^+
H_2O, H_2O(v), H_2O^+, H_3O^+, OH, OH^*, OH^+, OH^-, HO_2, H_2O_2, $H_2O^+(H_2O)^a$, $O_2^+(H_2O)^a$, $H_3O^+(H_2O)^a$, $O_2^-(H_2O)^a$, $O_2^-(H_2O)_2^a$, $O^-(H_2O)^a$, $OH^-(H_2O)^a$, $OH^-(H_2O)_2^a$
O_2, O_2(v), O_2(r)[a], $O_2(^1\Delta)$, $O_2(^1\Sigma)^a$, O_2^+, O_2^-, O_4^{+a}, O, O(^{1}D), O^+, O^-, O_3^a, O_3^{*a}, O_3^{-a}
CH_4, CH_4(v), CH_4^+, CH_5^+, CH_3, CH_3(v), CH_3^+, CH_2, CH_2(v), CH_2^+, CH_2^-, CH, CH^+, C, C^+
C_2H_6, C_2H_6(v), $C_2H_6^+$, C_2H_5, $C_2H_5^+$, C_2H_4, $C_2H_4^+$, C_2H_3, $C_2H_3^+$, C_2H_2, $C_2H_2^+$, $C_2H_2^-$, C_2H, C_2H^+, C_2, C_2^+
C_3H_8, C_3H_7N (n-Propyl radical), C_3H_7I (iso-Propyl radical), C_3H_6, C_3H_5, C_3H_4, C_3H_3, C_3H_2
CHO, CHO^+, CH_2O, CH_2O^+, CH_3O, CH_3O^+, CH_2OH, CH_2OH^+, CH_3OH, CH_3OH^+, $CH_3OH_2^+$

[a] Species only included in *GlobalKin*.

Table 2. Dominant reactions.

	Reaction	References
1.	$e + CH_4 \rightarrow CH_3 + H + e$	[55,56]
2.	$Ar^* + CH_4 \rightarrow CH_3 + H + Ar$ Ar^* = Ar($1s_1$), Ar($1s_2$), Ar($1s_3$), and Ar($1s_4$)	[57]
3.	$CH_2 + CH_4 \rightarrow CH_3 + CH_3$	[49]
4.	$e + C_2H_6 \rightarrow CH_3 + CH_3 + e$	[58]
5.	$CH_4^+ + CH_4 \rightarrow CH_5^+ + CH_3$	[a]
6.	$CH + CH_4 \rightarrow CH_2 + CH_3$	[49]
7.	$e + CH_5^+ \rightarrow CH_3 + H + H$	[59]
8.	$CH_3/CH_3(v) + CH_3 \rightarrow C_2H_6$	[49]
9.	$CH_3 + C_2H_5 \rightarrow C_3H_8$	[49]
10.	$CH_3 + OH \rightarrow CH_3OH$	[49]
11.	$Ar^* + CH_4 \rightarrow CH_2 + H + H + Ar$ Ar^* = Ar($1s_1$), Ar($1s_2$), Ar($1s_3$), and Ar($1s_4$)	[57]
12.	$e + CH_4 \rightarrow CH_2 + H_2 + e$	[55,56]
13.	$e + C_2H_4 \rightarrow CH_2 + CH_2 + e$	[58]
14.	$CH_2 + CH_4 \rightarrow C_2H_5 + H$	[49]
15.	$C_2H_4 + H \rightarrow C_2H_5$	[49]
16.	$C_2H_5 + H \rightarrow C_2H_4 + H_2$	[49]
17.	$H + H + M \rightarrow H_2 + M$, M = Ar, CH_4	[a]
18.	$e + H_2O \rightarrow OH + H + e$	[60]
19.	$e + H_2O \rightarrow OH + H^-$	[60]
20.	$Ar^* + H_2O \rightarrow OH + H + Ar$ Ar^* = Ar($1s_1$), Ar($1s_2$), Ar($1s_3$), Ar($1s_4$), Ar(4P), and Ar(4D)	[61,62]
21.	$H + OH + M \rightarrow H_2O + M$, M = Ar, CH_4	[a]

22.	$CH_4/CH_4(v) + OH \rightarrow H_2O + CH_3$	[49]
23.	$e + CH_4 \rightarrow CH + H_2 + H + e$	[55,56]
24.	$e + C_2H_5^+ \rightarrow C_2H_2 + H_2 + H$	[59,63]
25.	$e + C_2H_5^+ \rightarrow C_2H_2 + H + H + H$	[59,63]
26.	$C_2H_3 + H \rightarrow C_2H_2 + H_2$	[49]
27.	$C_2H_2 + H \rightarrow C_2H_3$	[49]
28.	$CH_3 + C_2H_3 \rightarrow C_3H_6$	[64]
29.	$C_3H_7I + CH_3 \rightarrow CH_4 + C_3H_6$	[65]
30.	$C_3H_5 + H \rightarrow C_3H_6$	[49]
31.	$CH_3O + H \rightarrow CH_2O + H_2$	[b]
32.	$CH_2 + H_2 \rightarrow CH_3 + H$	[49], At low CH_4 percentages
33.	$CH + H_2 \rightarrow CH_3$	[49], At low CH_4 percentages
34.	$e + CH_3OH \rightarrow CH_3 + OH + e$	[66–69][c], At low CH_4 percentages
35.	$CH_2 + C_2H_6 \rightarrow CH_3 + C_2H_5$	[50], At low CH_4 percentages

[a]Estimated by analogy to Ref. [70].

[b]NIST Chemical Kinetics Database https://kinetics.nist.gov/kinetics/.

[c]Estimated by analogy to CH_4.

Table 3. Properties for different number of droplets

Number of Droplets	Individual Droplet Radius (μm)	Total Surface Area (10^{-3} cm^2)	Diffusion Length (μm)
1	50	0.314	63.7
5	29.2	0.537	117
20	18.4	0.853	73.9
50	13.6	1.16	54.4
100	10.8	1.46	43.2
200	8.55	1.84	34.3
500	6.30	2.49	25.3
1000	5.00	3.14	20.1

TOC Graphic

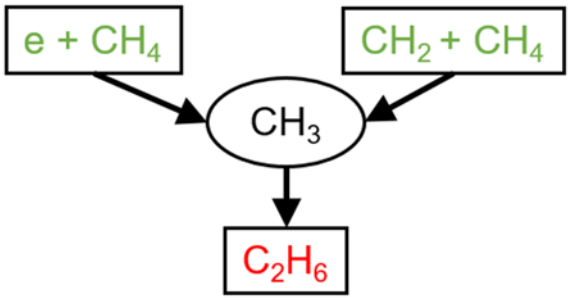

Supporting Information for "CH_3 Radical Generation in Microplasmas for Up-Conversion of Methane"

Mackenzie Meyer[1], Sanjana Kerketta[1], Ryan Hartman[2], Mark J. Kushner[1,3]

[1] University of Michigan, Electrical Engineering and Computer Science Department, 1301 Beal Ave., Ann Arbor, MI 48109-2122 USA maemeyer@umich.edu, kerketta@umich.edu, mjkush@umich.edu

[2] New York University, Department of Chemical and Biomolecular Engineering, New York, NY, 11201 USA ryan.hartman@nyu.edu

[3] Author to whom correspondence should be addressed.

The Supporting Information contains the reactions involving carbon-containing species, the corresponding rate coefficients, and the sources for those rates.

The rate coefficients are specified in cm^3/s unless otherwise noted. Some reaction rates are calculated based on the cross-section for the reaction. In those cases, the rate is specified as σ.

Vibrational states $CH_4(v)$, $CH_3(v)$, $CH_2(v)$, and $C_2H_6(v)$ were included in the model. Reactions for the ground state were duplicated for the vibrational states. In this case, the activation energy was reduced by the vibrational energy.

Table S1. Electron-impact reactions.

Reaction	Rate (cm^3/s)	References
CH_4		
$e + CH_4 \rightarrow CH_4 + e$	σ	[1]
$e + CH_4 \rightarrow CH_4(v) + e$	σ	[2–5]
$e + CH_4 \rightarrow CH_4(v) + e$	σ	[2–5]
$e + CH_4 \rightarrow CH_3 + H + e$	σ	[6,7]
$e + CH_4 \rightarrow CH_2 + H_2 + e$	σ	[6,7]
$e + CH_4 \rightarrow CH + H_2 + H + e$	σ	[6,7]
$e + CH_4 \rightarrow CH_4^+ + e + e$	σ	[6]
$e + CH_4 \rightarrow CH_3^+ + H + e + e$	σ	[6]
$e + CH_4 \rightarrow CH_2^+ + H_2 + e + e$	σ	[6]
$e + CH_4 \rightarrow CH^+ + H_2 + H + e + e$	σ	[6]
$e + CH_4 \rightarrow H^+ + CH_3 + e + e$	σ	[6]
$e + CH_4 \rightarrow CH_3 + H^-$	σ	[8,9]
$e + CH_4 \rightarrow CH_2^- + H_2$	σ	[8,9]
$CH_4(v)$		
$e + CH_4(v) \rightarrow CH_4(v) + e$	σ	[a]
$e + CH_4(v) \rightarrow CH_4 + e$	σ	[a,b]
$e + CH_4(v) \rightarrow CH_4 + e$	σ	[a,b]
$e + CH_4(v) \rightarrow CH_3 + H + e$	σ	[a]
$e + CH_4(v) \rightarrow CH_2 + H_2 + e$	σ	[a]
$e + CH_4(v) \rightarrow CH + H_2 + H + e$	σ	[a]
$e + CH_4(v) \rightarrow CH_4^+ + e + e$	σ	[a]
$e + CH_4(v) \rightarrow CH_3^+ + H + e + e$	σ	[a]
$e + CH_4(v) \rightarrow CH_2^+ + H_2 + e + e$	σ	[a]
$e + CH_4(v) \rightarrow CH^+ + H_2 + H + e + e$	σ	[a]
$e + CH_4(v) \rightarrow H^+ + CH_3 + e + e$	σ	[a]
$e + CH_4(v) \rightarrow CH_3 + H^-$	σ	[a]
$e + CH_4(v) \rightarrow CH_2^- + H_2$	σ	[a]
CH_3		
$e + CH_3 \rightarrow CH_3 + e$	σ	[c]
$e + CH_3 \rightarrow CH_3(v) + e$	σ	[c]
$e + CH_3 \rightarrow CH_3(v) + e$	σ	[c]
$e + CH_3 \rightarrow CH_2 + H + e$	σ	[10]
$e + CH_3 \rightarrow CH + H_2 + e$	σ	[10]
$e + CH_3 \rightarrow C + H_2 + H + e$	σ	[10]
$e + CH_3 \rightarrow CH_3^+ + e + e$	σ	[10]
$e + CH_3 \rightarrow CH_2^+ + H + e + e$	σ	[10]

$e + CH_3 \rightarrow CH^+ + H_2 + e + e$	σ	[10]
$e + CH_3 \rightarrow C^+ + H_2 + H + e + e$	σ	[10]
$e + CH_3 \rightarrow H_2^+ + CH + e + e$	σ	[10]
$e + CH_3 \rightarrow H^+ + CH_2 + e + e$	σ	[10]
$CH_3(v)$		
$e + CH_3(v) \rightarrow CH_3(v) + e$	σ	[a]
$e + CH_3(v) \rightarrow CH_3 + e$	σ	[a,b]
$e + CH_3(v) \rightarrow CH_3 + e$	σ	[a,b]
$e + CH_3(v) \rightarrow CH_2 + H + e$	σ	[a]
$e + CH_3(v) \rightarrow CH + H_2 + e$	σ	[a]
$e + CH_3(v) \rightarrow C + H_2 + H + e$	σ	[a]
$e + CH_3(v) \rightarrow CH_3^+ + e + e$	σ	[a]
$e + CH_3(v) \rightarrow CH_2^+ + H + e + e$	σ	[a]
$e + CH_3(v) \rightarrow CH^+ + H_2 + e + e$	σ	[a]
$e + CH_3(v) \rightarrow C^+ + H_2 + H + e + e$	σ	[a]
$e + CH_3(v) \rightarrow H_2^+ + CH + e + e$	σ	[a]
$e + CH_3(v) \rightarrow H^+ + CH_2 + e + e$	σ	[a]
CH_2		
$e + CH_2 \rightarrow CH_2 + e$	σ	[c]
$e + CH_2 \rightarrow CH_2(v) + e$	σ	[c]
$e + CH_2 \rightarrow CH_2(v) + e$	σ	[c]
$e + CH_2 \rightarrow CH + H + e$	σ	[10]
$e + CH_2 \rightarrow C + H_2 + e$	σ	[10]
$e + CH_2 \rightarrow C + H + H + e$	σ	[10]
$e + CH_2 \rightarrow CH_2^+ + e + e$	σ	[10]
$e + CH_2 \rightarrow CH^+ + H + e + e$	σ	[10]
$e + CH_2 \rightarrow C^+ + H_2 + e + e$	σ	[10]
$e + CH_2 \rightarrow H_2^+ + C + e + e$	σ	[10]
$e + CH_2 \rightarrow H^+ + CH + e + e$	σ	[10]
C_2H_6		
$e + C_2H_6 \rightarrow C_2H_6 + e$	σ	[11]
$e + C_2H_6 \rightarrow C_2H_6(v) + e$	σ	[11]
$e + C_2H_6 \rightarrow C_2H_6(v) + e$	σ	[11]
$e + C_2H_6 \rightarrow CH_3 + CH_3 + e$	σ	[11]
$e + C_2H_6 \rightarrow CH_3 + CH_3 + e$	σ	[11]
$e + C_2H_6 \rightarrow C_2H_6^+ + e + e$	σ	[11]
$e + C_2H_6 \rightarrow C_2H_5 + H^-$	σ	[11]
$C_2H_6(v)$		
$e + C_2H_6(v) \rightarrow C_2H_6(v) + e$	σ	[11][a]

$e + C_2H_6(v) \rightarrow C_2H_6 + e$	σ	[11][a,b]
$e + C_2H_6(v) \rightarrow CH_3 + CH_3 + e$	σ	[11][a]
$e + C_2H_6(v) \rightarrow CH_3 + CH_3 + e$	σ	[11][a]
$e + C_2H_6(v) \rightarrow C_2H_6^+ + e + e$	σ	[11][a]
$e + C_2H_6(v) \rightarrow C_2H_5 + H^-$	σ	[11][a]
C_2H_4		
$e + C_2H_4 \rightarrow C_2H_4 + e$	σ	[11]
$e + C_2H_4 \rightarrow C_2H_4 + e$	σ	Vibrational excitation, [11]
$e + C_2H_4 \rightarrow C_2H_4 + e$	σ	Vibrational excitation, [11]
$e + C_2H_4 \rightarrow C_2H_4 + e$	σ	Electronic excitation, [11]
$e + C_2H_4 \rightarrow CH_2 + CH_2 + e$	σ	[11]
$e + C_2H_4 \rightarrow CH_2 + CH_2 + e$	σ	[11]
$e + C_2H_4 \rightarrow C_2H_4^+ + e + e$	σ	[11]
C_2H_2		
$e + C_2H_2 \rightarrow C_2H_2 + e$	σ	[12]
$e + C_2H_2 \rightarrow C_2H_2 + e$	σ	Vibrational excitation, [12]
$e + C_2H_2 \rightarrow C_2H_2 + e$	σ	Vibrational excitation, [12]
$e + C_2H_2 \rightarrow C_2H_2 + e$	σ	Vibrational excitation, [12]
$e + C_2H_2 \rightarrow C_2H_2 + e$	σ	Electronic excitation, [12]
$e + C_2H_2 \rightarrow C_2H_2 + e$	σ	Electronic excitation, [12]
$e + C_2H_2 \rightarrow C_2H + H + e$	σ	[12]
$e + C_2H_2 \rightarrow C_2H_2^+ + e + e$	σ	[12]
$e + C_2H_2 \rightarrow C_2H_2^-$	σ	[12]
CH_3OH		
$e + CH_3OH \rightarrow CH_3OH + e$	σ	[c]
$e + CH_3OH \rightarrow CH_3O + H + e$	σ	[13–16][c]
$e + CH_3OH \rightarrow CH_2O + H + H + e$	σ	[13–16][c]
$e + CH_3OH \rightarrow CH_3 + OH + e$	σ	[13–16][c]
$e + CH_3OH \rightarrow CH_3OH^+ + e + e$	σ	[17]
$e + CH_3OH \rightarrow CH_2OH^+ + H + e + e$	σ	[17]
$e + CH_3OH \rightarrow CH_2O^+ + H + H + e + e$	σ	[17]
$e + CH_3OH \rightarrow CHO^+ + H_2 + H + e + e$	σ	[17]
$e + CH_3OH \rightarrow CH_3^+ + OH + e + e$	σ	[17]
$e + CH_3OH \rightarrow CH_2^+ + OH + H + e + e$	σ	[17]
$e + CH_3OH \rightarrow CH^+ + OH + H_2 + e + e$	σ	[17]
$e + CH_3OH \rightarrow C^+ + OH + H + H_2 + e + e$	σ	[17]

[a]Estimated from ground state with threshold shifted by vibrational energy.

[b]Superelastic cross-section calculated by detailed balance.

[c]Estimated by analogy to CH_4.

Table S2. Electron-ion recombination.

Reaction	Rate (cm^3/s)	References
Electron-CH_x^+ recombination		
$e + CH_5^+ \rightarrow CH_4 + H$	$1.84 \times 10^{-8}\ T_e^{-0.3}$	[18]
$e + CH_5^+ \rightarrow CH_3 + H_2$	$1.84 \times 10^{-8}\ T_e^{-0.3}$	[18]
$e + CH_5^+ \rightarrow CH_3 + H + H$	$2.57 \times 10^{-7}\ T_e^{-0.3}$	[18]
$e + CH_5^+ \rightarrow CH_2 + H_2 + H$	$6.61 \times 10^{-8}\ T_e^{-0.3}$	[18]
$e + CH_5^+ \rightarrow CH + H_2 + H_2$	$1.10 \times 10^{-8}\ T_e^{-0.3}$	[18]
$e + CH_4^+ \rightarrow CH_3 + H$	$1.02 \times 10^{-7}\ T_e^{-0.66}$	[19]
$e + CH_4^+ \rightarrow CH_2 + H_2$	$3.41 \times 10^{-8}\ T_e^{-0.66}$	[19]
$e + CH_4^+ \rightarrow CH_2 + H + H$	$2.896 \times 10^{-7}\ T_e^{-0.66}$	[19]
$e + CH_4^+ \rightarrow CH + H_2 + H$	$1.306 \times 10^{-7}\ T_e^{-0.66}$	[19]
$e + CH_4^+ \rightarrow C + H_2 + H_2$	$1.136 \times 10^{-8}\ T_e^{-0.66}$	[19]
$e + CH_3^+ \rightarrow CH_2 + H$	$2.27 \times 10^{-7}\ T_e^{-0.66}$	[20,21]
$e + CH_3^+ \rightarrow CH + H_2$	$7.95 \times 10^{-8}\ T_e^{-0.66}$	[20,21]
$e + CH_3^+ \rightarrow CH + H + H$	$9.09 \times 10^{-7}\ T_e^{-0.66}$	[20,21]
$e + CH_3^+ \rightarrow C + H_2 + H$	$1.70 \times 10^{-7}\ T_e^{-0.66}$	[20,21]
$e + CH_2^+ \rightarrow CH + H$	$1.790 \times 10^{-8}\ T_e^{-0.6}$	[22]
$e + CH_2^+ \rightarrow C + H_2$	$8.572 \times 10^{-9}\ T_e^{-0.6}$	[22]
$e + CH_2^+ \rightarrow C + H + H$	$4.500 \times 10^{-8}\ T_e^{-0.6}$	[22]
$e + CH^+ \rightarrow C + H$	$3.232 \times 10^{-8}\ T_e^{-0.42}$	[18]
$e + C^+ \rightarrow C$	$4 \times 10^{-13}\ T_e^{-0.5}$	[a]
$e + e + C^+ \rightarrow C + e$	$5 \times 10^{-27}\ T_e^{-4.0}$	[23][b]
Electron-$C_2H_x^+$ recombination		
$e + C_2H_6^+ \rightarrow C_2H_5 + H$	$2.22 \times 10^{-7}\ T_e^{-0.5}$	[18,24][c]
$e + C_2H_6^+ \rightarrow C_2H_4 + H + H$	$3.40 \times 10^{-7}\ T_e^{-0.5}$	[18,24][c]
$e + C_2H_6^+ \rightarrow C_2H_4 + H_2$	$5.92 \times 10^{-8}\ T_e^{-0.5}$	[18,24][c]
$e + C_2H_6^+ \rightarrow C_2H_3 + H_2 + H$	$2.22 \times 10^{-8}\ T_e^{-0.5}$	[18,24][c]
$e + C_2H_6^+ \rightarrow CH_4 + CH_2$	$2.96 \times 10^{-8}\ T_e^{-0.5}$	[18,24][c]
$e + C_2H_6^+ \rightarrow CH_3 + CH_3$	$5.92 \times 10^{-8}\ T_e^{-0.5}$	[18,24][c]
$e + C_2H_5^+ \rightarrow C_2H_4 + H$	$8.88 \times 10^{-8}\ T_e^{-0.5}$	[18,24]
$e + C_2H_5^+ \rightarrow C_2H_3 + H + H$	$2.22 \times 10^{-7}\ T_e^{-0.5}$	[18,24]
$e + C_2H_5^+ \rightarrow C_2H_3 + H_2$	$1.48 \times 10^{-8}\ T_e^{-0.5}$	[18,24]
$e + C_2H_5^+ \rightarrow C_2H_2 + H_2 + H$	$1.85 \times 10^{-7}\ T_e^{-0.5}$	[18,24]
$e + C_2H_5^+ \rightarrow C_2H_2 + H + H + H$	$1.04 \times 10^{-7}\ T_e^{-0.5}$	[18,24]
$e + C_2H_5^+ \rightarrow CH_4 + CH$	$1.48 \times 10^{-8}\ T_e^{-0.5}$	[18,24]
$e + C_2H_5^+ \rightarrow CH_3 + CH_2$	$1.11 \times 10^{-7}\ T_e^{-0.5}$	[18,24]
$e + C_2H_4^+ \rightarrow C_2H_4^+ + e$	σ	[a]
$e + C_2H_4^+ \rightarrow C_2H_4$	σ	[21][d]
$e + C_2H_4^+ \rightarrow C_2H_3 + H$	$5.32 \times 10^{-9}\ T_e^{-0.76}$	[18,24]

$e + C_2H_4^+ \rightarrow C_2H_2 + H + H$	$2.20 \times 10^{-8}\ T_e^{-0.76}$	[18,24]
$e + C_2H_4^+ \rightarrow C_2H_2 + H_2$	$2.13 \times 10^{-9}\ T_e^{-0.76}$	[18,24]
$e + C_2H_4^+ \rightarrow C_2H + H + H_2$	$3.55 \times 10^{-9}\ T_e^{-0.76}$	[18,24]
$e + C_2H_4^+ \rightarrow CH_2 + CH_2$	$1.42 \times 10^{-9}\ T_e^{-0.76}$	[18,24]
$e + C_2H_4^+ \rightarrow CH_3 + CH$	$7.09 \times 10^{-10}\ T_e^{-0.76}$	[18,24]
$e + C_2H_3^+ \rightarrow C_2H_2 + H$	$2.10 \times 10^{-8}\ T_e^{-0.5}$	[18,24]
$e + C_2H_3^+ \rightarrow C_2H + H + H$	$4.27 \times 10^{-8}\ T_e^{-0.5}$	[18,24]
$e + C_2H_3^+ \rightarrow C_2H + H_2$	$4.34 \times 10^{-9}\ T_e^{-0.5}$	[18,24]
$e + C_2H_3^+ \rightarrow C_2 + H_2 + H$	$1.74 \times 10^{-9}\ T_e^{-0.5}$	[18,24]
$e + C_2H_3^+ \rightarrow CH_3 + C$	$4.34 \times 10^{-10}\ T_e^{-0.5}$	[18,24]
$e + C_2H_3^+ \rightarrow CH_2 + CH$	$2.17 \times 10^{-9}\ T_e^{-0.5}$	[18,24]
$e + C_2H_2^+ \rightarrow C_2H + H$	$2.17 \times 10^{-8}\ T_e^{-0.5}$	[18,24]
$e + C_2H_2^+ \rightarrow C_2 + H + H$	$1.30 \times 10^{-8}\ T_e^{-0.5}$	[18,24]
$e + C_2H_2^+ \rightarrow C_2 + H_2$	$8.69 \times 10^{-10}\ T_e^{-0.5}$	[18,24]
$e + C_2H_2^+ \rightarrow CH_2 + C$	$2.17 \times 10^{-9}\ T_e^{-0.5}$	[18,24]
$e + C_2H_2^+ \rightarrow CH + CH$	$5.65 \times 10^{-9}\ T_e^{-0.5}$	[18,24]
$e + C_2H^+ \rightarrow C_2 + H$	$2.04 \times 10^{-8}\ T_e^{-0.5}$	[18,24]
$e + C_2H^+ \rightarrow CH + C$	$1.65 \times 10^{-8}\ T_e^{-0.5}$	[18,24]
$e + C_2H^+ \rightarrow C + C + H$	$6.51 \times 10^{-9}\ T_e^{-0.5}$	[18,24]
$e + C_2^+ \rightarrow C + C$	$4.83 \times 10^{-8}\ T_e^{-0.5}$	[18,24]
Electron-oxygenated hydrocarbon recombination		
$e + CH_3OH_2^+ \rightarrow CH_3OH + H$	$2.00 \times 10^{-7}\ T_e^{-0.5}$	[a]
$e + CH_3OH^+ \rightarrow CH_2OH + H$	$0.67 \times 10^{-7}\ T_e^{-0.5}$	[a]
$e + CH_3OH^+ \rightarrow CH_3O + H$	$0.67 \times 10^{-7}\ T_e^{-0.5}$	[a]
$e + CH_3OH^+ \rightarrow CH_3 + OH$	$0.67 \times 10^{-7}\ T_e^{-0.5}$	[a]
$e + CH_2OH^+ \rightarrow CH_2O + H$	$2.00 \times 10^{-7}\ T_e^{-0.5}$	[a]
$e + CH_3O^+ \rightarrow CH_2O + H$	$2.00 \times 10^{-7}\ T_e^{-0.5}$	[a]
$e + CH_2O^+ \rightarrow CHO + H$	$2.00 \times 10^{-7}\ T_e^{-0.5}$	[a]
$e + CHO^+ \rightarrow CHO$	$2.00 \times 10^{-7}\ T_e^{-0.5}$	[a]
$e + e + CH_3OH_2^+ \rightarrow CH_3OH + H + e$	$5.00 \times 10^{-27}\ T_e^{-4.5}\ cm^6/s$	[a]
$e + e + CH_3OH^+ \rightarrow CH_2OH + H + e$	$1.67 \times 10^{-27}\ T_e^{-4.5}\ cm^6/s$	[a]
$e + e + CH_3OH^+ \rightarrow CH_3O + H + e$	$1.67 \times 10^{-27}\ T_e^{-4.5}\ cm^6/s$	[a]
$e + e + CH_3OH^+ \rightarrow CH_3 + OH + e$	$1.67 \times 10^{-27}\ T_e^{-4.5}\ cm^6/s$	[a]
$e + e + CH_2OH^+ \rightarrow CH_2O + H + e$	$5.00 \times 10^{-27}\ T_e^{-4.5}\ cm^6/s$	[a]
$e + e + CH_3O^+ \rightarrow CH_2O + H + e$	$5.00 \times 10^{-27}\ T_e^{-4.5}\ cm^6/s$	[a]
$e + e + CH_2O^+ \rightarrow CHO + H + e$	$5.00 \times 10^{-27}\ T_e^{-4.5}\ cm^6/s$	[a]
$e + e + CHO^+ \rightarrow CHO + e$	$5.00 \times 10^{-27}\ T_e^{-4.5}\ cm^6/s$	[a]

[a]Estimated.

[b]Calculated by detailed balance.

[c]Estimated by analogy to $C_2H_5^+$.

[d]Estimated by analogy to N_2^+.

Table S3. Penning ionization and dissociation.

Reaction	Rate (cm^3/s)	References
CH_x		
$Ar^* + CH_4 \rightarrow CH_4^+ + Ar + e$ Ar^* = Ar(4P), Ar(4D)	$5 \times 10^{-11} (T_{gas}/300)^{0.5}$	[a]
$Ar^* + CH_4 \rightarrow CH_3 + H + Ar$ Ar^* = Ar($1s_1$), Ar($1s_2$), Ar($1s_3$), Ar($1s_4$)	$1.75 \times 10^{-10} (T_{gas}/300)^{0.5}$	[25]
$Ar^* + CH_4 \rightarrow CH_2 + H + H + Ar$ Ar^* = Ar($1s_1$), Ar($1s_2$), Ar($1s_3$), Ar($1s_4$)	$3.25 \times 10^{-10} (T_{gas}/300)^{0.5}$	[25]
$Ar^* + CH_3 \rightarrow CH_3^+ + Ar + e$ Ar^* = Ar($1s_1$), Ar($1s_2$), Ar($1s_3$), Ar($1s_4$), Ar(4P), Ar(4D)	$5 \times 10^{-11} (T_{gas}/300)^{0.5}$	[a]
$Ar^* + CH_2 \rightarrow CH_2^+ + Ar + e$ Ar^* = Ar($1s_1$), Ar($1s_2$), Ar($1s_3$), Ar($1s_4$), Ar(4P), Ar(4D)	$5 \times 10^{-11} (T_{gas}/300)^{0.5}$	[a]
$Ar^* + CH \rightarrow CH^+ + Ar + e$ Ar^* = Ar($1s_1$), Ar($1s_2$), Ar($1s_3$), Ar($1s_4$), Ar(4P), Ar(4D)	$5 \times 10^{-11} (T_{gas}/300)^{0.5}$	[a]
CH_x(v)		
$Ar^* + CH_4(v) \rightarrow CH_4^+ + e + Ar$ Ar^* = Ar(4P), Ar(4D)	$5 \times 10^{-11} (T_{gas}/300)^{0.5}$	[a]
$Ar^* + CH_4(v) \rightarrow CH_3 + H + Ar$ Ar^* = Ar($1s_1$), Ar($1s_2$), Ar($1s_3$), Ar($1s_4$)	$1.75 \times 10^{-10} (T_{gas}/300)^{0.5}$	[25]
$Ar^* + CH_4(v) \rightarrow CH_2 + H + H + Ar$ Ar^* = Ar($1s_1$), Ar($1s_2$), Ar($1s_3$), Ar($1s_4$)	$3.25 \times 10^{-10} (T_{gas}/300)^{0.5}$	[25]
$Ar^* + CH_3(v) \rightarrow CH_3^+ + Ar + e$ Ar^* = Ar($1s_1$), Ar($1s_2$), Ar($1s_3$), Ar($1s_4$), Ar(4P), Ar(4D)	$5 \times 10^{-11} (T_{gas}/300)^{0.5}$	[a]
$Ar^* + CH_2(v) \rightarrow CH_2^+ + Ar + e$ Ar^* = Ar($1s_1$), Ar($1s_2$), Ar($1s_3$), Ar($1s_4$), Ar(4P), Ar(4D)	$5 \times 10^{-11} (T_{gas}/300)^{0.5}$	[a]

[a] Estimated.

Table S4. Charge-exchange reactions with ground state molecules.

Reaction	Rate (cm^3/s)	References
Ar^+		
$Ar^+ + CH_4 \rightarrow CH_4^+ + Ar$	$2.94 \times 10^{-11} (T_{gas}/300)^{0.5}$	[26]
$Ar^+ + CH_4 \rightarrow CH_3^+ + H + Ar$	$8.33 \times 10^{-10} (T_{gas}/300)^{0.5}$	[26]
$Ar^+ + CH_4 \rightarrow CH_2^+ + H_2 + Ar$	$1.18 \times 10^{-10} (T_{gas}/300)^{0.5}$	[26]
$Ar^+ + CH_3 \rightarrow CH_3^+ + Ar$	$1.12 \times 10^{-10} (T_{gas}/300)^{0.5}$	a
$Ar^+ + CH_2 \rightarrow CH_2^+ + Ar$	$7.59 \times 10^{-11} (T_{gas}/300)^{0.5}$	a
$Ar^+ + CH \rightarrow CH^+ + Ar$	$6.23 \times 10^{-11} (T_{gas}/300)^{0.5}$	a
Ar_2^+		
$Ar_2^+ + CH_4 \rightarrow CH_4^+ + Ar + Ar$	$2.94 \times 10^{-11} (T_{gas}/300)^{0.5}$	[26][b]
$Ar_2^+ + CH_4 \rightarrow CH_3^+ + H + Ar + Ar$	$9.51 \times 10^{-10} (T_{gas}/300)^{0.5}$	[26][b]
$Ar_2^+ + CH_3 \rightarrow CH_3^+ + Ar + Ar$	$1.04 \times 10^{-10} (T_{gas}/300)^{0.5}$	a
$Ar_2^+ + CH_2 \rightarrow CH_2^+ + Ar + Ar$	$7.08 \times 10^{-11} (T_{gas}/300)^{0.5}$	a
$Ar_2^+ + CH \rightarrow CH^+ + Ar + Ar$	$5.83 \times 10^{-11} (T_{gas}/300)^{0.5}$	a
H_3^+		
$H_3^+ + CH_4 \rightarrow CH_5^+ + H_2$	$2.4 \times 10^{-9} (T_{gas}/300)^{0.5}$	[27]
$H_3^+ + CH_3 \rightarrow CH_4^+ + H_2$	$2.1 \times 10^{-9} (T_{gas}/300)^{0.5}$	[27]
$H_3^+ + CH_2 \rightarrow CH_3^+ + H_2$	1.7×10^{-9}	[27]
$H_3^+ + CH \rightarrow CH_2^+ + H_2$	$1.2 \times 10^{-9} (T_{gas}/300)^{0.5}$	[27]
$H_3^+ + C \rightarrow CH^+ + H_2$	2×10^{-9}	[27]
$H_3^+ + C_2H_6 \rightarrow C_2H_5^+ + H_2 + H_2$	2.4×10^{-9}	[27]
$H_3^+ + C_2H_5 \rightarrow C_2H_6^+ + H_2$	1.4×10^{-9}	[27]
$H_3^+ + C_2H_4 \rightarrow C_2H_5^+ + H_2$	1.15×10^{-9}	[27]
$H_3^+ + C_2H_4 \rightarrow C_2H_3^+ + H_2 + H_2$	1.15×10^{-9}	[27]
$H_3^+ + C_2H_3 \rightarrow C_2H_4^+ + H_2$	$2 \times 10^{-9} (T_{gas}/300)^{-0.5}$	[27]
$H_3^+ + C_2H \rightarrow C_2H_2^+ + H_2$	1.7×10^{-9}	[27]
$H_3^+ + C_2H_2 \rightarrow C_2H_3^+ + H_2$	3.5×10^{-9}	[27]
$H_3^+ + C_2 \rightarrow C_2H^+ + H_2$	1.8×10^{-9}	[27]
H_2^+		
$H_2^+ + CH_4 \rightarrow CH_5^+ + H$	$1.14 \times 10^{-10} (T_{gas}/300)^{0.5}$	[27]
$H_2^+ + CH_4 \rightarrow CH_4^+ + H_2$	$1.4 \times 10^{-9} (T_{gas}/300)^{0.5}$	[27]
$H_2^+ + CH_4 \rightarrow CH_3^+ + H_2 + H$	2.3×10^{-9}	[27]
$H_2^+ + CH_3 \rightarrow CH_3^+ + H_2$	$2.78 \times 10^{-10} (T_{gas}/300)^{0.5}$	c
$H_2^+ + CH_2 \rightarrow CH_3^+ + H$	10^{-9}	[27]
$H_2^+ + CH_2 \rightarrow CH_2^+ + H_2$	$10^{-9} (T_{gas}/300)^{0.5}$	[27]
$H_2^+ + CH \rightarrow CH_2^+ + H$	$7.1 \times 10^{-10} (T_{gas}/300)^{0.5}$	[27]
$H_2^+ + CH \rightarrow CH^+ + H_2$	$7.1 \times 10^{-10} (T_{gas}/300)^{0.5}$	[27]
$H_2^+ + C \rightarrow CH^+ + H$	2.4×10^{-9}	[27]
$H_2^+ + C_2H_6 \rightarrow C_2H_6^+ + H_2$	2.94×10^{-10}	[27]

$H_2^+ + C_2H_6 \rightarrow C_2H_5^+ + H_2 + H$	1.37×10^{-9}	[27]
$H_2^+ + C_2H_6 \rightarrow C_2H_4^+ + H_2 + H_2$	2.35×10^{-9}	[27]
$H_2^+ + C_2H_4 \rightarrow C_2H_4^+ + H_2$	2.21×10^{-9}	[27]
$H_2^+ + C_2H_4 \rightarrow C_2H_3^+ + H_2 + H$	1.81×10^{-9}	[27]
$H_2^+ + C_2H_4 \rightarrow C_2H_2^+ + H_2 + H_2$	8.82×10^{-10}	[27]
$H_2^+ + C_2H_2 \rightarrow C_2H_3^+ + H$	4.8×10^{-10}	[27]
$H_2^+ + C_2H_2 \rightarrow C_2H_2^+ + H_2$	4.82×10^{-9}	[27]
$H_2^+ + C_2H \rightarrow C_2H_2^+ + H$	10^{-9}	[27]
$H_2^+ + C_2H \rightarrow C_2H^+ + H_2$	10^{-9}	[27]
$H_2^+ + C_2 \rightarrow C_2H^+ + H$	1.1×10^{-9}	[27]
$H_2^+ + C_2 \rightarrow C_2^+ + H_2$	1.1×10^{-9}	[27]
H^+		
$H^+ + CH_4 \rightarrow CH_4^+ + H$	$1.5 \times 10^{-9} (T_{gas}/300)^{0.5}$	[27]
$H^+ + CH_4 \rightarrow CH_3^+ + H_2$	2.3×10^{-9}	[27]
$H^+ + CH_3 \rightarrow CH_3^+ + H$	$3.4 \times 10^{-9} (T_{gas}/300)^{0.5}$	[27]
$H^+ + CH_2 \rightarrow CH_2^+ + H$	$1.4 \times 10^{-9} (T_{gas}/300)^{0.5}$	[27]
$H^+ + CH_2 \rightarrow CH^+ + H_2$	$1.4 \times 10^{-9} (T_{gas}/300)^{0.5}$	[27]
$H^+ + CH \rightarrow CH^+ + H$	$1.9 \times 10^{-9} (T_{gas}/300)^{0.5}$	[27]
$H^+ + C_2H_6 \rightarrow C_2H_4^+ + H_2 + H$	1.4×10^{-9}	[27]
$H^+ + C_2H_6 \rightarrow C_2H_3^+ + H_2 + H_2$	2.8×10^{-9}	[27]
$H^+ + C_2H_5 \rightarrow C_2H_4^+ + H_2$	1.65×10^{-9}	[27]
$H^+ + C_2H_5 \rightarrow C_2H_3^+ + H_2 + H$	3.06×10^{-9}	[27]
$H^+ + C_2H_4 \rightarrow C_2H_4^+ + H$	10^{-9}	[27]
$H^+ + C_2H_4 \rightarrow C_2H_3^+ + H_2$	3×10^{-9}	[27]
$H^+ + C_2H_4 \rightarrow C_2H_2^+ + H_2 + H$	10^{-9}	[27]
$H^+ + C_2H_3 \rightarrow C_2H_3^+ + H$	$2 \times 10^{-9} (T_{gas}/300)^{-0.5}$	[27]
$H^+ + C_2H_3 \rightarrow C_2H_2^+ + H_2$	$2 \times 10^{-9} (T_{gas}/300)^{-0.5}$	[27]
$H^+ + C_2H_2 \rightarrow C_2H_2^+ + H$	5.4×10^{-10}	[27]
$H^+ + C_2H \rightarrow C_2H^+ + H$	1.5×10^{-9}	[27]
$H^+ + C_2H \rightarrow C_2^+ + H_2$	1.5×10^{-9}	[27]
$H^+ + C_2 \rightarrow C_2^+ + H$	3.1×10^{-9}	[27]
O_2^+		
$O_2^+ + CH_3 \rightarrow CH_3^+ + O_2$	$1.15 \times 10^{-10} (T_{gas}/300)^{0.5}$	c
$O_2^+ + CH_2 \rightarrow CH_2^+ + O_2$	$7.83 \times 10^{-11} (T_{gas}/300)^{0.5}$	c
$O_2^+ + CH \rightarrow CH^+ + O_2$	$6.41 \times 10^{-11} (T_{gas}/300)^{0.5}$	c
O^+		
$O^+ + CH_4 \rightarrow CH_4^+ + O$	$8.9 \times 10^{-10} (T_{gas}/300)^{0.5}$	c
$O^+ + CH_4 \rightarrow CH_3^+ + OH$	$1.1 \times 10^{-10} (T_{gas}/300)^{0.5}$	c
$O^+ + CH_3 \rightarrow CH_3^+ + O$	$1.32 \times 10^{-10} (T_{gas}/300)^{0.5}$	c
$O^+ + CH_2 \rightarrow CH_2^+ + O$	$8.95 \times 10^{-11} (T_{gas}/300)^{0.5}$	c
$O^+ + CH \rightarrow CH^+ + O$	$7.28 \times 10^{-11} (T_{gas}/300)^{0.5}$	c
H_2O^+		
$H_2O^+ + CH_4 \rightarrow H_3O^+ + CH_3$	1.40×10^{-9}	[28]

$H_2O^+ + CH_3 \rightarrow CH_3^+ + H_2O$	$1.29 \times 10^{-10} (T_{gas}/300)^{0.5}$	c
$H_2O^+ + CH_2 \rightarrow CH_2^+ + H_2O$	$4.70 \times 10^{-10} (T_{gas}/300)^{0.5}$	[28]
$H_2O^+ + CH \rightarrow CH^+ + H_2O$	$3.40 \times 10^{-10} (T_{gas}/300)^{0.5}$	[28]
OH^+		
$OH^+ + CH_4 \rightarrow CH_5^+ + O$	$1.89 \times 10^{-10} (T_{gas}/300)^{0.5}$	c
$OH^+ + CH_4 \rightarrow H_3O^+ + CH_2$	$1.07 \times 10^{-9} (T_{gas}/300)^{0.5}$	c
$OH^+ + CH_3 \rightarrow CH_3^+ + OH$	$1.31 \times 10^{-10} (T_{gas}/300)^{0.5}$	c
$OH^+ + CH_2 \rightarrow CH_2^+ + OH$	$8.82 \times 10^{-11} (T_{gas}/300)^{0.5}$	c
$OH^+ + CH \rightarrow CH^+ + OH$	$7.19 \times 10^{-11} (T_{gas}/300)^{0.5}$	c
CH_5^+		
$CH_5^+ + Ar^* \rightarrow Ar^+ + CH_4 + H$ $Ar^* = Ar(1s_1)$, $Ar(1s_2)$, $Ar(1s_3)$, $Ar(1s_4)$, Ar(4P), Ar(4D)	$3.31 \times 10^{-10} (T_{gas}/300)^{0.5}$	c
$CH_5^+ + Ar_2^* \rightarrow Ar_2^+ + CH_4 + H$	$6.73 \times 10^{-11} (T_{gas}/300)^{0.5}$	c
$CH_5^+ + H \rightarrow CH_4^+ + H_2$	$1.5 \times 10^{-10} (T_{gas}/300)^{0.5}$	[27]
$CH_5^+ + CH_2 \rightarrow CH_3^+ + CH_4$	9.6×10^{-10}	[27]
$CH_5^+ + CH \rightarrow CH_2^+ + CH_4$	$6.9 \times 10^{-10} (T_{gas}/300)^{0.5}$	[27]
$CH_5^+ + C \rightarrow CH^+ + CH_4$	1.2×10^{-9}	[27]
$CH_5^+ + C_2H_6 \rightarrow C_2H_5^+ + H_2 + CH_4$	2.25×10^{-10}	[27]
$CH_5^+ + C_2H_4 \rightarrow C_2H_5^+ + CH_4$	1.5×10^{-9}	[27]
$CH_5^+ + C_2H_2 \rightarrow C_2H_3^+ + CH_4$	1.6×10^{-9}	[27]
$CH_5^+ + C_2H \rightarrow C_2H_2^+ + CH_4$	9×10^{-10}	[27]
$CH_5^+ + C_2 \rightarrow C_2H^+ + CH_4$	9.5×10^{-10}	[27]
CH_4^+		
$CH_4^+ + Ar^* \rightarrow Ar^+ + CH_4$ $Ar^* = Ar(1s_1)$, $Ar(1s_2)$, $Ar(1s_3)$, $Ar(1s_4)$, Ar(4P), Ar(4D)	$3.38 \times 10^{-10} (T_{gas}/300)^{0.5}$	c
$CH_4^+ + Ar_2^* \rightarrow Ar_2^+ + CH_4$	$6.9 \times 10^{-11} (T_{gas}/300)^{0.5}$	c
$CH_4^+ + H_2 \rightarrow CH_5^+ + H$	$4.89 \times 10^{-11} (T_{gas}/300)^{-0.14} \exp(-4329/T_{gas})$	[27]
$CH_4^+ + H \rightarrow CH_3^+ + H_2$	10^{-11}	c
$CH_4^+ + O_2 \rightarrow O_2^+ + CH_4$	$3.90 \times 10^{-10} (T_{gas}/300)^{0.5}$	[28]
$CH_4^+ + O_2(v) \rightarrow O_2^+ + CH_4$	$8.92 \times 10^{-11} (T_{gas}/300)^{0.5}$	c
$CH_4^+ + O_2(^1\Delta) \rightarrow O_2^+ + CH_4$	$7.06 \times 10^{-11} (T_{gas}/300)^{0.5}$	c
$CH_4^+ + O_2(^1\Sigma) \rightarrow O_2^+ + CH_4$	$8.92 \times 10^{-11} (T_{gas}/300)^{0.5}$	c
$CH_4^+ + O(^1D) \rightarrow O^+ + CH_4$	$7.38 \times 10^{-11} (T_{gas}/300)^{0.5}$	c
$CH_4^+ + CH_4 \rightarrow CH_5^+ + CH_3$	$1.5 \times 10^{-9} (T_{gas}/300)^{0.5}$	c
$CH_4^+ + CH_3 \rightarrow CH_3^+ + CH_4$	$1.32 \times 10^{-10} (T_{gas}/300)^{0.5}$	c
$CH_4^+ + CH_2 \rightarrow CH_2^+ + CH_4$	$8.94 \times 10^{-11} (T_{gas}/300)^{0.5}$	c
$CH_4^+ + CH \rightarrow CH^+ + CH_4$	$7.28 \times 10^{-11} (T_{gas}/300)^{0.5}$	c
$CH_4^+ + C_2H_6 \rightarrow C_2H_4^+ + CH_4 + H_2$	1.91×10^{-9}	[27]
$CH_4^+ + C_2H_4 \rightarrow C_2H_5^+ + CH_3$	4.23×10^{-10}	[27]

$CH_4^+ + C_2H_4 \rightarrow C_2H_4^+ + CH_4$	1.38×10^{-9}	[27]
$CH_4^+ + C_2H_2 \rightarrow C_2H_3^+ + CH_3$	1.23×10^{-9}	[27]
$CH_4^+ + C_2H_2 \rightarrow C_2H_2^+ + CH_4$	1.13×10^{-9}	[27]
CH_3^+		
$CH_3^+ + Ar^* \rightarrow Ar^+ + CH_3$ $Ar^* = Ar(1s_1)$, $Ar(1s_2)$, $Ar(1s_3)$, $Ar(1s_4)$, Ar(4P), Ar(4D)	$3.46 \times 10^{-10} (T_{gas}/300)^{0.5}$	c
$CH_3^+ + Ar_2^* \rightarrow Ar_2^+ + CH_3$	$7.09 \times 10^{-11} (T_{gas}/300)^{0.5}$	c
$CH_3^+ + CH_4 \rightarrow CH_4^+ + CH_3$	1.36×10^{-10}	[27]
$CH_3^+ + CH_4 \rightarrow C_2H_5^+ + H_2$	1.2×10^{-9}	[27]
$CH_3^+ + CH_2 \rightarrow C_2H_3^+ + H_2$	9.9×10^{-10}	[27]
$CH_3^+ + CH \rightarrow C_2H_2^+ + H_2$	$7.1 \times 10^{-10} (T_{gas}/300)^{-0.5}$	[27]
$CH_3^+ + C \rightarrow C_2H^+ + H_2$	1.2×10^{-9}	[27]
$CH_3^+ + C_2H_6 \rightarrow C_2H_5^+ + CH_4$	1.48×10^{-9}	[27]
$CH_3^+ + C_2H_4 \rightarrow C_2H_3^+ + CH_4$	3.5×10^{-10}	[27]
$CH_3^+ + C_2H_3 \rightarrow C_2H_3^+ + CH_3$	$3 \times 10^{-10} (T_{gas}/300)^{-0.5}$	[27]
CH_2^+		
$CH_2^+ + Ar^* \rightarrow Ar^+ + CH_2$ $Ar^* = Ar(1s_1)$, $Ar(1s_2)$, $Ar(1s_3)$, $Ar(1s_4)$, Ar(4P), Ar(4D)	$3.55 \times 10^{-10} (T_{gas}/300)^{0.5}$	c
$CH_2^+ + Ar_2^* \rightarrow Ar_2^+ + CH_2$	$7.3 \times 10^{-11} (T_{gas}/300)^{0.5}$	c
$CH_2^+ + H_2 \rightarrow CH_3^+ + H$	1.6×10^{-9}	[27]
$CH_2^+ + CH_4 \rightarrow CH_3^+ + CH_3$	$1.38 \times 10^{-10} (T_{gas}/300)^{0.5}$	c
$CH_2^+ + CH_4 \rightarrow C_2H_5^+ + H$	3.6×10^{-10}	[27]
$CH_2^+ + CH_4 \rightarrow C_2H_4^+ + H_2$	8.4×10^{-10}	[27]
$CH_2^+ + CH_4 \rightarrow C_2H_3^+ + H_2 + H$	2.31×10^{-10}	[27]
$CH_2^+ + CH_4 \rightarrow C_2H_2^+ + H_2 + H_2$	3.97×10^{-10}	[27]
$CH_2^+ + CH_3 \rightarrow CH_3^+ + CH_2$	$1.37 \times 10^{-10} (T_{gas}/300)^{0.5}$	c
$CH_2^+ + CH_2 \rightarrow CH_2^+ + CH_2$	$10^{-9} (T_{gas}/300)^{0.5}$	c
$CH_2^+ + C \rightarrow C_2H^+ + H$	1.2×10^{-9}	[27]
CH^+		
$CH^+ + Ar^* \rightarrow Ar^+ + CH$ $Ar^* = Ar(1s_1)$, $Ar(1s_2)$, $Ar(1s_3)$, $Ar(1s_4)$, Ar(4P), Ar(4D)	$3.65 \times 10^{-10} (T_{gas}/300)^{0.5}$	c
$CH^+ + Ar_2^* \rightarrow Ar_2^+ + CH$	$7.54 \times 10^{-11} (T_{gas}/300)^{0.5}$	c
$CH^+ + H_2 \rightarrow CH_2^+ + H$	$1.2 \times 10^{-9} (T_{gas}/300)^{0.5}$	c
$CH^+ + H \rightarrow C^+ + H_2$	$7.5 \times 10^{-10} (T_{gas}/300)^{-0.37} \exp(-3500/T_{gas})$	[27]
$CH^+ + CH_4 \rightarrow C_2H_4^+ + H$	6.5×10^{-11}	[27]
$CH^+ + CH_4 \rightarrow C_2H_3^+ + H_2$	1.09×10^{-9}	[27]
$CH^+ + CH_4 \rightarrow C_2H_2^+ + H_2 + H$	1.43×10^{-10}	[27]

$CH^+ + CH_3 \rightarrow CH_3^+ + CH$	$1.4 \times 10^{-10} (T_{gas}/300)^{0.5}$	c
$CH^+ + CH_2 \rightarrow CH_2^+ + CH$	$9.41 \times 10^{-11} (T_{gas}/300)^{0.5}$	c
$CH^+ + CH_2 \rightarrow C_2H^+ + H_2$	10^{-9}	[27]
$CH^+ + CH \rightarrow CH^+ + CH$	$10^{-9} (T_{gas}/300)^{0.5}$	c
$CH^+ + CH \rightarrow C_2^+ + H_2$	$7.4 \times 10^{-10} (T_{gas}/300)^{-0.5}$	[27]
$CH^+ + C \rightarrow C_2^+ + H$	1.2×10^{-9}	[27]
$C_2H_6^+$		
$C_2H_6^+ + H \rightarrow C_2H_5^+ + H_2$	10^{-10}	[27]
$C_2H_6^+ + C_2H_4 \rightarrow C_2H_4^+ + C_2H_6$	1.15×10^{-9}	[27]
$C_2H_6^+ + C_2H_2 \rightarrow C_2H_5^+ + C_2H_3$	2.47×10^{-10}	[27]
$C_2H_5^+$		
$C_2H_5^+ + H \rightarrow C_2H_4^+ + H_2$	10^{-11}	[27]
$C_2H_4^+$		
$C_2H_4^+ + H \rightarrow C_2H_3^+ + H_2$	3×10^{-10}	[27]
$C_2H_4^+ + C_2H_3 \rightarrow C_2H_5^+ + C_2H_2$	$5 \times 10^{-10} (T_{gas}/300)^{-0.5}$	[27]
$C_2H_4^+ + C_2H_3 \rightarrow C_2H_3^+ + C_2H_4$	$5 \times 10^{-10} (T_{gas}/300)^{-0.5}$	[27]
$C_2H_3^+$		
$C_2H_3^+ + H \rightarrow C_2H_2^+ + H_2$	6.8×10^{-11}	[27]
$C_2H_3^+ + C_2H_6 \rightarrow C_2H_5^+ + C_2H_4$	2.91×10^{-10}	[27]
$C_2H_3^+ + C_2H_4 \rightarrow C_2H_5^+ + C_2H_2$	8.9×10^{-10}	[27]
$C_2H_3^+ + C_2H_3 \rightarrow C_2H_5^+ + C_2H$	$5 \times 10^{-10} (T_{gas}/300)^{-0.5}$	[27]
$C_2H_3^+ + C_2H \rightarrow C_2H_2^+ + C_2H_2$	3.3×10^{-10}	[27]
$C_2H_2^+$		
$C_2H_2^+ + H_2 \rightarrow C_2H_3^+ + H$	10^{-11}	[27]
$C_2H_2^+ + CH_4 \rightarrow C_2H_3^+ + CH_3$	4.1×10^{-9}	[27]
$C_2H_2^+ + C_2H_6 \rightarrow C_2H_5^+ + C_2H_3$	1.31×10^{-10}	[27]
$C_2H_2^+ + C_2H_6 \rightarrow C_2H_4^+ + C_2H_4$	2.48×10^{-10}	[27]
$C_2H_2^+ + C_2H_4 \rightarrow C_2H_4^+ + C_2H_2$	4.14×10^{-10}	[27]
$C_2H_2^+ + C_2H_3 \rightarrow C_2H_3^+ + C_2H_2$	$3.3 \times 10^{-10} (T_{gas}/300)^{-0.5}$	[27]
C_2H^+		
$C_2H^+ + H_2 \rightarrow C_2H_2^+ + H$	1.1×10^{-9}	[27]
$C_2H^+ + CH_4 \rightarrow C_2H_2^+ + CH_3$	3.74×10^{-10}	[27]
$C_2H^+ + CH_2 \rightarrow CH_3^+ + C_2$	4.4×10^{-10}	[27]
$C_2H^+ + CH \rightarrow CH_2^+ + C_2$	$3.2 \times 10^{-10} (T_{gas}/300)^{-0.5}$	[27]
C_2^+		
$C_2^+ + H_2 \rightarrow C_2H^+ + H$	1.1×10^{-9}	[27]
$C_2^+ + CH_4 \rightarrow C_2H_2^+ + CH_2$	1.82×10^{-10}	[27]
$C_2^+ + CH_4 \rightarrow C_2H^+ + CH_3$	2.38×10^{-10}	[27]
$C_2^+ + CH_2 \rightarrow CH_2^+ + C_2$	4.5×10^{-10}	[27]
$C_2^+ + CH \rightarrow CH^+ + C_2$	$3.2 \times 10^{-10} (T_{gas}/300)^{-0.5}$	[27]
$C_2^+ + C \rightarrow C^+ + C_2$	1.1×10^{-10}	[27]

[a]Estimated.
[b]Estimated by analogy to Ar^+.
[c]Estimated by analogy to Ref. [29].

Table S5. Charge-exchange reactions with vibrationally excited molecules.

Reaction	Rate (cm^3/s)	References
$CH_4(v)$		
$Ar^+ + CH_4(v) \rightarrow CH_4^+ + Ar$	$2.94 \times 10^{-11} (T_{gas}/300)^{0.5}$	[26]
$Ar^+ + CH_4(v) \rightarrow CH_3^+ + H + Ar$	$8.33 \times 10^{-10} (T_{gas}/300)^{0.5}$	[26]
$Ar^+ + CH_4(v) \rightarrow CH_2^+ + H_2 + Ar$	$1.18 \times 10^{-10} (T_{gas}/300)^{0.5}$	[26]
$Ar_2^+ + CH_4(v) \rightarrow CH_4^+ + Ar + Ar$	$2.94 \times 10^{-11} (T_{gas}/300)^{0.5}$	[26][a]
$Ar_2^+ + CH_4(v) \rightarrow CH_3^+ + H + Ar + Ar$	$9.51 \times 10^{-10} (T_{gas}/300)^{0.5}$	[26][a]
$H_3^+ + CH_4(v) \rightarrow CH_5^+ + H_2$	$2.4 \times 10^{-9} (T_{gas}/300)^{0.5}$	[b]
$H_2^+ + CH_4(v) \rightarrow CH_5^+ + H$	$1.14 \times 10^{-10} (T_{gas}/300)^{0.5}$	[b]
$H_2^+ + CH_4(v) \rightarrow CH_4^+ + H_2$	$1.4 \times 10^{-9} (T_{gas}/300)^{0.5}$	[b]
$H_2^+ + CH_4(v) \rightarrow CH_3^+ + H_2 + H$	2.3×10^{-9}	[b]
$H^+ + CH_4(v) \rightarrow CH_4^+ + H$	$1.5 \times 10^{-9} (T_{gas}/300)^{0.5}$	[b]
$H^+ + CH_4(v) \rightarrow CH_3^+ + H_2$	2.3×10^{-9}	[b]
$O^+ + CH_4(v) \rightarrow CH_4^+ + O$	$8.9 \times 10^{-10} (T_{gas}/300)^{0.5}$	[b]
$O^+ + CH_4(v) \rightarrow CH_3^+ + OH$	$1.1 \times 10^{-10} (T_{gas}/300)^{0.5}$	[b]
$OH^+ + CH_4(v) \rightarrow CH_5^+ + O$	$1.89 \times 10^{-10} (T_{gas}/300)^{0.5}$	[b]
$OH^+ + CH_4(v) \rightarrow H_3O^+ + CH_2$	$1.07 \times 10^{-9} (T_{gas}/300)^{0.5}$	[b]
$H_2O^+ + CH_4(v) \rightarrow H_3O^+ + CH_3$	$1.12 \times 10^{-9} (T_{gas}/300)^{0.5}$	[b]
$CH_4^+ + CH_4(v) \rightarrow CH_5^+ + CH_3$	$1.5 \times 10^{-9} (T_{gas}/300)^{0.5}$	[b]
$CH_4^+ + CH_4(v) \rightarrow CH_4^+ + CH_4$	$10^{-9} (T_{gas}/300)^{0.5}$	[b]
$CH_3^+ + CH_4(v) \rightarrow CH_4^+ + CH_3$	1.36×10^{-10}	[27]
$CH_3^+ + CH_4(v) \rightarrow C_2H_5^+ + H_2$	1.2×10^{-9}	[27]
$CH_2^+ + CH_4(v) \rightarrow CH_3^+ + CH_3$	$1.38 \times 10^{-10} (T_{gas}/300)^{0.5}$	[b]
$CH_2^+ + CH_4(v) \rightarrow C_2H_5^+ + H$	3.6×10^{-10}	[27]
$CH_2^+ + CH_4(v) \rightarrow C_2H_4^+ + H_2$	8.4×10^{-10}	[27]
$CH_2^+ + CH_4(v) \rightarrow C_2H_3^+ + H_2 + H$	2.31×10^{-10}	[27]
$CH_2^+ + CH_4(v) \rightarrow C_2H_2^+ + H_2 + H_2$	3.97×10^{-10}	[27]
$CH^+ + CH_4(v) \rightarrow C_2H_4^+ + H$	6.5×10^{-11}	[27]
$CH^+ + CH_4(v) \rightarrow C_2H_3^+ + H_2$	1.09×10^{-9}	[27]
$CH^+ + CH_4(v) \rightarrow C_2H_2^+ + H_2 + H$	1.43×10^{-10}	[27]
$C_2H_2^+ + CH_4(v) \rightarrow C_2H_3^+ + CH_3$	4.1×10^{-9}	[27]
$C_2H^+ + CH_4(v) \rightarrow C_2H_2^+ + CH_3$	3.74×10^{-10}	[27]
$C_2^+ + CH_4(v) \rightarrow C_2H_2^+ + CH_2$	1.82×10^{-10}	[27]
$C_2^+ + CH_4(v) \rightarrow C_2H^+ + CH_3$	2.38×10^{-10}	[27]
$CH_3(v)$		
$Ar^+ + CH_3(v) \rightarrow CH_3^+ + Ar$	$1.12 \times 10^{-10} (T_{gas}/300)^{0.5}$	[c]
$Ar_2^+ + CH_3(v) \rightarrow CH_3^+ + Ar + Ar$	$1.04 \times 10^{-10} (T_{gas}/300)^{0.5}$	[c]
$H_3^+ + CH_3(v) \rightarrow CH_4^+ + H_2$	$2.1 \times 10^{-9} (T_{gas}/300)^{0.5}$	[b]
$H_2^+ + CH_3(v) \rightarrow CH_3^+ + H_2$	$2.78 \times 10^{-10} (T_{gas}/300)^{0.5}$	[b]
$H^+ + CH_3(v) \rightarrow CH_3^+ + H$	$3.4 \times 10^{-9} (T_{gas}/300)^{0.5}$	[b]

$O_2^+ + CH_3(v) \rightarrow CH_3^+ + O_2$	$1.15 \times 10^{-10} (T_{gas}/300)^{0.5}$	b
$O^+ + CH_3(v) \rightarrow CH_3^+ + O$	$1.32 \times 10^{-10} (T_{gas}/300)^{0.5}$	b
$H_2O^+ + CH_3(v) \rightarrow CH_3^+ + H_2O$	$1.29 \times 10^{-10} (T_{gas}/300)^{0.5}$	b
$CH_4^+ + CH_3(v) \rightarrow CH_3^+ + CH_4$	$1.32 \times 10^{-10} (T_{gas}/300)^{0.5}$	b
$CH_3^+ + CH_3(v) \rightarrow CH_3^+ + CH_3$	$10^{-9} (T_{gas}/300)^{0.5}$	b
$CH_2^+ + CH_3(v) \rightarrow CH_3^+ + CH_2$	$1.37 \times 10^{-10} (T_{gas}/300)^{0.5}$	b
$CH^+ + CH_3(v) \rightarrow CH_3^+ + CH$	$1.4 \times 10^{-10} (T_{gas}/300)^{0.5}$	b
$CH_2(v)$		
$Ar^+ + CH_2(v) \rightarrow CH_2^+ + Ar$	$7.59 \times 10^{-11} (T_{gas}/300)^{0.5}$	c
$Ar_2^+ + CH_2(v) \rightarrow CH_2^+ + Ar + Ar$	$7.08 \times 10^{-11} (T_{gas}/300)^{0.5}$	c
$H_3^+ + CH_2(v) \rightarrow CH_3^+ + H_2$	1.7×10^{-9}	[27]
$H_2^+ + CH_2(v) \rightarrow CH_3^+ + H$	10^{-9}	[27]
$H_2^+ + CH_2(v) \rightarrow CH_2^+ + H_2$	$10^{-9} (T_{gas}/300)^{0.5}$	[27]
$H^+ + CH_2(v) \rightarrow CH_2^+ + H$	$1.4 \times 10^{-9} (T_{gas}/300)^{0.5}$	[27]
$H^+ + CH_2(v) \rightarrow CH^+ + H_2$	$1.4 \times 10^{-9} (T_{gas}/300)^{0.5}$	[27]
$O_2^+ + CH_2(v) \rightarrow CH_2^+ + O_2$	$7.83 \times 10^{-11} (T_{gas}/300)^{0.5}$	b
$O^+ + CH_2(v) \rightarrow CH_2^+ + O$	$8.95 \times 10^{-11} (T_{gas}/300)^{0.5}$	b
$OH^+ + CH_2(v) \rightarrow CH_2^+ + OH$	$8.82 \times 10^{-11} (T_{gas}/300)^{0.5}$	b
$H_2O^+ + CH_2(v) \rightarrow CH_2^+ + H_2O$	$8.71 \times 10^{-11} (T_{gas}/300)^{0.5}$	b
$CH_5^+ + CH_2(v) \rightarrow CH_3^+ + CH_4$	9.6×10^{-10}	[27]
$CH_4^+ + CH_2(v) \rightarrow CH_2^+ + CH_4$	$8.94 \times 10^{-11} (T_{gas}/300)^{0.5}$	b
$CH_3^+ + CH_2(v) \rightarrow C_2H_3^+ + H_2$	9.9×10^{-10}	[27]
$CH_2^+ + CH_2(v) \rightarrow CH_2^+ + CH_2$	$10^{-9} (T_{gas}/300)^{0.5}$	b
$CH^+ + CH_2(v) \rightarrow CH_2^+ + CH$	$9.41 \times 10^{-11} (T_{gas}/300)^{0.5}$	b
$CH^+ + CH_2(v) \rightarrow C_2H^+ + H_2$	10^{-9}	[27]
$C_2H^+ + CH_2(v) \rightarrow CH_3^+ + C_2$	4.4×10^{-10}	[27]
$C_2^+ + CH_2(v) \rightarrow CH_2^+ + C_2$	4.5×10^{-10}	[27]
$C_2H_6(v)$		
$H_3^+ + C_2H_6(v) \rightarrow C_2H_5^+ + H_2 + H_2$	2.4×10^{-9}	[27]
$H_2^+ + C_2H_6(v) \rightarrow C_2H_6^+ + H_2$	2.94×10^{-10}	[27]
$H_2^+ + C_2H_6(v) \rightarrow C_2H_5^+ + H_2 + H$	1.37×10^{-9}	[27]
$H_2^+ + C_2H_6(v) \rightarrow C_2H_4^+ + H_2 + H_2$	2.35×10^{-9}	[27]
$H_2^+ + C_2H_6(v) \rightarrow C_2H_3^+ + H_2 + H_2 + H$	6.86×10^{-10}	[27]
$H_2^+ + C_2H_6(v) \rightarrow C_2H_2^+ + H_2 + H_2 + H_2$	1.96×10^{-10}	[27]
$H^+ + C_2H_6(v) \rightarrow C_2H_4^+ + H_2 + H$	1.4×10^{-9}	[27]
$H^+ + C_2H_6(v) \rightarrow C_2H_3^+ + H_2 + H_2$	2.8×10^{-9}	[27]
$H^+ + C_2H_6(v) \rightarrow C_2H_5^+ + H_2$	1.3×10^{-9}	[27]
$CH_5^+ + C_2H_6(v) \rightarrow C_2H_5^+ + H_2 + CH_4$	2.25×10^{-10}	[27]
$CH_4^+ + C_2H_6(v) \rightarrow C_2H_4^+ + CH_4 + H_2$	1.91×10^{-9}	[27]
$CH_3^+ + C_2H_6(v) \rightarrow C_2H_5^+ + CH_4$	1.48×10^{-9}	[27]
$C_2H_3^+ + C_2H_6(v) \rightarrow C_2H_5^+ + C_2H_4$	2.91×10^{-10}	[27]

$C_2H_2^+ + C_2H_6(v) \rightarrow C_2H_5^+ + C_2H_3$	1.31×10^{-10}	[27]
$C_2H_2^+ + C_2H_6(v) \rightarrow C_2H_4^+ + C_2H_4$	2.48×10^{-10}	[27]

[a]Estimated by analogy to Ar^+.

[b]Estimated by analogy to Ref. [29].

[c]Estimated.

Table S6. Neutral species reactions.

Reaction	Rate (cm^3/s)	References
CH_4		
$CH_4 + H \rightarrow H_2 + CH_3$	$1.59 \times 10^{-12} (T_{gas}/300)^{2.5} \exp(-4825/T_{gas})$	[30]
$CH_4 + OH \rightarrow H_2O + CH_3$	$5.7 \times 10^{-13} (T_{gas}/300)^{2.18} \exp(-1350/T_{gas})$	[30]
CH_3		
$CH_3 + H \rightarrow CH_2 + H_2$	$8.61 \times 10^{-10} (T_{gas}/300)^{-0.56} \exp(-8000/T_{gas})$	[30]
$CH_3 + OH \rightarrow CH_3OH$	$7.95 \times 10^{-11} (T_{gas}/300)^{-0.79}$	[30]
$CH_3 + OH \rightarrow CH_2OH + H$	$1.2 \times 10^{-12} \exp(-2760/T_{gas})$	[30]
$CH_3 + CH_3 \rightarrow C_2H_6$	6×10^{-11}	[30]
CH_2		
$CH_2 + H_2 \rightarrow H + CH_3$	9×10^{-11}	[30]
$CH_2 + H \rightarrow H_2 + CH$	2×10^{-10}	[30]
$CH_2 + CH_4 \rightarrow C_2H_5 + H$	$1.4 \times 10^{-11} \exp(250/T_{gas})$	[30]
$CH_2 + CH_4 \rightarrow CH_3 + CH_3$	$1.4 \times 10^{-11} \exp(250/T_{gas})$	[30]
$CH_2 + CH_3 \rightarrow H + C_2H_4$	1.2×10^{-10}	[30]
$CH_2 + CH_2 \rightarrow C_2H_2 + H_2$	3×10^{-11}	[31]
CH		
$CH + H_2 \rightarrow CH_3$	$2 \times 10^{-11} (T_{gas}/300)^{0.15}$	[30]
$CH + H_2 \rightarrow CH_2 + H$	$2.9 \times 10^{-10} \exp(-1670/T_{gas})$	[30]
$CH + CH_4 \rightarrow C_2H_4 + H$	$5.16 \times 10^{-11} (T_{gas}/300)^{-0.94} \exp(-29/T_{gas})$	[30]
$CH + CH_4 \rightarrow CH_2 + CH_3$	$5.16 \times 10^{-11} (T_{gas}/300)^{-0.94} \exp(-29/T_{gas})$	[30]
C_2H_6		
$C_2H_6 + H \rightarrow H_2 + C_2H_5$	$1.63 \times 10^{-10} \exp(-4640/T_{gas})$	[30]
$C_2H_6 + OH \rightarrow H_2O + C_2H_5$	$1.37 \times 10^{-12} (T_{gas}/300)^{2} \exp(-500/T_{gas})$	[30]
$C_2H_6 \rightarrow CH_3 + CH_3$	$1.82 \times 10^{18} (T_{gas}/300)^{-1.37} \exp(-45900/T_{gas})$	[30]
$C_2H_6 + CH_2 \rightarrow CH_3 + C_2H_5$	1.9×10^{-10}	[31]
C_2H_5		
$C_2H_5 + H \rightarrow H_2 + C_2H_4$	7×10^{-11}	[30]
$C_2H_5 + CH_3 \rightarrow C_3H_8$	6.1×10^{-11}	[30]
$C_2H_5 + CH_3 \rightarrow CH_4 + C_2H_4$	1.5×10^{-12}	[30]
$C_2H_5 + CH_2 \rightarrow C_2H_4 + CH_3$	1.5×10^{-11}	[31]
$C_2H_5 + CH_2 \rightarrow C_3H_6 + H$	1.5×10^{-11}	[31]

$C_2H_5 + C_2H_5 \rightarrow C_2H_4 + C_2H_6$	2.3×10^{-12}	[30]
C_2H_4		
$C_2H_4 + H \rightarrow C_2H_5$	$9.78 \times 10^{-12} (T_{gas}/300)^{1.28} \exp(-650/T_{gas})$	[30]
$C_2H_4 + OH \rightarrow C_2H_3 + H_2O$	$1.69 \times 10^{-13} (T_{gas}/300)^{2.75} \exp(-2100/T_{gas})$	[31]
$C_2H_4 + CH_3 \rightarrow C_3H_7N$	$3.5 \times 10^{-13} \exp(-3700/T_{gas})$	[30]
$C_2H_4 + CH_2 \rightarrow C_3H_5 + H$	$5.3 \times 10^{-12} \exp(-2660/T_{gas})$	[30]
C_2H_3		
$C_2H_3 + H \rightarrow C_2H_4$	1.6×10^{-10}	[30]
$C_2H_3 + H \rightarrow H_2 + C_2H_2$	7×10^{-11}	[30]
$C_2H_3 + OH \rightarrow C_2H_2 + H_2O$	5×10^{-11}	[31]
$C_2H_3 \rightarrow C_2H_2 + H$	$4.02 \times 10^{12} (T_{gas}/300)^{1.62} \exp(-18650/T_{gas})$	[30]
$C_2H_3 + CH_3 \rightarrow C_2H_2 + CH_4$	$1.5 \times 10^{-11} \exp(385/T_{gas})$	[32]
$C_2H_3 + CH_3 \rightarrow C_3H_5 + H$	$1.32 \times 10^{-11} \exp(236/T_{gas})$	[32]
$C_2H_3 + CH_3 \rightarrow C_3H_6$	$1.98 \times 10^{-11} \exp(236/T_{gas})$	[32]
$C_2H_3 + CH_2 \rightarrow C_2H_2 + CH_3$	3×10^{-11}	[31]
$C_2H_3 + C_2H_3 \rightarrow C_2H_4 + C_2H_2$	1.4×10^{-10}	[30]
C_2H_2		
$C_2H_2 + H \rightarrow C_2H_3$	$1.06 \times 10^{-11} (T_{gas}/300)^{1.64} \exp(-1055/T_{gas})$	[30]
$C_2H_2 + H \rightarrow H_2 + C_2H$	$1.93 \times 10^{-10} (T_{gas}/300)^{1.64} \exp(-15250/T_{gas})$	[30]
$C_2H_2 + OH \rightarrow C_2H + H_2O$	$1.04 \times 10^{-13} (T_{gas}/300)^{2.68} \exp(-6060/T_{gas})$	[31]
$C_2H_2 + CH_2 \rightarrow C_3H_3 + H$	$3.3 \times 10^{-10} (T_{gas}/300)^{-0.9}$	[30]
$C_2H_2 + CH \rightarrow C_3H_2 + H$	$3.1 \times 10^{-10} \exp(61/T_{gas})$	[30]
C_2H		
$C_2H + H_2 \rightarrow C_2H_2 + H$	$1.95 \times 10^{-12} (T_{gas}/300)^{2.32} \exp(-444/T_{gas})$	[30]
$C_2H + CH_4 \rightarrow C_2H_2 + CH_3$	$7.67 \times 10^{-12} (T_{gas}/300)^{0.94} \exp(-328/T_{gas})$	[30]
$C_2H + CH_2 \rightarrow C_2H_2 + CH$	3×10^{-11}	[31]
$C_2H + C_2H_6 \rightarrow C_2H_2 + C_2H_5$	$3.33 \times 10^{-11} (T_{gas}/300)^{0.28} \exp(62/T_{gas})$	[30]
C_3H_8		
$C_3H_8 + OH \rightarrow C_3H_7N + H_2O$	$2.23 \times 10^{-15} (T_{gas}/300)^{2.8} \exp(156/T_{gas})$	[33]

$C_3H_8 + OH \rightarrow C_3H_7I + H_2O$	$1.80 \times 10^{-14} (T_{gas}/300)^{2.8} \exp(156/T_{gas})$	[33]
$C_3H_8 + CH_2 \rightarrow C_2H_5 + C_2H_5$	1.6×10^{-10}	[33]
$C_3H_8 + CH_2 \rightarrow C_3H_7I + CH_3$	7.1×10^{-11}	[33]
$C_3H_8 + C_2H_5 \rightarrow C_3H_7N + C_2H_6$	$1.65 \times 10^{-15} (T_{gas}/300)^{3.65} \exp(-4600/T_{gas})$	[33]
$C_3H_8 + C_2H_5 \rightarrow C_3H_7I + C_2H_6$	$9.31 \times 10^{-16} (T_{gas}/300)^{3.46} \exp(-3758/T_{gas})$	[33]
$C_3H_8 + C_2H_3 \rightarrow C_3H_7N + C_2H_4$	$1.49 \times 10^{-13} (T_{gas}/300)^{3.3} \exp(-5285/T_{gas})$	[33]
$C_3H_8 + C_2H_3 \rightarrow C_3H_7I + C_2H_4$	$8.12 \times 10^{-14} (T_{gas}/300)^{3.1} \exp(-4443/T_{gas})$	[33]
$C_3H_8 + C_2H \rightarrow C_2H_2 + C_3H_7N$	6×10^{-12}	[33]
$C_3H_8 + C_2H \rightarrow C_2H_2 + C_3H_7I$	2×10^{-12}	[33]
C_3H_7N		
$C_3H_7N + H \rightarrow CH_3 + C_2H_5$	7.2×10^{-12}	[33]
$C_3H_7N + H \rightarrow C_3H_8$	5.28×10^{-11}	[33]
$C_3H_7N + H \rightarrow C_3H_6 + H_2$	3×10^{-12}	[33]
$C_3H_7N + CH_4 \rightarrow CH_3 + C_3H_8$	$3.63 \times 10^{-16} (T_{gas}/300)^{4.02} \exp(-5473/T_{gas})$	[33]
$C_3H_7N + CH_3 \rightarrow CH_4 + C_3H_6$	$3.06 \times 10^{-12} (T_{gas}/300)^{-0.32}$	[33]
$C_3H_7N + CH_2 \rightarrow C_2H_5 + C_2H_4$	3×10^{-11}	[33]
$C_3H_7N + CH_2 \rightarrow C_3H_6 + CH_3$	3×10^{-12}	[33]
$C_3H_7N + C_2H_6 \rightarrow C_2H_5 + C_3H_8$	$1.22 \times 10^{-15} (T_{gas}/300)^{3.82} \exp(-4550/T_{gas})$	[33]
$C_3H_7N + C_2H_5 \rightarrow C_3H_8 + C_2H_4$	1.9×10^{-12}	[33]
$C_3H_7N + C_2H_5 \rightarrow C_3H_6 + C_2H_6$	2.4×10^{-12}	[33]
$C_3H_7N + C_2H_3 \rightarrow C_3H_8 + C_2H_2$	2×10^{-12}	[33]
$C_3H_7N + C_2H_3 \rightarrow C_3H_6 + C_2H_4$	2×10^{-12}	[33]
$C_3H_7N + C_2H_2 \rightarrow C_3H_5 + C_2H_4$	$1.2 \times 10^{-12} \exp(-4531/T_{gas})$	[33]
$C_3H_7N + C_2H \rightarrow C_2H_2 + C_3H_6$	10^{-11}	[33]
$C_3H_7N + C_2H \rightarrow C_3H_3 + C_2H_5$	2×10^{-11}	[33]
C_3H_7I		
$C_3H_7I + H_2 \rightarrow C_3H_8 + H$	$1.73 \times 10^{-15} (T_{gas}/300)^{3.28} \exp(-4360/T_{gas})$	[30]
$C_3H_7I + OH \rightarrow C_3H_6 + H_2O$	4×10^{-11}	[33]
$C_3H_7I \rightarrow C_3H_6 + H$	$2.01 \times 10^{12} (T_{gas}/300)^{1.76} \exp(-17870/T_{gas})$	[30]
$C_3H_7I + CH_4 \rightarrow CH_3 + C_3H_8$	$9.52 \times 10^{-17} (T_{gas}/300)^{4.4}$	[33]

	$\exp(-5434/T_{gas})$	
$C_3H_7I + CH_3 \rightarrow CH_4 + C_3H_6$	$7.52 \times 10^{-12} (T_{gas}/300)^{-0.68}$	[33]
$C_3H_7I + CH_2 \rightarrow C_3H_6 + CH_3$	5×10^{-11}	[33]
$C_3H_7I + C_2H_6 \rightarrow C_3H_8 + C_2H_5$	$3.55 \times 10^{-16} (T_{gas}/300)^{4.2} \exp(-4386/T_{gas})$	[33]
$C_3H_7I + C_2H_5 \rightarrow C_3H_8 + C_2H_4$	$4.16 \times 10^{-12} (T_{gas}/300)^{-0.35}$	[33]
$C_3H_7I + C_2H_5 \rightarrow C_3H_6 + C_2H_6$	$5.20 \times 10^{-12} (T_{gas}/300)^{-0.35}$	[33]
$C_3H_7I + C_2H \rightarrow C_3H_6 + C_2H_2$	6×10^{-12}	[33]
$C_3H_7I + C_3H_8 \rightarrow C_3H_8 + C_3H_7N$	$3.55 \times 10^{-16} (T_{gas}/300)^{4.2} \exp(-4386/T_{gas})$	[33]
$C_3H_7I + C_3H_7I \rightarrow C_3H_6 + C_3H_8$	4.2×10^{-12}	[30]
C_3H_6		
$C_3H_6 + CH_2 \rightarrow C_3H_5 + CH_3$	8.7×10^{-11}	[34]
$C_3H_6 + C_2H_5 \rightarrow C_2H_4 + C_3H_7N$	$8.72 \times 10^{-15} \exp(-3625/T_{gas})$	[34]
$C_3H_6 + C_2H_5 \rightarrow C_3H_5 + C_2H_6$	$1.73 \times 10^{-15} (T_{gas}/300)^{3.5} \exp(-3340/T_{gas})$	[34]
$C_3H_6 + C_2H_3 \rightarrow C_3H_5 + C_2H_4$	$1.72 \times 10^{-15} (T_{gas}/300)^{3.5} \exp(-2356/T_{gas})$	[34]
$C_3H_6 + C_2H \rightarrow C_3H_5 + C_2H_2$	10^{-11}	[34]
$C_3H_6 + C_3H_7N \rightarrow C_3H_5 + C_3H_8$	$1.73 \times 10^{-15} (T_{gas}/300)^{3.5} \exp(-3340/T_{gas})$	[34]
C_3H_5		
$C_3H_5 + H \rightarrow C_2H_3 + CH_3$	1.48×10^{-10}	[30]
$C_3H_5 + H \rightarrow C_3H_6$	1.4×10^{-10}	[30]
$C_3H_5 + OH \rightarrow H_2O + C_3H_4$	10^{-11}	[30]
$C_3H_5 + H_2 \rightarrow C_3H_6 + H$	$1.59 \times 10^{-13} (T_{gas}/300)^{2.4} \exp(-9550/T_{gas})$	[30]
$C_3H_5 + CH_4 \rightarrow C_3H_6 + CH_3$	$1.74 \times 10^{-14} (T_{gas}/300)^{3.4} \exp(-11670/T_{gas})$	[30]
$C_3H_5 + CH_2 \rightarrow C_2H_3 + C_2H_4$	6.67×10^{-11}	[34]
$C_3H_5 + C_2H_6 \rightarrow C_3H_6 + C_2H_5$	$5.83 \times 10^{-14} (T_{gas}/300)^{3.3} \exp(-9990/T_{gas})$	[30]
$C_3H_5 + C_3H_8 \rightarrow C_3H_6 + C_3H_7N$	$5.83 \times 10^{-14} (T_{gas}/300)^{3.3} \exp(-9990/T_{gas})$	[30]
$C_3H_5 + C_3H_8 \rightarrow C_3H_6 + C_3H_7I$	$1.94 \times 10^{-14} (T_{gas}/300)^{3.3} \exp(-8660/T_{gas})$	[30]
$C_3H_5 + C_3H_7N \rightarrow C_3H_6 + C_3H_6$	$2.4 \times 10^{-12} \exp(66/T_{gas})$	[34]
$C_3H_5 + C_3H_7N \rightarrow C_3H_4 + C_3H_8$	$1.2 \times 10^{-12} \exp(66/T_{gas})$	[34]

$C_3H_5 + C_3H_7I \rightarrow C_3H_6 + C_3H_6$	$5.16 \times 10^{-12} (T_{gas}/300)^{-0.35} \exp(66/T_{gas})$	[34]
$C_3H_5 + C_3H_7I \rightarrow C_3H_4 + C_3H_8$	$1.03 \times 10^{-12} (T_{gas}/300)^{-0.35} \exp(66/T_{gas})$	[34]
$C_3H_5 + C_3H_5 \rightarrow C_3H_6 + C_3H_4$	10^{-13}	[30]
CH_3OH		
$CH_3OH + H \rightarrow CH_3 + H_2O$	$3.3 \times 10^{-10} \exp(-2690/T_{gas})$	a
$CH_3OH + H \rightarrow CH_3O + H_2$	$1.35 \times 10^{-12} (T_{gas}/300)^{1.24} \exp(-2260/T_{gas})$	[30]
$CH_3OH + H \rightarrow CH_2OH + H_2$	$5.38 \times 10^{-12} (T_{gas}/300)^{1.24} \exp(-2260/T_{gas})$	[30]
$CH_3OH + OH \rightarrow H_2O + CH_2OH$	$4.99 \times 10^{-13} (T_{gas}/300)^{1.92} \exp(144/T_{gas})$	[30]
$CH_3OH + OH \rightarrow CH_3O + H_2O$	$8.81 \times 10^{-14} (T_{gas}/300)^{1.92} \exp(144/T_{gas})$	[30]
$CH_3OH + OH \rightarrow CH_2O + H_2O + H$	$1.11 \times 10^{-12} (T_{gas}/300)^{1.44} \exp(-56.5/T_{gas})$	a
$CH_3OH + O \rightarrow CH_3O + OH$	$1.31 \times 10^{-13} (T_{gas}/300)^{2.5} \exp(-1550/T_{gas})$	[35]
$CH_3OH + O \rightarrow CH_2OH + OH$	$8.73 \times 10^{-13} (T_{gas}/300)^{2.5} \exp(-1550/T_{gas})$	[35]
$CH_3OH + O(^1D) \rightarrow CH_3O + OH$	2.66×10^{-10}	a
$CH_3OH + O(^1D) \rightarrow CH_2OH + OH$	2.6×10^{-10}	a
$CH_3OH \rightarrow CH_3 + OH$	$1.9 \times 10^{16} \exp(-46192/T_{gas})\ s^{-1}$	[35]
$CH_3OH + CH_3 \rightarrow CH_4 + CH_3O$	$1.18 \times 10^{-14} (T_{gas}/300)^{3.45} \exp(-4020/T_{gas})$	[30]
$CH_3OH + CH_3 \rightarrow CH_4 + CH_2OH$	$5.80 \times 10^{-15} (T_{gas}/300)^{3.45} \exp(-4020/T_{gas})$	[30]
$CH_3OH + CH_2 \rightarrow CH_3O + CH_3$	$1.15 \times 10^{-15} (T_{gas}/300)^{3.1} \exp(-3490/T_{gas})$	[35]
$CH_3OH + CH_2 \rightarrow CH_2OH + CH_3$	$4.48 \times 10^{-15} (T_{gas}/300)^{3.2} \exp(-3609/T_{gas})$	[35]
$CH_3OH + C_3H_7N \rightarrow C_3H_8 + CH_2OH$	$3.77 \times 10^{-15} (T_{gas}/300)^{3.17} \exp(-4610/T_{gas})$	[33]
$CH_3OH + C_3H_7I \rightarrow C_3H_8 + CH_2OH$	$7.76 \times 10^{-14} (T_{gas}/300)^{3.7} \exp(-5300/T_{gas})$	[33]
CH_2OH		
$CH_2OH + O \rightarrow CH_2O + OH$	7×10^{-11}	a
$CH_2OH + H \rightarrow CH_3 + OH$	1.6×10^{-10}	a
$CH_2OH + H \rightarrow CH_2O + H_2$	10^{-11}	a

$CH_2OH + O_2 \rightarrow CH_2O + HO_2$	9.6×10^{-12}	[a]
$CH_2OH + OH \rightarrow CH_2O + H_2O$	4×10^{-11}	[a]
$CH_2OH + H_2O \rightarrow CH_3OH + OH$	$4.29 \times 10^{-14} (T_{gas}/300)^{3} \exp(-10440/T_{gas})$	[a]
$CH_2OH \rightarrow CH_2O + H$	$4.8 \times 10^{-5} (T_{gas}/300)^{-2.5} \exp(-17200/T_{gas})\ s^{-1}$	[a]
$CH_2OH + CH_2 \rightarrow CH_2O + CH_3$	2.01×10^{-12}	[a]
$CH_2OH + C_3H_7N \rightarrow C_3H_6 + CH_3OH$	8×10^{-13}	[33]
$CH_2OH + C_3H_7I \rightarrow C_3H_6 + CH_3OH$	4.8×10^{-12}	[33]
$CH_2OH + C_3H_6 \rightarrow C_3H_5 + CH_3OH$	$2.03 \times 10^{-15} (T_{gas}/300)^{2.95} \exp(-6033/T_{gas})$	[34]
CH_3O		
$CH_3O + O \rightarrow CH_3 + O_2$	2.5×10^{-11}	[a]
$CH_3O + O \rightarrow CH_2O + OH$	10^{-11}	[a]
$CH_3O + H \rightarrow CH_2O + H_2$	3×10^{-11}	[a]
$CH_3O + O_2 \rightarrow CH_2O + HO_2$	$7.82 \times 10^{-14} \exp(-1150/T_{gas})$	[a]
$CH_3O + CH_2 \rightarrow CH_2O + CH_3$	3.01×10^{-11}	[a]
$CH_3O + CH_3OH \rightarrow CH_3OH + CH_2OH$	$5 \times 10^{-13} \exp(-2050/T_{gas})$	[a]
CH_2O		
$CH_2O + O \rightarrow CHO + OH$	$1.79 \times 10^{-11} (T_{gas}/300)^{0.57} \exp(-1390/T_{gas})$	[a]
$CH_2O + H \rightarrow CHO + H_2$	$8.82 \times 10^{-12} (T_{gas}/300)^{1.77} \exp(-1510/T_{gas})$	[31]
$CH_2O + OH \rightarrow CHO + H_2O$	$4.77 \times 10^{-12} (T_{gas}/300)^{1.18} \exp(225/T_{gas})$	[31]
$CH_2O + CH_3 \rightarrow CHO + CH_4$	$1.68 \times 10^{-16} (T_{gas}/300)^{6.1} \exp(-990/T_{gas})$	[36]
$CH_2O + CH_3O \rightarrow CHO + CH_3OH$	$1.70 \times 10^{-13} \exp(-1500/T_{gas})$	[31]
CHO		
$CHO + H_2 \rightarrow CH_2O + H$	$2.70 \times 10^{-13} (T_{gas}/300)^{2} \exp(-8972/T_{gas})$	[30]
$CHO + CH_2OH \rightarrow CH_2O + CH_2O$	3.01×10^{-10}	[a]

[a]From NIST Chemical Kinetics Database.

Table S7. Reactions with vibrationally excited states.

Reaction	Rate (cm^3/s)	References
$CH_4(v)$		
$CH_4(v) + Ar \rightarrow CH_4 + Ar$	$3.4 \times 10^{-15} (T_{gas}/300)^{0.5}$	[37]
$CH_4(v) + M \rightarrow CH_4 + M$ $M = CH_4, CH_3, CH_2$	$2.1 \times 10^{-14} (T_{gas}/300)^{0.5}$	[38]
$CH_4(v) + M \rightarrow CH_4 + M$ $M = C_2H_6, C_2H_5, C_2H_4, C_2H_3, C_2H_2, C_2H, C_3H_8, C_3H_7N, C_3H_7I, C_3H_6, C_3H_5, C_3H_4, C_3H_3, C_3H_2$	$3.2 \times 10^{-14} (T_{gas}/300)^{0.5}$	[39]
$CH_4(v) + M \rightarrow CH_4 + M$ $M = H_2O, H_2, O_2, O_3$	$10^{-14} (T_{gas}/300)^{0.5}$	[38]
$CH_4(v) + H \rightarrow H_2 + CH_3$	$1.59 \times 10^{-12} (T_{gas}/300)^{2.5} \exp(-2855/T_{gas})$	[30]
$CH_4(v) + OH \rightarrow H_2O + CH_3$	$5.7 \times 10^{-13} (T_{gas}/300)^{2.18}$	[30]
$CH_4(v) + CH \rightarrow CH_2 + CH_3$	$5.16 \times 10^{-11} (T_{gas}/300)^{-0.94}$	[30]
$CH_4(v) + CH \rightarrow C_2H_4 + H$	$5.16 \times 10^{-11} (T_{gas}/300)^{-0.94}$	[30]
$CH_4(v) + C_2H \rightarrow C_2H_2 + CH_3$	$7.67 \times 10^{-12} (T_{gas}/300)^{0.94}$	[30]
$CH_4(v) + C_3H_7N \rightarrow CH_3 + C_3H_8$	$3.63 \times 10^{-16} (T_{gas}/300)^{4.02} \exp(-3503/T_{gas})$	[33]
$CH_4(v) + C_3H_7I \rightarrow CH_3 + C_3H_8$	$9.52 \times 10^{-17} (T_{gas}/300)^{4.4} \exp(-3464/T_{gas})$	[33]
$CH_4(v) + C_3H_5 \rightarrow C_3H_6 + CH_3$	$1.74 \times 10^{-14} (T_{gas}/300)^{3.4} \exp(-9700/T_{gas})$	[30]
$CH_3(v)$		
$CH_3(v) + Ar \rightarrow CH_3 + Ar$	$3.4 \times 10^{-15} (T_{gas}/300)^{0.5}$	[37]
$CH_3(v) + M \rightarrow CH_3 + M$ $M = CH_4, CH_3, CH_2$	$2.1 \times 10^{-14} (T_{gas}/300)^{0.5}$	[38]
$CH_3(v) + M \rightarrow CH_3 + M$ $M = C_2H_6, C_2H_5, C_2H_4, C_2H_3, C_2H_2, C_2H, C_3H_8, C_3H_7N, C_3H_7I, C_3H_6, C_3H_5, C_3H_4, C_3H_3, C_3H_2$	$3.2 \times 10^{-14} (T_{gas}/300)^{0.5}$	[39]
$CH_3(v) + M \rightarrow CH_3 + M$ $M = H_2O, H_2, O_2, O_3$	$10^{-14} (T_{gas}/300)^{0.5}$	[38]
$CH_3(v) + H \rightarrow CH_2 + H_2$	$8.61 \times 10^{-10} (T_{gas}/300)^{-0.56} \exp(-6030/T_{gas})$	[30]
$CH_3(v) + OH \rightarrow CH_3OH$	$7.95 \times 10^{-11} (T_{gas}/300)^{-0.79}$	[30]
$CH_3(v) + OH \rightarrow H + CH_2OH$	$1.2 \times 10^{-12} \exp(-790/T_{gas})$	[30]
$CH_3(v) + CH_3 \rightarrow C_2H_6$	6×10^{-11}	[30]
$CH_3(v) + CH_3(v) \rightarrow C_2H_6$	6×10^{-11}	[30]
$CH_3(v) + C_2H_5 \rightarrow CH_4 + C_2H_4$	1.5×10^{-12}	[30]

$CH_3(v) + C_2H_5 \rightarrow C_3H_8$	6.1×10^{-11}	[30]
$CH_3(v) + C_2H_4 \rightarrow C_3H_7N$	$3.5 \times 10^{-13} \exp(-1730/T_{gas})$	[30]
$CH_3(v) + C_2H_3 \rightarrow C_2H_2 + CH_4$	$1.5 \times 10^{-11} \exp(-385/T_{gas})$	[32]
$CH_3(v) + C_2H_3 \rightarrow C_3H_6$	$1.98 \times 10^{-11} \exp(-236/T_{gas})$	[32]
$CH_3(v) + C_2H_3 \rightarrow C_3H_5 + H$	$1.32 \times 10^{-11} \exp(-236/T_{gas})$	[32]
$CH_3(v) + C_3H_7N \rightarrow CH_4 + C_3H_6$	$3.06 \times 10^{-12} (T_{gas}/300)^{-0.32}$	[33]
$CH_3(v) + C_3H_7I \rightarrow CH_4 + C_3H_6$	$7.52 \times 10^{-12} (T_{gas}/300)^{-0.68}$	[33]
$CH_3(v) + CH_3OH \rightarrow CH_4 + CH_2OH$	$5.8 \times 10^{-15} (T_{gas}/300)^{3.45} \exp(-2050/T_{gas})$	[30]
$CH_3(v) + CH_3OH \rightarrow CH_4 + CH_3O$	$1.18 \times 10^{-14} (T_{gas}/300)^{3.45} \exp(-2050/T_{gas})$	[30]
$CH_3(v) + CH_2O \rightarrow CH_4 + CHO$	$1.68 \times 10^{-16} (T_{gas}/300)^{6.1}$	[36]
$CH_2(v)$		
$CH_2(v) + Ar \rightarrow CH_2 + Ar$	$3.4 \times 10^{-15} (T_{gas}/300)^{0.5}$	[37]
$CH_2(v) + M \rightarrow CH_2 + M$ $M = CH_4, CH_3, CH_2$	$2.1 \times 10^{-14} (T_{gas}/300)^{0.5}$	[38]
$CH_2(v) + M \rightarrow CH_2 + M$ $M = C_2H_6, C_2H_5, C_2H_4, C_2H_3, C_2H_2, C_2H, C_3H_8, C_3H_7N, C_3H_7I, C_3H_6, C_3H_5, C_3H_4, C_3H_3, C_3H_2$	$3.2 \times 10^{-14} (T_{gas}/300)^{0.5}$	[39]
$CH_2(v) + M \rightarrow CH_2 + M$ $M = H_2O, H_2, O_2, O_3$	$10^{-14} (T_{gas}/300)^{0.5}$	[38]
$CH_2(v) + H_2 \rightarrow H + CH_3$	9×10^{-11}	[30]
$CH_2(v) + H \rightarrow H_2 + CH$	2×10^{-10}	[30]
$CH_2(v) + CH_4 \rightarrow CH_3 + CH_3$	$1.4 \times 10^{-11} \exp(250/T_{gas})$	[30]
$CH_2(v) + CH_4 \rightarrow C_2H_5 + H$	$1.4 \times 10^{-11} \exp(250/T_{gas})$	[30]
$CH_2 + CH_4(v) \rightarrow CH_3 + CH_3$	$1.4 \times 10^{-11} \exp(250/T_{gas})$	[30]
$CH_2 + CH_4(v) \rightarrow C_2H_5 + H$	$1.4 \times 10^{-11} \exp(250/T_{gas})$	[30]
$CH_2(v) + CH_4(v) \rightarrow CH_3 + CH_3$	$1.4 \times 10^{-11} \exp(250/T_{gas})$	[30]
$CH_2(v) + CH_4(v) \rightarrow C_2H_5 + H$	$1.4 \times 10^{-11} \exp(250/T_{gas})$	[30]
$CH_2(v) + CH_3 \rightarrow H + C_2H_4$	1.2×10^{-10}	[30]
$CH_2 + CH_3(v) \rightarrow H + C_2H_4$	1.2×10^{-10}	[30]
$CH_2(v) + CH_3(v) \rightarrow H + C_2H_4$	1.2×10^{-10}	[30]
$CH_2(v) + CH_2 \rightarrow C_2H_2 + H_2$	3×10^{-11}	[31]
$CH_2(v) + CH_2(v) \rightarrow C_2H_2 + H_2$	3×10^{-11}	[31]
$CH_2(v) + C_2H_5 \rightarrow C_2H_4 + CH_3$	1.5×10^{-11}	[31]
$CH_2(v) + C_2H_5 \rightarrow C_3H_6 + H$	1.5×10^{-11}	[31]
$CH_2(v) + C_2H_4 \rightarrow C_3H_5 + H$	$5.3 \times 10^{-12} \exp(-1270/T_{gas})$	[30]
$CH_2(v) + C_2H_3 \rightarrow C_2H_2 + CH_3$	3×10^{-11}	[31]
$CH_2(v) + C_2H_2 \rightarrow H + C_3H_3$	$3.3 \times 10^{-10} (T_{gas}/300)^{-0.9}$	[30]

$CH_2(v) + C_2H \rightarrow C_2H_2 + CH$	3×10^{-11}	[31]
$CH_2(v) + C_3H_8 \rightarrow C_2H_5 + C_2H_5$	1.6×10^{-10}	[33]
$CH_2(v) + C_3H_8 \rightarrow C_3H_7I + CH_3$	7.1×10^{-11}	[33]
$CH_2(v) + C_3H_7N \rightarrow C_2H_5 + C_2H_4$	3×10^{-11}	[33]
$CH_2(v) + C_3H_7N \rightarrow C_3H_6 + CH_3$	3×10^{-12}	[33]
$CH_2(v) + C_3H_7I \rightarrow C_3H_6 + CH_3$	5×10^{-11}	[33]
$CH_2(v) + C_3H_6 \rightarrow C_3H_5 + CH_3$	8.7×10^{-11}	[34]
$CH_2(v) + C_3H_5 \rightarrow C_2H_3 + C_2H_4$	6.67×10^{-11}	[34]
$CH_2(v) + CH_3OH \rightarrow CH_3 + CH_2OH$	$4.48 \times 10^{-15} (T_{gas}/300)^{3.2} \exp(-2219/T_{gas})$	[35]
$CH_2(v) + CH_3OH \rightarrow CH_3 + CH_3O$	$1.15 \times 10^{-15} (T_{gas}/300)^{3.1} \exp(-2100/T_{gas})$	[35]
$CH_2(v) + CH_2OH \rightarrow CH_3 + CH_2O$	2.01×10^{-12}	[a]
$CH_2(v) + CH_3O \rightarrow CH_3 + CH_2O$	3.01×10^{-11}	[a]
$C_2H_6(v)$		
$C_2H_6(v) + Ar \rightarrow C_2H_6 + Ar$	$3.4 \times 10^{-15} (T_{gas}/300)^{0.5}$	[37]
$C_2H_6(v) + M \rightarrow C_2H_6 + M$ $M = CH_4, CH_3, CH_2$	$2.1 \times 10^{-14} (T_{gas}/300)^{0.5}$	[38]
$C_2H_6(v) + M \rightarrow C_2H_6 + M$ $M = C_2H_5, C_2H_4, C_2H_3, C_2H_2, C_2H, C_3H_8, C_3H_7N, C_3H_7I, C_3H_6, C_3H_5, C_3H_4, C_3H_3, C_3H_2$	$3.2 \times 10^{-14} (T_{gas}/300)^{0.5}$	[39]
$C_2H_6(v) + M \rightarrow C_2H_6 + M$ $M = H_2O, H_2, O_2, O_3$	$10^{-14} (T_{gas}/300)^{0.5}$	[38]
$C_2H_6(v) + H \rightarrow H_2 + C_2H_5$	$1.63 \times 10^{-10} \exp(-2795/T_{gas})$	[30]
$C_2H_6(v) + OH \rightarrow H_2O + C_2H_5$	$1.37 \times 10^{-12} (T_{gas}/300)^{2}$	[30]
$C_2H_6(v) \rightarrow CH_3 + CH_3$	$1.82 \times 10^{18} (T_{gas}/300)^{-1.37} \exp(-44055/T_{gas})$	[30]
$C_2H_6 + CH_2(v) \rightarrow CH_3 + C_2H_5$	1.9×10^{-10}	[31]
$C_2H_6(v) + CH_2 \rightarrow CH_3 + C_2H_5$	1.9×10^{-10}	[31]
$C_2H_6(v) + CH_2(v) \rightarrow CH_3 + C_2H_5$	1.9×10^{-10}	[31]
$C_2H_6(v) + C_2H \rightarrow C_2H_2 + C_2H_5$	$3.33 \times 10^{-11} (T_{gas}/300)^{0.28} \exp(62/T_{gas})$	[30]
$C_2H_6(v) + C_3H_7N \rightarrow C_2H_5 + C_3H_8$	$1.22 \times 10^{-15} (T_{gas}/300)^{3.82} \exp(-2705/T_{gas})$	[33]
$C_2H_6(v) + C_3H_7I \rightarrow C_2H_5 + C_3H_8$	$3.55 \times 10^{-16} (T_{gas}/300)^{4.2} \exp(-2541/T_{gas})$	[33]
$C_2H_6(v) + C_3H_5 \rightarrow C_3H_6 + C_2H_5$	$5.83 \times 10^{-14} (T_{gas}/300)^{3.3} \exp(-8145/T_{gas})$	[30]

[a]From NIST Chemical Kinetics Database.

Table S8. Ion-ion recombination.

Reaction	Rate (cm^3/s)	References
CH_x^+		
$CH_x^+ + CH_2^- \rightarrow CH_{x-1} + H + CH_2$ x = 5, 4, 3, 2, 1	$2 \times 10^{-7} (T_{gas}/300)^{-0.5}$	a
$CH_x^+ + C_2H_2^- \rightarrow CH_{x-1} + H + C_2H_2$ x = 5, 4, 3, 2, 1	$2 \times 10^{-7} (T_{gas}/300)^{-0.5}$	a
$CH_x^+ + H^- \rightarrow CH_{x-1} + H + H$ x = 5, 4, 3, 2, 1	$2 \times 10^{-7} (T_{gas}/300)^{-0.5}$	a
$CH_x^+ + O_3^- \rightarrow CH_{x-1} + H + O_3$ x = 5, 4, 3, 2, 1	$2 \times 10^{-7} (T_{gas}/300)^{-0.5}$	a
$CH_x^+ + O_2^- \rightarrow CH_{x-1} + H + O_2$ x = 5, 4, 3, 2, 1	$2 \times 10^{-7} (T_{gas}/300)^{-0.5}$	a
$CH_x^+ + O^- \rightarrow CH_{x-1} + H + O$ x = 5, 4, 3, 2, 1	$2 \times 10^{-7} (T_{gas}/300)^{-0.5}$	a
$CH_x^+ + OH^- \rightarrow CH_{x-1} + H + OH$ x = 5, 4, 3, 2, 1	$2 \times 10^{-7} (T_{gas}/300)^{-0.5}$	a
$CH_x^+ + O_2^-(H_2O) \rightarrow CH_{x-1} + H + O_2 + H_2O$ x = 5, 4, 3, 2, 1	$2 \times 10^{-7} (T_{gas}/300)^{-0.5}$	a
$CH_x^+ + O^-(H_2O) \rightarrow CH_{x-1} + H + O + H_2O$ x = 5, 4, 3, 2, 1	$2 \times 10^{-7} (T_{gas}/300)^{-0.5}$	a
$CH_x^+ + OH^-(H_2O) \rightarrow CH_{x-1} + H + OH + H_2O$ x = 5, 4, 3, 2, 1	$2 \times 10^{-7} (T_{gas}/300)^{-0.5}$	a
$CH_x^+ + O_2^-(H_2O)_2 \rightarrow CH_{x-1} + H + O_2 + H_2O + H_2O$ x = 5, 4, 3, 2, 1	$2 \times 10^{-7} (T_{gas}/300)^{-0.5}$	a
$CH_x^+ + OH^-(H_2O)_2 \rightarrow CH_{x-1} + H + OH + H_2O + H_2O$ x = 5, 4, 3, 2, 1	$2 \times 10^{-7} (T_{gas}/300)^{-0.5}$	a
C^+		
$C^+ + M^- \rightarrow C + M$ M = H, OH, O, O_2, O_3, CH_2, C_2H_2	$2 \times 10^{-7} (T_{gas}/300)^{-0.5}$	a
$C^+ + M^-(H_2O) \rightarrow C + M + H_2O$ M = O_2, O, OH	$2 \times 10^{-7} (T_{gas}/300)^{-0.5}$	a
$C^+ + M^-(H_2O)_2 \rightarrow C + M + H_2O + H_2O$ M = O_2, OH	$2 \times 10^{-7} (T_{gas}/300)^{-0.5}$	a
$C_2H_6^+$		
$C_2H_6^+ + M^- \rightarrow C_2H_5 + H + M$ M = H, OH, O, O_2, O_3, CH_2, C_2H_2	$10^{-7} (T_{gas}/300)^{-0.5}$	a
$C_2H_6^+ + M^- \rightarrow C_2H_4 + H + H + M$ M = H, OH, O, O_2, O_3, CH_2, C_2H_2	$10^{-7} (T_{gas}/300)^{-0.5}$	a
$C_2H_6^+ + M^-(H_2O) \rightarrow C_2H_5 + H + M + H_2O$	$10^{-7} (T_{gas}/300)^{-0.5}$	a

M = O_2, O, OH		
$C_2H_6^+ + M^-(H_2O) \rightarrow C_2H_4 + H + H + M + H_2O$ M = O_2, O, OH	$10^{-7} (T_{gas}/300)^{-0.5}$	[a]
$C_2H_6^+ + M^-(H_2O)_2 \rightarrow C_2H_5 + H + M + H_2O + H_2O$ M = O_2, OH	$10^{-7} (T_{gas}/300)^{-0.5}$	[a]
$C_2H_6^+ + M^-(H_2O)_2 \rightarrow C_2H_4 + H + H + M + H_2O + H_2O$ M = O_2, OH	$10^{-7} (T_{gas}/300)^{-0.5}$	[a]
$C_2H_5^+$		
$C_2H_5^+ + M^- \rightarrow CH_3 + CH_2 + M$ M = H, OH, O, O_2, O_3, CH_2, C_2H_2	$3 \times 10^{-8} (T_{gas}/300)^{-0.5}$	[a]
$C_2H_5^+ + M^- \rightarrow C_2H_3 + H + H + M$ M = H, OH, O, O_2, O_3, CH_2, C_2H_2	$1.7 \times 10^{-7} (T_{gas}/300)^{-0.5}$	[a]
$C_2H_5^+ + M^-(H_2O) \rightarrow CH_3 + CH_2 + M + H_2O$ M = O_2, O, OH	$3 \times 10^{-8} (T_{gas}/300)^{-0.5}$	[a]
$C_2H_5^+ + M^-(H_2O) \rightarrow C_2H_3 + H + H + M + H_2O$ M = O_2, O, OH	$1.7 \times 10^{-7} (T_{gas}/300)^{-0.5}$	[a]
$C_2H_5^+ + M^-(H_2O)_2 \rightarrow CH_3 + CH_2 + M + H_2O + H_2O$ M = O_2, OH	$3 \times 10^{-8} (T_{gas}/300)^{-0.5}$	[a]
$C_2H_5^+ + M^-(H_2O)_2 \rightarrow C_2H_3 + H + H + M + H_2O + H_2O$ M = O_2, OH	$1.7 \times 10^{-7} (T_{gas}/300)^{-0.5}$	[a]
$C_2H_4^+$		
$C_2H_4^+ + M^- \rightarrow C_2H_2 + H + H + M$ M = H, OH, O, O_2, O_3, CH_2, C_2H_2	$2 \times 10^{-7} (T_{gas}/300)^{-0.5}$	[a]
$C_2H_4^+ + M^-(H_2O) \rightarrow C_2H_2 + H + H + M + H_2O$ M = O_2, O, OH	$2 \times 10^{-7} (T_{gas}/300)^{-0.5}$	[a]
$C_2H_4^+ + M^-(H_2O)_2 \rightarrow C_2H_2 + H + H + M + H_2O + H_2O$ M = O_2, OH	$2 \times 10^{-7} (T_{gas}/300)^{-0.5}$	[a]
$C_2H_3^+$		
$C_2H_3^+ + M^- \rightarrow C_2H_2 + H + M$ M = H, OH, O, O_2, O_3, CH_2, C_2H_2	$2 \times 10^{-7} (T_{gas}/300)^{-0.5}$	[a]
$C_2H_3^+ + M^-(H_2O) \rightarrow C_2H_2 + H + M + H_2O$ M = O_2, O, OH	$2 \times 10^{-7} (T_{gas}/300)^{-0.5}$	[a]
$C_2H_3^+ + M^-(H_2O)_2 \rightarrow C_2H_2 + H + M + H_2O + H_2O$ M = O_2, OH	$2 \times 10^{-7} (T_{gas}/300)^{-0.5}$	[a]
$C_2H_2^+$		
$C_2H_2^+ + M^- \rightarrow CH + CH + M$ M = H, OH, O, O_2, O_3, CH_2, C_2H_2	$2 \times 10^{-7} (T_{gas}/300)^{-0.5}$	[a]
$C_2H_2^+ + M^-(H_2O) \rightarrow CH + CH + M + H_2O$ M = O_2, O, OH	$2 \times 10^{-7} (T_{gas}/300)^{-0.5}$	[a]
$C_2H_2^+ + M^-(H_2O)_2 \rightarrow CH + CH + M + H_2O + H_2O$	$2 \times 10^{-7} (T_{gas}/300)^{-0.5}$	[a]

M = O_2, OH		
C_2H^+		
$C_2H^+ + M^- \rightarrow CH + C + M$ M = H, OH, O, O_2, O_3, CH_2, C_2H_2	$2 \times 10^{-7} (T_{gas}/300)^{-0.5}$	[a]
$C_2H^+ + M^-(H_2O) \rightarrow CH + C + M + H_2O$ M = O_2, O, OH	$2 \times 10^{-7} (T_{gas}/300)^{-0.5}$	[a]
$C_2H^+ + M^-(H_2O)_2 \rightarrow CH + C + M + H_2O + H_2O$ M = O_2, OH	$2 \times 10^{-7} (T_{gas}/300)^{-0.5}$	[a]
C_2^+		
$C_2^+ + M^- \rightarrow C + C + M$ M = H, OH, O, O_2, O_3, CH_2, C_2H_2	$2 \times 10^{-7} (T_{gas}/300)^{-0.5}$	[a]
$C_2^+ + M^-(H_2O) \rightarrow C + C + M + H_2O$ M = O_2, O, OH	$2 \times 10^{-7} (T_{gas}/300)^{-0.5}$	[a]
$C_2^+ + M^-(H_2O)_2 \rightarrow C + C + M + H_2O + H_2O$ M = O_2, OH	$2 \times 10^{-7} (T_{gas}/300)^{-0.5}$	[a]
$CH_3OH_2^+$		
$CH_3OH_2^+ + M^- \rightarrow CH_3OH + H + M$ M = H, OH, O, O_2, O_3, CH_2, C_2H_2	$2 \times 10^{-7} (T_{gas}/300)^{-0.5}$	[a]
$CH_3OH_2^+ + M^-(H_2O) \rightarrow CH_3OH + H + M + H_2O$ M = O_2, O, OH	$2 \times 10^{-7} (T_{gas}/300)^{-0.5}$	[a]
$CH_3OH_2^+ + M^-(H_2O)_2 \rightarrow CH_3OH + H + M + H_2O +$ H_2O M = O_2, OH	$2 \times 10^{-7} (T_{gas}/300)^{-0.5}$	[a]
CH_3OH^+		
$CH_3OH^+ + M^- \rightarrow CH_3 + OH + M$ M = H, OH, O, O_2, O_3, CH_2, C_2H_2	$2 \times 10^{-7} (T_{gas}/300)^{-0.5}$	[a]
$CH_3OH^+ + M^-(H_2O) \rightarrow CH_3 + OH + M + H_2O$ M = O_2, O, OH	$2 \times 10^{-7} (T_{gas}/300)^{-0.5}$	[a]
$CH_3OH^+ + M^-(H_2O)_2 \rightarrow CH_3 + OH + M + H_2O + H_2O$ M = O_2, OH	$2 \times 10^{-7} (T_{gas}/300)^{-0.5}$	[a]
CH_2OH^+		
$CH_2OH^+ + M^- \rightarrow CH_2OH + M$ M = H, OH, O, O_2, O_3, CH_2, C_2H_2	$2 \times 10^{-7} (T_{gas}/300)^{-0.5}$	[a]
$CH_2OH^+ + M^-(H_2O) \rightarrow CH_2OH + M + H_2O$ M = O_2, O, OH	$2 \times 10^{-7} (T_{gas}/300)^{-0.5}$	[a]
$CH_2OH^+ + M^-(H_2O)_2 \rightarrow CH_2OH + M + H_2O + H_2O$ M = O_2, OH	$2 \times 10^{-7} (T_{gas}/300)^{-0.5}$	[a]
CH_3O^+		
$CH_3O^+ + M^- \rightarrow CH_2O + H + M$ M = H, OH, O, O_2, O_3, CH_2, C_2H_2	$2 \times 10^{-7} (T_{gas}/300)^{-0.5}$	[a]

$CH_3O^+ + M^-(H_2O) \rightarrow CH_3O + H + M + H_2O$ $M = O_2, O, OH$	$2 \times 10^{-7} (T_{gas}/300)^{-0.5}$	[a]
$CH_3O^+ + M^-(H_2O)_2 \rightarrow CH_3O + H + M + H_2O + H_2O$ $M = O_2, OH$	$2 \times 10^{-7} (T_{gas}/300)^{-0.5}$	[a]
CH_2O^+		
$CH_2O^+ + M^- \rightarrow CHO + H + M$ $M = H, OH, O, O_2, O_3, CH_2, C_2H_2$	$2 \times 10^{-7} (T_{gas}/300)^{-0.5}$	[a]
$CH_2O^+ + M^-(H_2O) \rightarrow CHO + H + M + H_2O$ $M = O_2, O, OH$	$2 \times 10^{-7} (T_{gas}/300)^{-0.5}$	[a]
$CH_2O^+ + M^-(H_2O)_2 \rightarrow CHO + H + M + H_2O + H_2O$ $M = O_2, OH$	$2 \times 10^{-7} (T_{gas}/300)^{-0.5}$	[a]
CHO^+		
$CHO^+ + M^- \rightarrow CHO + M$ $M = H, OH, O, O_2, O_3, CH_2, C_2H_2$	$2 \times 10^{-7} (T_{gas}/300)^{-0.5}$	[a]
$CHO^+ + M^-(H_2O) \rightarrow CHO + M + H_2O$ $M = O_2, O, OH$	$2 \times 10^{-7} (T_{gas}/300)^{-0.5}$	[a]
$CHO^+ + M^-(H_2O)_2 \rightarrow CHO + M + H_2O + H_2O$ $M = O_2, OH$	$2 \times 10^{-7} (T_{gas}/300)^{-0.5}$	[a]
CH_2^- and $C_2H_2^-$		
$M^- + Ar^+ \rightarrow M + Ar$ $M = CH_2, C_2H_2$	$2 \times 10^{-7} (T_{gas}/300)^{-0.5}$	[a]
$M^- + Ar_2^+ \rightarrow M + Ar + Ar$ $M = CH_2, C_2H_2$	$2 \times 10^{-7} (T_{gas}/300)^{-0.5}$	[a]
$M^- + ArH^+ \rightarrow M + Ar + H$ $M = CH_2, C_2H_2$	$2 \times 10^{-7} (T_{gas}/300)^{-0.5}$	[a]
$M^- + H_3^+ \rightarrow M + H_2 + H$ $M = CH_2, C_2H_2$	$2 \times 10^{-7} (T_{gas}/300)^{-0.5}$	[a]
$M^- + H_2^+ \rightarrow M + H + H$ $M = CH_2, C_2H_2$	$2 \times 10^{-7} (T_{gas}/300)^{-0.5}$	[a]
$M^- + H^+ \rightarrow M + H$ $M = CH_2, C_2H_2$	$2 \times 10^{-7} (T_{gas}/300)^{-0.5}$	[a]
$M^- + OH^+ \rightarrow M + O + H$ $M = CH_2, C_2H_2$	$2 \times 10^{-7} (T_{gas}/300)^{-0.5}$	[a]
$M^- + O_4^+ \rightarrow M + O_2 + O_2$ $M = CH_2, C_2H_2$	$2 \times 10^{-7} (T_{gas}/300)^{-0.5}$	[a]
$M^- + O_2^+ \rightarrow M + O + O$ $M = CH_2, C_2H_2$	$2 \times 10^{-7} (T_{gas}/300)^{-0.5}$	[a]
$M^- + O^+ \rightarrow M + O$ $M = CH_2, C_2H_2$	$2 \times 10^{-7} (T_{gas}/300)^{-0.5}$	[a]
$M^- + H_3O^+ \rightarrow M + H_2O + H$	$2 \times 10^{-7} (T_{gas}/300)^{-0.5}$	[a]

$M = CH_2, C_2H_2$		
$M^- + H_2O^+ \rightarrow M + OH + H$ $M = CH_2, C_2H_2$	$2 \times 10^{-7} (T_{gas}/300)^{-0.5}$	[a]
$M^- + H_2O^+(H_2O) \rightarrow M + H_2O + OH + H$ $M = CH_2, C_2H_2$	$2 \times 10^{-7} (T_{gas}/300)^{-0.5}$	[a]
$M^- + O_2^+(H_2O) \rightarrow M + H_2O + O_2$ $M = CH_2, C_2H_2$	$2 \times 10^{-7} (T_{gas}/300)^{-0.5}$	[a]
$M^- + H_3O^+(H_2O) \rightarrow M + H + H_2O + H_2O$ $M = CH_2, C_2H_2$	$2 \times 10^{-7} (T_{gas}/300)^{-0.5}$	[a]

[a]Estimated by analogy to Ref. [29].

References

[1] M.-Y. Song, J.-S. Yoon, H. Cho, Y. Itikawa, G. P. Karwasz, V. Kokoouline, Y. Nakamura and J. Tennyson, J. Phys. Chem. Ref. Data **44,** 023101 (2015).

[2] C. W. Duncan and I. C. Walker, J. Chem. Soc. Faraday Trans. 2 **68,** 1514 (1972).

[3] W. Sohn, K. Jung and H. Ehrhardt, J. Phys. B At. Mol. Phys. **16,** 891 (1983).

[4] H. Tanaka, M. Kubo, N. Onodera and A. Suzuki, J. Phys. B At. Mol. Phys. **16,** 2861 (1983).

[5] K. Rohr, J. Phys. B At. Mol. Phys. **13,** 4897 (1980).

[6] H. Chatham, D. Hils, R. Robertson and A. Gallagher, J. Chem. Phys. **81,** 1770 (1984).

[7] H. F. Winters, J. Chem. Phys. **63,** 3462 (1975).

[8] L. v. Trepka and H. Neuert, Zeitschrift für Naturforsch. A **18,** 1295 (1963).

[9] T. E. Sharp and J. T. Dowell, J. Chem. Phys. **46,** 1530 (1967).

[10] R. K. Janev and D. Reiter, Phys. Plasmas **9,** 4071 (2002).

[11] M. Hayashi, Swarm Studies and Inelastic Electron-Molecule Collisions, 167–187 (1987).

[12] Y. Nakamura, J. Phys. D. Appl. Phys. **43,** 365201 (2010).

[13] M. Lucas, Y. Liu, R. Bryant, J. Minor and J. Zhang, Chem. Phys. Lett. **619,** 18 (2015).

[14] S. Satyapal, J. Park, R. Bersohn and B. Katz, J. Chem. Phys. **91,** 6873 (1989).

[15] C. C. Marston, K. Weide, R. Schinke and H. U. Suter, J. Chem. Phys. **98,** 4718 (1993).

[16] S.-H. Lee, H.-I. Lee and Y. T. Lee, J. Chem. Phys. **121,** 11053 (2004).

[17] K. L. Nixon, W. A. D. Pires, R. F. C. Neves, H. V. Duque, D. B. Jones, M. J. Brunger and M. C. A. Lopes, Int. J. Mass Spectrom. **404,** 48 (2016).

[18] A. I. Florescu-Mitchell and J. B. A. Mitchell, Phys. Rep. **430,** 277 (2006).

[19] R. D. Thomas, I. Kashperka, E. Vigren, W. D. Geppert, M. Hamberg, M. Larsson, M. af Ugglas and V. Zhaunerchyk, J. Phys. Chem. A **117,** 9999 (2013).

[20] L. Vejby-Christensen, L. H. Andersen, O. Heber, D. Kella, H. B. Pedersen, H. T. Schmidt and D. Zajfman, Astrophys. J. **483,** 531 (1997).

[21] J. Brian and A. Mitchell, Phys. Rep. **186,** 215 (1990).

[22] A. Larson, A. Le Padellec, J. Semaniak, C. Stromholm, M. Larsson, S. Rosen, R. Peverall, H. Danared, N. Djuric, G. H. Dunn and S. Datz, Astrophys. J. **505,** 459 (1998).

[23] H. Deutsch, P. Scheier, K. Becker and T. . Märk, Chem. Phys. Lett. **382,** 26 (2003).

[24] R. K. Janev and D. Reiter, Phys. Plasmas **11,** 780 (2004).

[25] P. Tosi, D. Bassi, B. Brunetti and F. Vecchiocattivi, Int. J. Mass Spectrom. Ion Process. **149–150,** 345 (1995).

[26] V. G. Anicich, J. Phys. Chem. Ref. Data **22,** 1469 (1993).

[27] J. Woodall, M. Agundez, M.-K. A. J and T. J. Millar, Astron. Astrophys. **466,** 1197 (2007).

[28] D. McElroy, C. Walsh, A. J. Markwick, M. A. Cordiner, K. Smith and T. J. Millar, Astron. Astrophys. **550,** A36 (2013).

[29] A. A. Konnov, Combust. Flame **156,** 2093 (2009).

[30] D. L. Baulch, C. T. Bowman, C. J. Cobos, R. A. Cox, T. Just, J. A. Kerr, M. J. Pilling, D. Stocker, J. Troe, W. Tsang, R. W. Walker and J. Warnatz, J. Phys. Chem. Ref. Data **34,** 757 (2005).

[31] W. Tsang and R. F. Hampson, J. Phys. Chem. Ref. Data **15,** 1087 (1986).

[32] S. I. Stoliarov, V. D. Knyazev and I. R. Slagle, J. Phys. Chem. A **104,** 9687 (2000).

[33] W. Tsang, J. Phys. Chem. Ref. Data **17,** 887 (1988).

[34] W. Tsang, J. Phys. Chem. Ref. Data **20,** 221 (1991).

[35] W. Tsang, J. Phys. Chem. Ref. Data **17,** 887 (1988).

[36] D. L. Baulch, C. J. Cobos, R. A. Cox, P. Frank, G. Hayman, T. Just, J. A. Kerr, T. Murrells, M. J. Pilling, J. Troe, R. W. Walker and J. Warnatz, J. Phys. Chem. Ref. Data **23,** 847 (1994).

[37] M. H. De Vasconcelos and A. E. De Vries, Phys. A Stat. Mech. its Appl. **86,** 490 (1977).

[38] R. M. Siddles, G. J. Wilson and C. J. S. M. Simpson, Chem. Phys. **188,** 99 (1994).

[39] J. T. Yardley, M. N. Fertig and C. B. Moore, J. Chem. Phys. **52,** 1450 (1970).